University of Alberta

An Investigation of Silver Coated Hollow Glass Fiber for Applications at 800 nm

by

Mohammad Mohebbi

A thesis submitted to the Faculty of Graduate Studies and Research in partial fulfillment of the requirements for the degree of Doctor of Philosophy

Department of Electrical and Computer Engineering

Edmonton, Alberta
Spring 2003

National Library
of Canada

Acquisitions and
Bibliographic Services

395 Wellington Street
Ottawa ON K1A 0N4
Canada

Bibliothèque nationale
du Canada

Acquisisitons et
services bibliographiques

395, rue Wellington
Ottawa ON K1A 0N4
Canada

Your file Votre référence
ISBN: 0-612-82142-0
Our file Notre référence
ISBN: 0-612-82142-0

The author has granted a non-exclusive licence allowing the National Library of Canada to reproduce, loan, distribute or sell copies of this thesis in microform, paper or electronic formats.

The author retains ownership of the copyright in this thesis. Neither the thesis nor substantial extracts from it may be printed or otherwise reproduced without the author's permission.

L'auteur a accordé une licence non exclusive permettant à la Bibliothèque nationale du Canada de reproduire, prêter, distribuer ou vendre des copies de cette thèse sous la forme de microfiche/film, de reproduction sur papier ou sur format électronique.

L'auteur conserve la propriété du droit d'auteur qui protège cette thèse. Ni la thèse ni des extraits substantiels de celle-ci ne doivent être imprimés ou aturement reproduits sans son autorisation.

Canada

University of Alberta

Library Release Form

Name of Author: Mohammad Mohebbi

Title of Thesis: An Investigation of Silver Coated Hollow Glass Fiber for Applications at 800 nm

Degree: Doctor of Philosophy

Year this Degree Granted: 2003

Permission is hereby granted to the University of Alberta Library to reproduce single copies of this thesis and to lend or sell such copies for private, scholarly or scientific research purposes only.

The author reserves all other publication and other rights in association with the copyright in the thesis, and except as herein before provided, neither the thesis nor any substantial portion thereof may be printed or otherwise reproduced in any material form whatever without the author's prior written permission.

M. Mohebbi

328C Michener park
Edmonton, AB T6H 4M5

January 6, 2003

University of Alberta

Faculty of Graduate Studies and Research

The undersigned certify that they have read, and recommend to the Faculty of Graduate Studies and Research for acceptance, a thesis entitled An Investigation of Silver Coated Hollow Glass Fiber for Applications at 800 nm submitted by Mohammad Mohebbi in partial fulfillment of the requirements for the degree of Doctor of Philosophy.

Robert Fedosejevs
R. Fedosejevs

C. Capjack

Y. Tsui

Ray DeCorby
R. Decorby

M. Freeman

H. Haugen
(McMaster University)

Jan. 6, 2005

Abstract

A silver coated hollow glass fiber with a core diameter of 250 μm is studied for beam transport and nonlinear optical applications at 800 nm using a femtosecond Ti:sapphire laser. To reduce the losses, the inner glass surface of the waveguide is coated with a thin film of silver by a liquid phase deposition process. The measured transmission loss of the straight silver coated hollow fiber, 0.44 dB/m, is lower than the transmission loss of a similar fused silica hollow fiber, 1.94 dB/m. Beam diameter measurements indicate that a single HE_{11} mode propagates from output of the waveguide into free space. The bending loss of this waveguide was measured for bending radii of 30, 50, and 100 cm and compared to the theoretical values. Numerical modeling and experimental results for optical compression of femtosecond pulses are presented. Input pulses with energy of 250μJ and duration of 110 fs were compressed to 20 fs with energy of 220 μJ using the silver coated hollow fiber, filled with argon, and a prism pair. The same experiment was performed for the fused silica hollow fiber which produced 20 fs pulses with energy of 190 μJ. There was close agreement between the pulse compression numerical and experimental results. Nonlinear ellipse rotation for pulse contrast enhancement was also studied using the silver coated waveguide. The results were similar to those obtained for the fused silica waveguide, but with higher transmission.

Acknowledgement

I would like to thank Dr. Robert Fedosejevs for giving me the opportunity to pursue my graduate studies and for providing financial assistance.

I am grateful to Dr. J. A. Harrington for fabrication of the waveguide that was used in the experiments presented in this thesis. I would also like to thank the people in the machine shop for building my experimental equipment.

I am thankful to Geoff Redman, Michael Buhr, and Hideki Minami for their friendship. I also thank them for lending me their books.

I would like to thank my parents for their kindness, help, encouragement, and support throughout my life. They made everything possible for me. Special thanks to my wife Zahra for being so patient, kind, and supportive during my studies. I had to work long hours and she never complained and always greeted me with a smile.

Table of Contents

Chapter 1 Introduction 1

1.1 Background 1

1.2 Motivation 3

1.3 Research Project 4

1.4 Organization of the Thesis 6

Chapter 2 Wave Propagation in Hollow Fibers 8

2.1 Introduction 8

2.2 Modes and Propagation Constants 8

2.3 Attenuation of Bent Hollow Waveguide 19

2.4 Dispersion 22

Chapter 3 Beam Transport Experimental Results 26

3.1 Introduction 26

3.2 Mode Coupling 27

3.3 Fused Silica Hollow Fiber 31

3.4 Silver Coated Hollow Fiber 35

3.4.1 Fabrication 35

3.4.2 Transmission Measurements 38

3.4.3 Bending Loss 41

3.5 Discussion 43

Chapter 4 Theory of Optical Pulse Compression 46

4.1 Nonlinear Wave Propagation 46

4.1.1 Nonlinear Refractive Index 46

4.1.2 Nonlinear wave equation 48

4.2 Prism Compressor 54

4.2.1 General Description of Optical Pulse Compression 54

4.2.2 Angular Dispersion 57

4.2.3 Prism Dispersion 61

Chapter 5 Optical Pulse Compression Using Silver Coated Hollow Fiber 67

5.1 Introduction 67

5.2 Numerical Modeling 68

5.3 Experimental Results 92

5.4 Design Considerations for Hollow Fiber Chamber 106

5.5 Discussion 109

Chapter 6 Nonlinear Ellipse Rotation in Silver Coated Hollow Fiber 113

6.1 Introduction 113

6.2 Theory of NER 114

6.3 Experimental Results 117

Chapter 7 Conclusion 124

References 128

List of Figures

Fig. 2.1 A Hollow cylindrical waveguide. Core diameter is $2a$. The core can be free space or a material such as a noble gas. The cladding can be fused silica or a highly reflective metal. 9

Fig. 2.2 Comparison of the attenuation constants for three hybrid modes of a fused silica hollow cylindrical waveguide as a function of the core diameter. The wavelength is 800 nm. The HE_{11} mode has the lowest loss. For a core radius of 125 μm the intensity attenuation constant of the HE_{11} mode is 0.62 dB/m. 13

Fig. 2.3 Comparison of the attenuation constants for three hybrid modes of a silver coated hollow cylindrical waveguide as a function of the core diameter. The wavelength is 800 nm. The HE_{11} mode has the lowest loss among the hybrid modes. For a core radius of 125 μm the intensity attenuation constant of the HE_{11} mode is 0.033 dB/m. 14

Fig. 2.4 Electric field lines of the HE_{11} mode inside the core of a hollow cylindrical waveguide. Electric field is not continuous at the boundary between the core and the cladding. Therefore, electric field lines of the HE_{11} mode are discontinuous at the boundary. 16

Fig. 2.5 Electric field amplitude of HE_{11} mode inside the core of a hollow cylindrical waveguide. The electric field is maximum in the center of the core and is zero at the boundary between the core and the cladding. Radial distance is normalized with respect to the core radius. 16

Fig. 2.6 Electric field lines of the TE_{01} mode inside the core of a hollow cylindrical waveguide. Electric field lines are circles in a plane perpendicular to the z axis. The electric field of the TE_{01} mode is continuous at the boundary between the core and the cladding. 17

Fig. 2.7 Electric field amplitude of TE_{01} mode inside the core of a hollow cylindrical waveguide. The electric field is zero in the center of the core and at the boundary between the core and the cladding. Radial distance is normalized with respect to the core radius. 18

Fig. 2.8 Attenuation constant of the HE_{11} mode as a function of core diameter for a fused silica hollow waveguide and a silver coated hollow glass waveguide at 800 nm. The attenuation constant is inversely proportional to the cube of the core radius. Losses of the silver coated hollow fiber are much less for smaller values of core diameter. 19

Fig. 2.9 Group velocity dispersion of a fused silica hollow fiber filled with air as a function of core radius at a wavelength of 800 nm (solid line). The GVD

parameter for a core radius of 125 μm is β_2=12.8 fs^2/m. The material dispersion of air is also shown (dashed line). 24

Fig. 2.10 Third order dispersion of a fused silica hollow fiber filled with air as a function of core radius at a wavelength of 800 nm (solid line). The TOD parameter for a core radius of 125 μm is β_3=20.7 fs^2/m. The third order material dispersion of air is also shown (dashed line). 25

Fig. 3.1 The experimental setup for transmission and beam diameter measurements. The laser beam is attenuated by the half wave plate and polarizer combination. A lens is used to couple the laser beam into the hollow fiber. Images of the output beam are taken by a CCD detector, which are then used to measure the beam diameters at different distances from the exit of the hollow fiber. 27

Fig. 3.2 Coupling efficiency of the fundamental free space mode to the HE_{11} mode of a hollow cylindrical waveguide as a function of normalized beam waist. Maximum coupling efficiency of 98% occurs for a normalized beam waist of 0.64. 30

Fig. 3.3 The horizontal spatial intensity of the input beam. There is a small intensity offset due to dark current in the CCD detector. 32

Fig. 3.4 Output image of the beam from the fused silica hollow fiber at 20 cm from output end of the fiber. The actual beam is circular. The image was taken using a CCD detector with pixel size of 27 μm by 11.5 μm, which results in an elliptically appearing image. The image is 5.5 mm by 3.7 mm in the vertical and horizontal directions respectively. 33

Fig. 3.5 Spatial output intensity of the fused silica hollow fiber at 20 cm from output end of the fiber and a Gaussian fit to the data (line). The data is taken from a horizontal line through the center of the image shown in Fig. 3.4. There is a small intensity offset due to the dark current in the CCD detector. 34

Fig. 3.6 Comparison of theoretical and experimental beam diameters for output beam of the fused silica hollow fiber as a function of distance from output end of the fiber. The line represents the calculated values. Squares are the horizontal beam diameters and triangles are the vertical beam diameters measured experimentally. The measurement error bars are smaller than the size of the symbols. 35

Fig. 3.7 AFM image of the silver thin film deposited on a glass slide for 20 minutes. Image was provided by Prof. Harrington's research group at Rutgers University. 38

Fig. 3.8 Output image of the beam from the silver coated hollow fiber at 20 cm from output end of the fiber. The actual beam is circular. The image was taken using a CCD detector with pixel size of 27 μm by 11.5 μm, which results in an elliptically appearing image. The image is 5.5 mm by 3.7 mm in the vertical and horizontal directions respectively. 39

Fig. 3.9 Horizontal spatial output intensity (dots) at 20 cm from output end of the silver coated hollow fiber and a Gaussian fit to the data (line). The data is taken from a horizontal line through the center of the image shown in Fig. 3.8. 40

Fig. 3.10 Comparison of theoretical and experimental beam diameters for output beam of the silver coated hollow fiber as a function of distance from output end of the fiber. The line represents the calculated values. Triangles are the horizontal beam diameters and squares are the vertical beam diameters measured experimentally. 41

Fig. 4.1 A sequence of four prisms producing negative GVD. Prisms 1 and 2 are used to obtain the GVD. Prisms 3 and 4 correct the beam deformation..... 58

Fig. 4.2 Angular dispersion by an optical element. Rays of light are diffracted by the optical element and different spectral components propagate at different angles..... 59

Fig. 4.3 Geometry of a prism pair used to find the GVD and TOD parameters. The mirror is used to reflect the beam back along the same path through the prism pair. The reflected beam can be separated from the input beam by slight adjustment of this mirror. 61

Fig. 4.4 Refractive index of fused silica as a function of wavelength. The refractive index of fused silica at 0.8 μm is 1.4533. 64

Fig. 4.5 GVD of fused silica as a function of wavelength. The material dispersion of fused silica at 0.8μm is 361 fs^2/cm. 64

Fig. 4.6 GVD of a double-pass fused silica prism pair with apex angle of 69.08 degrees. Prism separation is 60 cm. The GVD parameter at 0.8 μm is β_2= 9.6 fs^2/cm. 65

Fig. 4.7 TOD of a double-pass fused silica prism pair with apex angle of 69.08 degrees. Prism separation is 60 cm. The TOD parameter at 0.8 μm is β_3= 14.2 fs^3/cm. 66

Fig. 5.1 GVD of the HE_{11} mode for the silver coated hollow fiber filled with argon at 2.4 atm (solid line). The core radius of the hollow fiber is 125 μm. The GVD parameter β_2=39.24 fs^2/m at 800 nm. The material

(dotted line) and waveguide (dashed line) dispersions are shown for comparison. 71

Fig. 5.2 Comparison of GVD for the silver coated (solid line) and fused silica (dashed line) hollow fibers filled with argon at 2.4 atm. 72

Fig. 5.3 Third order dispersion (TOD) of the HE_{11} mode for the silver coated hollow fiber filled with argon at 2.4 atm (solid line). The TOD parameter β_3=32.04 fs^3/m at 800 nm. The third order material (dotted line) and waveguide (dashed line) dispersions are shown for comparison. 73

Fig. 5.4 Comparison of TOD for the silver coated (solid line) and fused silica (dashed line) hollow fibers filled with argon at 2.4 atm. 74

Fig. 5.5 Input (dashed line) and output (solid line) pulse shapes obtained from simulating the propagation of hyperbolic secant optical pulses through the silver coated hollow fiber for an argon pressure of 2.4 atm. The propagation distance is 50 cm. The distortion of the output pulse is due to the nonlinear effects. Because of large value of the dispersion length (100 m), the output pulse has broadened very little. The output pulse without the self steepening effect is also shown (dotted line). 76

Fig. 5.6 Frequency chirp of the output pulse (shown in Fig. 5.5) for argon pressure of 2.4 atm. It shows a linear positive chirp in the central portion of the pulse. The frequency chirp is asymmetric and is larger near the trailing edge. This leads to larger spectral broadening for the blue-shifted frequency components. 77

Fig. 5.7 Output spectrum (solid line) of the silver coated hollow fiber at argon pressure of 2.4 atm obtained from the simulation. The spectral broadening is larger on the high frequency side of the spectrum. The peaks are characteristic of SPM induced spectral broadening. The input spectrum (dashed line) is also shown. 78

Fig. 5.8 Calculated compressed (solid line) and input (dashed line) pulses for the silver coated hollow fiber at argon pressure of 2.4 atm. A fused silica prism pair with spacing of 60 cm was used to compress the frequency broadened output pulses of the hollow fiber. Because the chirp is linear only in the central portion of the pulse, some of the energy in the wings is not compressed. 80

Fig. 5.9 Calculated compressed (solid line) and input (dashed line) pulses for prism separation of 50 cm. When the prism distance is reduced below the optimum value of 60 cm the amount of uncompressed energy in the wings increases. 81

Fig. 5.10 Compressed (solid line) and input (dashed line) pulses for prism separation of 70 cm. By increasing the prism distance above the optimum value of 60 cm, there is a slight decrease in the amount of compression. The amplitude of oscillations at the wings also increases. 82

Fig. 5.11 Compressed (solid line) and input (dashed line) pulses for prism separation of 80 cm. By increasing the prism distance beyond 70 cm, the amount of compression decreases. The amplitude of oscillations at the wings has also grown indicating that more uncompressed energy is contained in the wings. 83

Fig. 5.12 Input (dashed line) and output (solid line) pulse shapes obtained from simulating the propagation of Gaussian optical pulses through the silver coated hollow fiber for an argon pressure of 2.4 atm. 84

Fig. 5.13 Frequency chirp of the output pulse (shown in Fig. 5.12) for argon pressure of 2.4 atm, assuming a Gaussian input pulse..... 85

Fig. 5.14 Output spectrum (solid line) of the silver coated hollow fiber at argon pressure of 2.4 atm, obtained from the simulation for Gaussian input pulses. The input spectrum (dashed line) is shown for comparison. 86

Fig. 5.15 Calculated compressed (solid line) and input (dashed line) pulses for the silver coated hollow fiber at argon pressure of 2.4 atm, using Gaussian input pulses. A fused silica prism pair with spacing of 55 cm was assumed for compression in the simulation. 87

Fig. 5.16 Input (dashed line) and output (solid line) pulse shapes obtained from simulating the propagation of optical pulses through the silver coated hollow fiber for argon pressure of 1.5 atm. The propagation distance is 50 cm. The distortion of the output pulse is due to the nonlinear effects. 88

Fig. 5.17 Calculated frequency chirp of the output pulse for argon pressure of 1.5 atm. It shows a linear positive chirp in the central portion of the pulse. The frequency chirp is asymmetric and is larger near the trailing edge. The amount of frequency chirp is less compared to the frequency chirp for pressure of 2.4 atm. 89

Fig. 5.18 Output spectrum (solid line) of the silver coated hollow fiber at argon pressure of 1.5 atm obtained from the simulation. The peaks are characteristic of SPM induced spectral broadening. The number of peaks has reduced which is due to larger value of the nonlinear length (10 cm) for 1.5 atm compared to its value (6.3 cm) for 2.4 atm. The input spectrum (dashed line) is also shown..... 90

Fig. 5.19 Calculated compressed (solid line) and input (dashed line) pulses for the silver coated hollow fiber at argon pressure of 1.5 atm. A fused silica prism compressor was used to compress the frequency broadened output pulses of the hollow fiber. Because the chirp is linear only in the central portion of the pulse, some of the energy in the wings is not compressed. The compressed pulse width has increased to 30 fs for 1.5 atm compared to 20 fs for 2.4 atm. 91

Fig. 5.20 The experimental setup used for optical pulse compression. The hollow fiber is in a tube filled with argon gas. The lenses are antireflection coated. A fused silica prism pair is used to obtain compression. The reflected beam is separated from the input beam vertically by adjusting mirror M4 and the output beam is obtained using mirror M5. 92

Fig. 5.21 Measured output spectrum (solid line) of the silver coated hollow fiber filled with argon at 2.4 atm. Input pulse energy is 250 μJ and input pulse width is 110 fs. Spectrum of the input pulse (dashed line) is shown for comparison. The spectral width is 55.6 nm. 94

Fig. 5.22 Comparison of output spectrum measured from experiment (solid line) with output spectrum obtained from simulation (dashed line) for the silver coated hollow fiber. The input pulse energy is 250 μJ, the input pulse width is 110 fs, and the argon gas pressure is 2.4 atm. There is close agreement between the theoretical and experimental spectra..... 95

Fig. 5.23 Measured autocorrelation trace (dots) of the compressed pulses and calculated autocorrelation trace (solid line) assuming a Gaussian pulse shape. The argon pressure is 2.4 atm. The output pulses of the silver coated hollow fiber were compressed using a fused silica prism pair with separation of 60 cm. The autocorrelation of the compressed pulse of Fig. 5.8 is also shown (dashed line). 96

Fig. 5.24 Spatial output intensity of the silver coated hollow fiber at a distance of 25 cm from the output end of the fiber. Dots are the experimental data. The Gaussian fit (line) to the data is also shown. 98

Fig. 5.25 Comparison of calculated (line) and experimental beam diameters as a function of distance for the output beam of the silver coated hollow fiber. Distance is measured from the output end of the hollow fiber. Triangles are the horizontal beam diameters and squares are the vertical beam diameters measured experimentally..... 99

Fig. 5.26 Measured output spectrum (solid line) of the silver coated hollow fiber filled with argon at 1.5 atm. Input pulse energy is 250 μJ and input pulse width is 110 fs. Spectrum of the input pulse (dashed line) is shown for comparison. The spectral width is 28 nm. 100

Fig. 5.27 Comparison of output spectrum measured from experiment (solid line) with output spectrum obtained from simulation (dashed line) for the silver coated hollow fiber. The input pulse energy is 250 μJ, the input pulse width is 110 fs, and the argon gas pressure is 1.5 atm. 101

Fig. 5.28 Measured autocorrelation trace (dots) of the compressed pulses and calculated autocorrelation trace (line) assuming a Gaussian pulse shape. The argon pressure is 1.5 atm. The output pulses of the silver coated hollow fiber were compressed using a fused silica prism pair with separation of 70 cm. The autocorrelation of the compressed pulse of Fig. 5.19 is also shown (dashed line). 102

Fig. 5.29 Measured output spectrum (solid line) of the fused silica hollow fiber filled with argon at 2.4 atm. Input pulse energy is 250 μJ and input pulse width is 110 fs. Measured output spectrum of the silver coated hollow fiber (dashed line) is shown for comparison. The spectral width is 55.6 nm. 104

Fig. 5.30 Measured autocorrelation trace (dots) of the compressed pulses and calculated autocorrelation trace (line) assuming a Gaussian pulse shape. The argon pressure is 2.4 atm. The output pulses of the fused silica hollow fiber were compressed using a prism separation of 60 cm. 105

Fig. 5.31 The B-integral of the fused silica window is obtained by finding the beam radius w_2. The maximum distance from the lens with focal length f to the fused silica window is found to be 64.3 cm. Therefore, the distance d between the window and the input end of the fiber must be greater than 10.7 cm. This result was obtained for pulse energy of 400 μJ and pulse width of 110 fs. 107

Fig. 6.1 Nonlinear ellipse rotation experimental setup. A half wave plate is used to convert the horizontal input polarization to vertical. The first quarter wave plate changes the polarization of the beam to elliptic. The beam undergoes nonlinear ellipse rotation as it propagates inside the hollow fiber. After passing through the second quarter wave plate, a polarizer rejects the low intensity components of the beam and passes most of the energy near the peak of the pulse with the initial horizontal polarization. ... 118

Fig. 6.2 Fraction of energy in the pulse at the output of the polarizer as a function of energy entering the second quarter wave plate for the silver coated hollow fiber filled with argon at 3 atm. 119

Fig. 6.3 Fraction of energy in the pulse at the output of the polarizer as a function of argon pressure for the silver coated hollow glass fiber. The energy per pulse at the output of the waveguide was set at 100 μJ. 120

Fig. 6.4 Fraction of energy in the pulse at the output of the polarizer as a function of energy entering the second quarter wave plate for the fused silica hollow fiber at argon pressure of 3 atm. 121

Fig. 6.5 Fraction of energy in the pulse at the output of the polarizer as a function of pressure for the fused silica hollow fiber. The energy at the output of the waveguide was set at 100 μJ. 122

List of Tables

Table 3.1 Fraction of power contained in the first six free space Laguerre-Gaussian modes in the expansion of the HE_{11} mode. 30

Table 3.2 Bending loss of the silver coated hollow fiber for perpendicular polarization. 42

Table 3.3 Bending loss of the silver coated hollow fiber for parallel polarization. 42

List of Symbols

a	Hollow core radius
A_{eff}	Effective area of the mode
$A(z,t)$	Optical field envelope
c	Speed of light
$\vec{E}$	Electric field vector
f	Focal length
$F(x,y)$	Transverse modal distribution
I	Intensity
k	Free space propagation constant
k_i	Radial propagation constant in the core
k_e	Radial propagation constant in the cladding
L_D	Second order dispersion length
L'_D	Third order dispersion length
L_{NL}	Nonlinear length
$l(\omega)$	Optical path
n	Index of refraction
n_0	Linear index of refraction
n_2	Nonlinear index of refraction
p_0	Peak power of the pulse
$\vec{P}$	Polarization vector

$\vec{r}$	Position vector
T_0	1/e Intensity half width of the pulse
$U(z,\tau)$	Normalized amplitude envelope
v_g	Group velocity
w	Beam radius
α	Attenuation constant
β	Phase constant
β_2	Group velocity dispersion parameter
β_3	Third order dispersion parameter
γ	Axial propagation constant
γ	Nonlinear parameter
$\Delta\omega$	Spectral width
ε	Permittivity
η	Coupling coefficient
λ	Wavelength
μ	Permeability
ν	Refractive index of cladding
ϕ	Phase shift
χ	Susceptibility tensor
ω	Angular frequency
ω_0	Central angular frequency

Acronyms

GVD	Group velocity dispersion
HE	Hybrid electric
NER	Nonlinear ellipse rotation
SPM	Self phase modulation
TE	Transverse electric
TEM	Transverse electromagnetic
TM	Transverse magnetic
TOD	Third order dispersion

Chapter 1

Introduction

1.1 Background

Hollow core waveguides are used for transmitting high laser powers. These waveguides were originally developed for the delivery of CO_2 laser radiation [1]. There are two types of hollow waveguides: those with a wall material that has a refractive index n less than one ($n < 1$) and waveguides whose wall material has a refractive index greater than one ($n > 1$) [2]. Waveguides that have an air core with refractive index of one and a cladding material with $n < 1$ guide light in a manner similar to conventional solid core fibers. One of the first hollow waveguides of this type used lead and germanium doped silicates as the cladding material [3]. Hollow sapphire waveguides also have an $n < 1$ structure when transmitting light at a wavelength of 10.6 μm. The measured losses of hollow sapphire waveguide are higher than expected due to the roughness of the sapphire inner surface [4]. It also can not be bent to a small radius because of high modulus of sapphire. Leaky hollow waveguides, whose claddings have a refractive index greater than one, transmit light by grazing incidence reflections at the inner surface of the cladding. Hollow waveguides in general have a loss that depends strongly on wavelength, core diameter, and bending radius [5].

Hollow waveguides are fabricated by depositing metallic and dielectric coatings on the inside surface of metallic, plastic, or glass tubing. A number of different fabrication techniques have been used such as physical vapor deposition, chemical vapor deposition, sputtering, and liquid phase deposition. Physical vapor deposition was used to

deposit silver and dielectric layers on metallic substrates. This technique is difficult to use for fabrication of small bore hollow waveguides. Sputtering was used to deposit dielectric and metallic layers on a pipe made of aluminum, where a thick layer of nickel was then deposited over the sputtered layers [6]. This was followed by etching the pipe away and ending up with a hollow waveguide. Small bore hollow waveguides with metal films on the inside surface have been fabricated by chemical vapor deposition [7]. The most common technique for fabricating metallic films in hollow waveguides is liquid phase deposition [8]. This process is inexpensive, easy to perform, and suitable for fabricating silver and gold films.

In the infrared region of the spectrum, metallic and dielectric coatings have been used to reduce the losses of a fused silica hollow fiber [9]. By coating the inside surface of the waveguide with a highly reflective metallic layer the losses can be reduced. A dielectric layer is then deposited over the metal film in order to reduce the losses further. The thickness of this dielectric film is adjusted for minimum transmission loss. Different dielectric thicknesses give a minimum loss at different wavelengths. Hollow glass fibers with a metallic layer of silver and a dielectric film such as silver iodide on the inner surface have been effective for transmitting CO_2 laser light at a wavelength of 10.6 μm and Er:YAG laser light at a wavelength of 3 μm with low losses.

The roughness of metallic and dielectric coatings introduces scattering losses and adds to the total loss of the waveguide. Studies have been conducted in order to optimize the fabrication parameters for obtaining smoother films and lower waveguide losses [10]. Hollow fibers with bore sizes of 250 to 1000 μm have been fabricated for transmission at wavelengths of 3 and 10.6 μm with losses between 0.3 and 0.8 dB/m [10]. The use of

these hollow waveguides for beam delivery has offered good flexibility, easy handling, and small spot size which is required in some applications.

1.2 Motivation

With the recent development of Ti:sapphire oscillators and amplifiers [11], applications of high energy femtosecond optical pulses are rapidly growing. Direct generation of optical pulses shorter than 8 fs from a Ti:sapphire laser in the 800 nm region was achieved by 1996 [12]. It is now possible to produce laser pulses lasting a few femtoseconds and reaching focused intensities exceeding 10^{18} W/cm^2.

In an experiment which was performed in 1997 [13], input pulses with a duration of 13 fs and an energy of 45 nJ from a Ti:sapphire laser were used to produce a pulse width of 4.9 fs. This was achieved by self phase modulation (SPM) in a single mode fiber, which broadens the frequency spectrum, and subsequent compression in a compressor consisting of grating and prism pairs. In another experiment, the pulse duration was reduced to 4.6 fs by using a chirped mirror in the compressor [14].

Optical fibers can only be used for transmitting and chirping pulses that have low peak powers. The peak power of the input pulse should be lower than the damage threshold of silica which is used for making optical fibers. A fused silica hollow fiber with large diameter and filled with a noble gas has been used for chirping high energy optical pulses. In the first experiment which was reported in 1996 [15], a 70 cm fused silica hollow fiber filled with krypton was used to compress 140 fs pulses to 10 fs. In another experiment [16], a 60 cm fused silica hollow fiber was used to chirp and frequency broaden 20 fs input pulses from a Ti:sapphire amplifier by dispersion and

nonlinear effects in argon and krypton. A compressor consisting of a chirped mirror and two fused silica prism pairs was then used to compress the pulses to 4.5 fs.

Hollow fibers are needed for both the delivery of high power laser pulses to a target and nonlinear optical applications in the 800 nm region. However, a fused silica hollow fiber has high losses that are mainly due to the leaky nature of the mode caused by refraction at the inner glass surface [5]. Bending of the waveguide also adds greatly to the losses and, thus, makes a fused silica hollow fiber ineffective for beam delivery applications.

In this thesis a silver coated hollow glass fiber designed for transmitting optical pulses at a wavelength of 800 nm with low losses is studied. This silver coated waveguide can transport femtosecond optical pulses with much higher transmission compared with a fused silica waveguide and, thus, improve the optical efficiency for both straight and bent waveguides in beam delivery applications. Despite lower losses, the output mode can have high purity and be as good as that obtained from a fused silica hollow fiber. With single mode propagation, the silver coated hollow fiber can also be employed for nonlinear applications such as optical pulse compression and pulse contrast enhancement [17], with much higher throughput.

1.3 Research project

The research project reported in this thesis consists of the investigation of a silver coated hollow glass fiber fabricated for beam transport and nonlinear applications at 800 nm. The attenuation constants of several low order modes are compared as a function of core diameter for both silver coated and fused silica hollow waveguides. The power

coupling efficiency of a TEM_{00} input beam to the HE_{11} mode of a hollow fiber is discussed. Fabrication of the silver coating inside a hollow glass fiber is explained in detail. The beam transport properties of silver coated and uncoated fused silica hollow fibers are investigated experimentally using a Ti:sapphire laser and are compared to theoretical models. These include the bending losses of the silver coated hollow fiber. The beam profile is measured as a function of distance from the output of straight hollow fibers in order to verify that an HE_{11} mode exits each hollow fiber and propagates into the free space.

An optical pulse compressor is developed using both silver coated and uncoated fused silica hollow fibers filled with argon gas and a prism pair for compression of femtosecond pulses at 800 nm. The dispersion parameters of the HE_{11} mode propagating in a silver coated hollow fiber filled with argon are calculated. It is shown that the dispersion parameters are essentially the same as those for a fused silica hollow fiber. The propagation of optical pulses inside a hollow fiber is modeled using the generalized nonlinear Schrödinger equation. A split-step method is used for the simulation. A fused silica prism compressor is explained in detail and its model is used in the calculations. An optical compressor is designed and built using the simulation results. Optical compression experiments are performed using fused silica and silver coated hollow fibers with different pulse energies and gas pressures and the results are compared.

Nonlinear ellipse rotation of femtosecond pulses inside silver coated and fused silica hollow fibers is examined for pulse contrast enhancement. The polarization of the input laser beam is converted to elliptic using a quarter wave plate, which is then propagated through an argon filled hollow fiber. Experiments are carried out to determine

the effects of pulse energy and gas pressure on the polarization ellipse of the beam. It is shown that the ellipse rotation can be maximized at a certain energy, which depends on the angle between the fast axis of the quarter wave plate and the input linear polarization. By keeping the pulse energy constant, the effect of argon gas pressure on the rotation of polarization ellipse of the beam and the transmission of output pulses is determined.

1.4 Organization of the thesis

This thesis is composed of seven chapters. Chapter 1 is an introduction which contains the background material on hollow fibers, the motivation for this work, and a description of the research project.

In chapter 2 the modes that can propagate in a hollow fiber are described and the attenuation and phase constants of the modes are given. The attenuations, field amplitudes, and field lines of several modes are compared for silver coated and fused silica hollow fibers. Dispersion in a hollow fiber filled with air is also discussed.

Chapter 3 contains the beam transport experimental results for the silver coated and fused silica hollow fibers. The coupling of a free space TEM_{00} Gaussian mode to the HE_{11} mode of a hollow fiber is discussed. Fabrication of a silver coated hollow fiber is explained. Transmission loss and beam profile measurements obtained for both hollow fibers are presented. The bending loss measurements for the silver coated hollow fiber are compared with the theoretical values.

The theory of optical pulse compression is explained in chapter 4. The nonlinear wave equation describing the propagation of an optical pulse in a hollow fiber is derived. Both dispersive and nonlinear effects are included in this equation. The phenomenon of

self phase modulation which is a result of intensity dependence of the nonlinear refractive index is explained. Optical pulse compression is explained and the dispersion equations for a prism compressor are given. The geometry of a prism is used to find the second and third order dispersion coefficients. It is shown that the group velocity dispersion of a prism pair is negative and tunable and, thus, it can be used to compress positively chirped optical pulses.

The numerical and experimental results for optical pulse compression using silver coated and fused silica hollow fibers are presented in chapter 5. The group velocity and third order dispersions of the hollow fibers are compared. The compression results for the silver coated hollow fiber are obtained for argon gas pressures of 2.4 and 1.5 atm. The experimental results of optical pulse compression using a fused silica hollow fiber are given for different energies and argon gas pressures.

The experimental results of nonlinear ellipse rotation in silver coated and fused silica hollow fibers filled with argon are presented in chapter 6. The theory of this nonlinear effect is explained and equations are given. Experimental results obtained by varying the input pulse energy and argon gas pressure are discussed.

In chapter 7 the main conclusions of this project are given. The results obtained for silver coated and fused silica hollow fibers are compared. Methods for improving the performance of the silver coated hollow fiber are discussed.

Chapter 2

Wave propagation in hollow fibers

2.1 Introduction

In this chapter the modes that propagate in a hollow cylindrical waveguide are explained and their field configurations and propagation constants are discussed. A mode or characteristic equation is given. The propagation constants of the modes are found by solving this equation. The simplifying assumptions used to obtain the field components and the propagation constants are explained. It is seen that the attenuation constant is proportional to the square of wavelength and inversely proportional to the cube of core radius. An optical pulse broadens as it propagates along a hollow cylindrical waveguide. This is due to the material (filling gas) and waveguide dispersions. The group velocity dispersion (GVD) and the third order dispersion (TOD) are obtained for the HE_{11} mode assuming that the hollow waveguide is filled with air.

2.2 Modes and propagation constants

The waveguide consists of a hollow core and a cladding made of a dielectric material such as glass or a highly reflective metal as shown in Fig. 2.1. At optical wavelengths metal no longer acts as a good conductor instead it starts to behave as a dielectric with a large dielectric constant. Thus, both the dielectric and metallic waveguides can be described in terms of a general hollow circular waveguide that has a cladding material with a finite complex refractive index. We consider a waveguide that

has a straight axis and a cylindrical cross section. We also assume that the wall thickness of this hollow fiber is infinite.

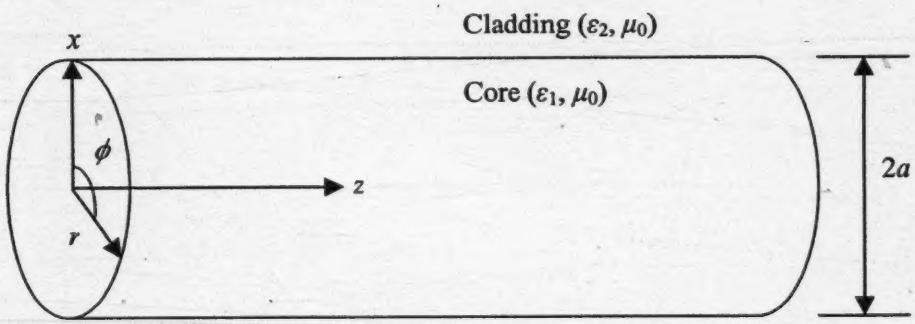

Fig. 2.1 A Hollow cylindrical waveguide. Core diameter is $2a$. The core can be free space or a material such as a noble gas. The cladding can be fused silica or a highly reflective metal.

The core can be free space (ε_0,μ_0) or another medium such as a noble gas (ε_1,μ_0). The wall consists of a metal or dielectric with complex dielectric constant ε_2. Both media are assumed to have magnetic permeability μ_0. The problem of finding the field components and propagation constants for the modes of the hollow fiber is greatly simplified if we use the assumption that

$$\lambda << a \tag{2.1}$$

where λ is the wavelength in free space. By using the inequality given by equation (2.1), we are considering the case where the core radius a is much larger than the free space wavelength λ.

The field components of the modes for a general cylindrical waveguide with arbitrary materials for the core and cladding have been determined by Stratton [18]. Three types of modes can propagate in a cylindrical waveguide: transverse electric modes

(TE) with field components E_ϕ, H_r, and H_z, transverse magnetic modes (TM) with field components H_ϕ, E_r, and E_z, and hybrid modes with all the electric and magnetic field components present.

A mode equation can be obtained by using the continuity of the tangential field components at the boundary between the core and the cladding. The propagation constants for the above modes in a straight hollow cylindrical waveguide are obtained by solving the following mode equation

$$\left[\frac{J_n'(k_i a)}{J_n(k_i a)} - \frac{k_i}{k_e}\frac{H_n^{(1)'}(k_e a)}{H_n^{(1)}(k_e a)}\right]\left[\frac{J_n'(k_i a)}{J_n(k_i a)} - \frac{\nu^2 k_i}{k_e}\frac{H_n^{(1)'}(k_e a)}{H_n^{(1)}(k_e a)}\right] = \left[\frac{n\lambda}{k k_i a}\right]^2\left[1-\left(\frac{k_i}{k_e}\right)^2\right]^2 \quad (2.2)$$

where ν is the ratio of the refractive index of the cladding medium to that of the core medium and $k = 2\pi/\lambda$ is the free space propagation constant. The radial propagation constants in the internal and external media, k_i and k_e, are defined by

$$k_i^2 = k_1^2 - \gamma^2 \quad (2.3)$$

$$k_e^2 = k_2^2 - \gamma^2 \quad (2.4)$$

where γ is the axial propagation constant of the mode, k_1 is the propagation constant in the core medium, and k_2 is the propagation constant in the cladding medium. In equation (2.2), J_n is the Bessel function of order n, J_n' is the first derivative of J_n with respect to its argument, $H_n^{(1)}$ is the Hankel function of the first kind of order n, and $H_n^{(1)'}$ is the derivative of $H_n^{(1)}$ with respect to its argument.

For n=0, we obtain transverse electric TE_{0m} and transverse magnetic TM_{0m} modes, where m is the order of the mode. The electric fields for the TE_{0m} modes are circles that are centered on the z axis and located in a transverse plane. The electric field lines for the

TM_{0m} modes are in the radial direction in the transverse plane. For n 0, we have hybrid modes, HE_{nm}. Therefore, the electric field lines of the modes are three dimensional. When the approximation given in equation (2.1) is used, the axial field component is small and the hybrid modes can be considered transverse. In this case the characteristic equation simplifies to [5]

$$J_{n-1}(k_i a) = i\nu_n \left(\frac{k_i}{k}\right) J_n(k_i a) \tag{2.5}$$

where

$$\nu_n = \begin{cases} \dfrac{1}{\sqrt{\nu^2 - 1}} & \text{for } TE_{0m} \text{ modes (n = 0)} \\ \dfrac{\nu^2}{\sqrt{\nu^2 - 1}} & \text{for } TM_{0m} \text{ modes (n = 0)} \\ \dfrac{1}{2}\dfrac{\nu^2 + 1}{\sqrt{\nu^2 - 1}} & \text{for } HE_{nm} \text{ modes (n} \neq 0) \end{cases} \tag{2.6}$$

Because of the approximation given in equation (2.1) and using equation (2.3), it is seen that the right hand side of equation (2.5) is close to zero. The characteristic equation is solved for $k_i a$, yielding

$$k_i a \approx u_{nm}\left(1 - \frac{i\nu_n}{ka}\right) \tag{2.7}$$

where u_{nm} is the mth root of the equation $J_{n-1}(u_{nm}) = 0$. Equation (2.7) is valid as long as $\lambda << a$. The propagation constant γ can be found using equations (2.3) and (2.7), giving

$$\gamma \approx k_1 \left[1 - \frac{1}{2}\left(\frac{u_{nm}}{k_1 a}\right)^2 \left(1 - \frac{i\nu_n \lambda}{\pi a}\right)\right] \tag{2.8}$$

The attenuation and phase constants for each mode are given by

$$\alpha_{nm} = \mathrm{Im}(\gamma) = \frac{u_{nm}^{\ 2}}{a^3}\frac{\mathrm{Re}(\nu_n)}{k_1 k} \tag{2.9}$$

$$\beta_{nm} = \mathrm{Re}(\gamma) = k_1\left\{1 - \frac{1}{2}\left(\frac{u_{nm}}{k_1 a}\right)^2\left[1 + \mathrm{Im}\left(\frac{\nu_n \lambda}{\pi a}\right)\right]\right\} \tag{2.10}$$

The attenuation constant is proportional to the square of the wavelength λ and inversely proportional to the cube of core radius of the waveguide a. Therefore, by choosing the radius of the hollow cylindrical waveguide sufficiently large compared to the wavelength, we can make the losses of the waveguide very small. The higher order modes have a larger attenuation.

For waveguides with a dielectric material such as fused silica in the cladding, the refractive index ν is real. By comparing the attenuation constant for different modes, we find that if $\nu > 2.02$ the mode with the lowest loss is TE_{01} and if $\nu < 2.02$ the HE_{11} mode has the lowest attenuation. Since the refractive index of most glasses is close to 1.5, for hollow glass fibers the HE_{11} mode has the lowest attenuation.

In Fig. 2.2, the attenuation constants of several hybrid modes in a fused silica hollow fiber are compared as a function of the core diameter for a wavelength of λ=800 nm. The attenuation constants decrease with increasing the diameter of the hollow core and the HE_{11} mode has the lowest attenuation. For a wavelength of λ=800 nm and a core radius of a=125 μm, the intensity attenuation constant for the HE_{11} mode is 0.142 m^{-1} or 0.62 dB/m. Therefore, the theoretical transmission of the HE_{11} mode for a 1 m long hollow glass waveguide is 86.8%. The transmission of a 50 cm long hollow glass waveguide will be 93.15%.

For the same wavelength and core radius, the intensity attenuation constant for the TE_{01} mode in a fused silica hollow fiber is 0.218 m^{-1} or 0.947 dB/m. The intensity attenuation constant for the TM_{01} mode is 0.49 m^{-1} or 2.13 dB/m which is larger than the attenuation constants of the HE_{11} and TE_{01} modes. The attenuation constants of the TE_{01} and TM_{01} modes are also shown in Fig. 2.2.

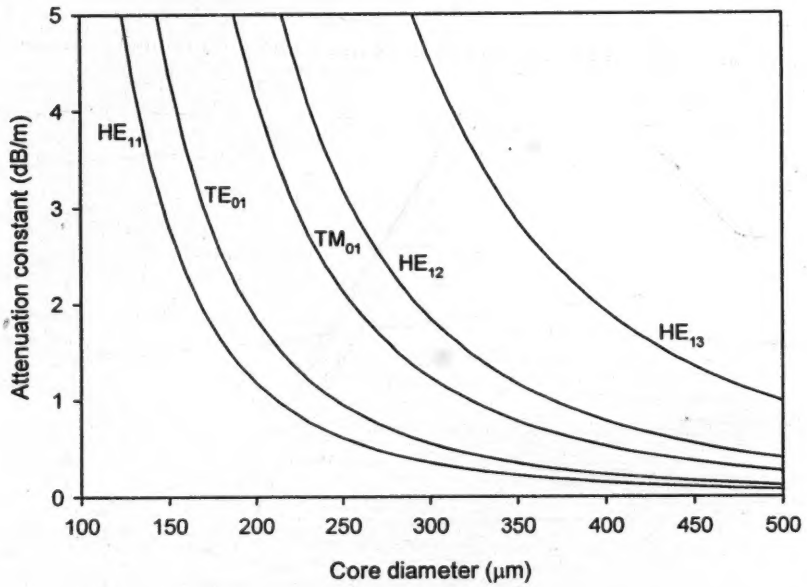

Fig. 2.2 Comparison of the attenuation constants for three hybrid modes of a fused silica hollow cylindrical waveguide as a function of the core diameter. The wavelength is 800 nm. The HE_{11} mode has the lowest loss. For a core radius of 125 μm the intensity attenuation constant of the HE_{11} mode is 0.62 dB/m.

The attenuation constants of the same three hybrid modes in a silver coated hollow fiber are compared as a function of core diameter in Fig. 2.3. The refractive index of silver at a wavelength of 800 nm is $0.15 - i5.3$ [19]. The attenuation constants are considerably smaller than the attenuation constants for a fused silica hollow waveguide. The HE_{11} mode has the lowest attenuation for the hybrid modes.

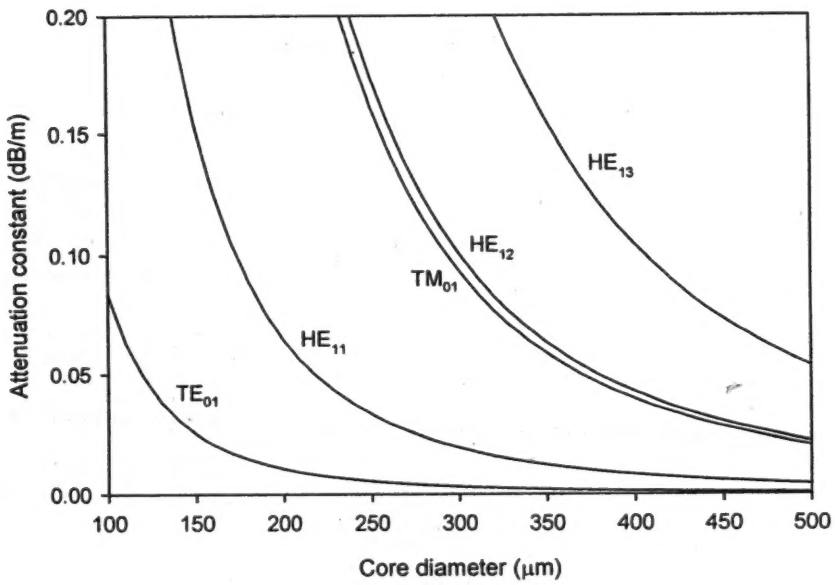

Fig. 2.3 Comparison of the attenuation constants for three hybrid modes of a silver coated hollow cylindrical waveguide as a function of the core diameter. The wavelength is 800 nm. The HE_{11} mode has the lowest loss among the hybrid modes. For a core radius of 125 μm the intensity attenuation constant of the HE_{11} mode is 0.033 dB/m.

For a wavelength of λ=800 nm and a core radius of a=125 μm, the intensity attenuation constant for the HE_{11} mode in a silver coated hollow fiber is 0.0076 m^{-1} or 0.033 dB/m. Therefore, the theoretical transmission of the HE_{11} mode for a 1 m silver coated hollow glass waveguide is 99.2%. The transmission of a 50 cm silver coated hollow glass waveguide will be 99.6%.

For the same wavelength and core radius, the intensity attenuation constant for the TE_{01} mode in a silver coated hollow fiber is 0.0012 m^{-1} or 0.0054 dB/m. The intensity attenuation constant for the TM_{01} mode is 0.037 m^{-1} or 0.16 dB/m which is larger than the attenuation constants of the HE_{11} and TE_{01} modes. The attenuation constants of the TE_{01} and TM_{01} modes are also shown in Fig. 2.3.

For the HE_{11} mode all the field components are present. Since the axial field component (z component) is proportional to λ/a and is very small, this mode can be considered to be almost transverse. Using the approximation $\lambda/a<<1$ and the field components of the HE_{11} mode, the equation for the field lines in the transverse plane, perpendicular to the z axis of the waveguide, is given by

$$r\cos\phi = r_0 \tag{2.11}$$

where r_0 is an integration constant, generating a family of field lines. The electric field lines of the HE_{11} mode are shown in Fig. 2.4. As can be seen, the HE_{11} mode can be considered a linearly polarized mode. The normal component of electric field for the HE_{11} mode is not continuous at the interface between the core and the cladding. The tangential component is continuous at the boundary. Therefore, the electric field lines of the HE_{11} mode are discontinuous at the boundary between the core and the cladding. The magnetic field lines of the HE_{11} mode are similar to its electric field lines only rotated by $\pi/2$ radians around the z axis.

The maximum value of the electric field in the cladding occurs at the boundary $r=a$ and is proportional to λ/a. Therefore, the field intensity in the cladding is very small. If we neglect terms of the order λ/a, the field amplitude in the core for the HE_{11} mode is given by

$$E = E_0 J_0(2.405\frac{r}{a}) \tag{2.12}$$

where E_0 is the amplitude at the center of the waveguide and u_{11}=2.405 is the first root of the Bessel equation $J_0(x)$. The field distribution of the HE_{11} mode is shown in Fig. 2.5.

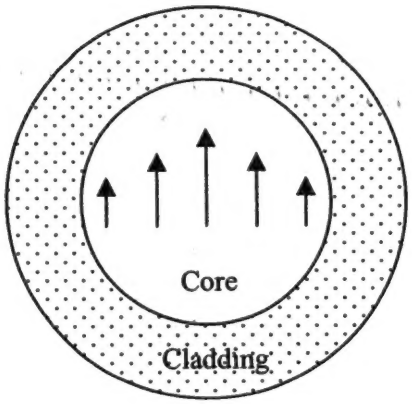

Fig. 2.4 Electric field lines of the HE_{11} mode inside the core of a hollow cylindrical waveguide. Electric field is not continuous at the boundary between the core and the cladding. Therefore, electric field lines of the HE_{11} mode are discontinuous at the boundary.

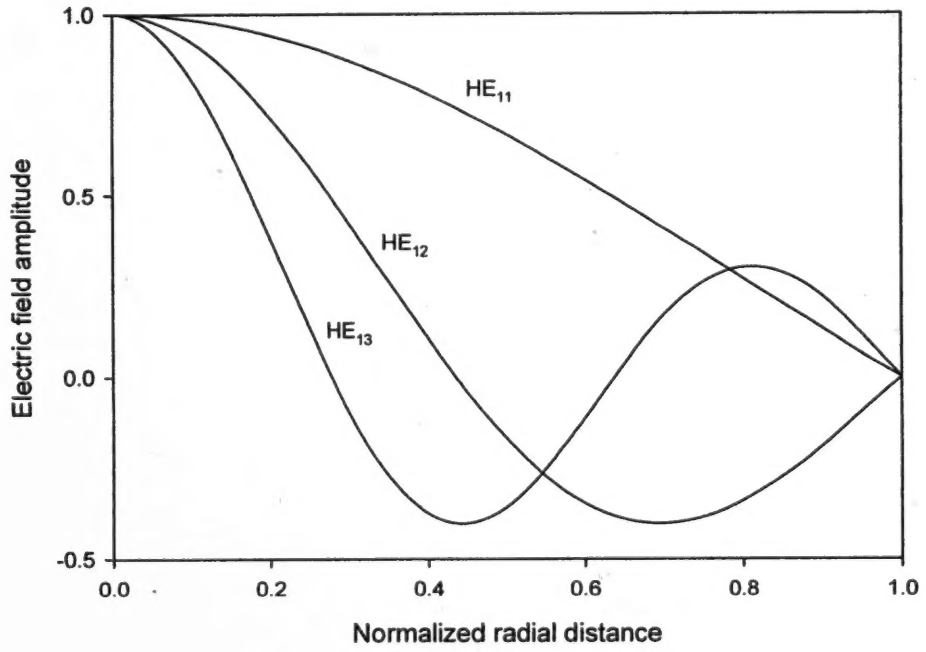

Fig. 2.5 Electric field amplitude of HE_{11} mode inside the core of a hollow cylindrical waveguide. The electric field is maximum in the center of the core and is zero at the boundary between the core and the cladding. Radial distance is normalized with respect to the core radius.

For the TE_{01} mode, only the transverse component of the electric field is present. The electric field lines of the TE_{01} mode are shown in Fig. 2.6. As can be seen, they form circles that are centered on the z axis. The field amplitude in the core for the TE_{01} mode is given by

$$E = E_0 J_1(3.832\frac{r}{a}) \tag{2.13}$$

where E_0 is an arbitrary amplitude and u_{21}=3.832 is the first root of the Bessel function $J_1(x)$. The electric field distribution of the TE_{01} mode is shown in Fig. 2.7. The field intensity in the center of the core and at the cladding surface is zero.

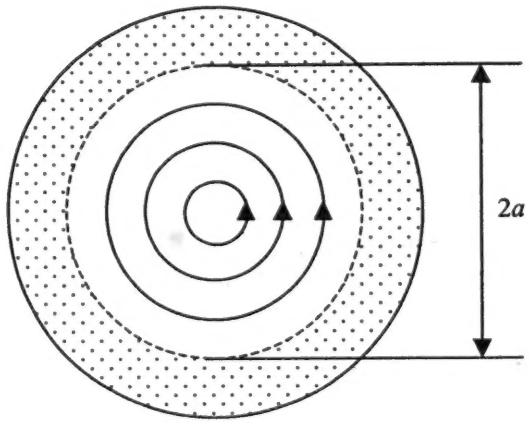

Fig. 2.6 Electric field lines of the TE_{01} mode inside the core of a hollow cylindrical waveguide. Electric field lines are circles in a plane perpendicular to the *z* axis. The electric field of the TE_{01} mode is continuous at the boundary between the core and the cladding.

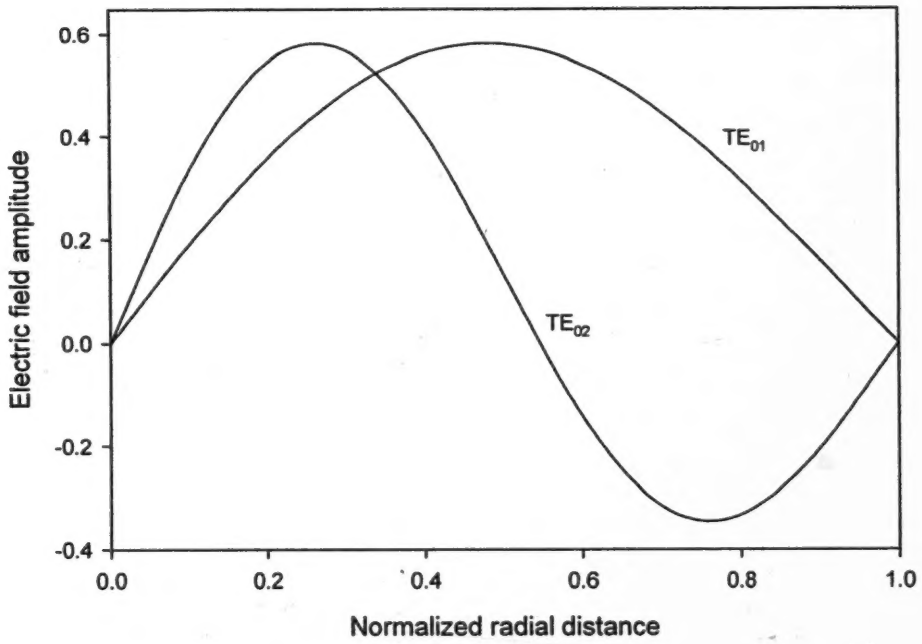

Fig. 2.7 Electric field amplitude of TE_{01} mode inside the core of a hollow cylindrical waveguide. The electric field is zero in the center of the core and at the boundary between the core and the cladding. Radial distance is normalized with respect to the core radius.

The TEM_{00} mode of lasers does not couple to the TE_{01} mode. Thus, the lowest order mode excited by an input TEM_{00} mode in a metallic hollow waveguide is the HE_{11} mode. Figure 2.8 shows the attenuation constant of the HE_{11} mode as a function of core diameter for a fused silica hollow waveguide and a silver coated hollow glass waveguide. The calculations are for a wavelength of 800 nm. The attenuation of the silver coated hollow waveguide is much lower for smaller values of core diameter. As the core diameter increases, the losses of both the fused silica hollow waveguide and the silver coated hollow waveguide become small. Therefore, the use of a silver coated hollow fiber will be advantageous for core diameters less than approximately 500 μm.

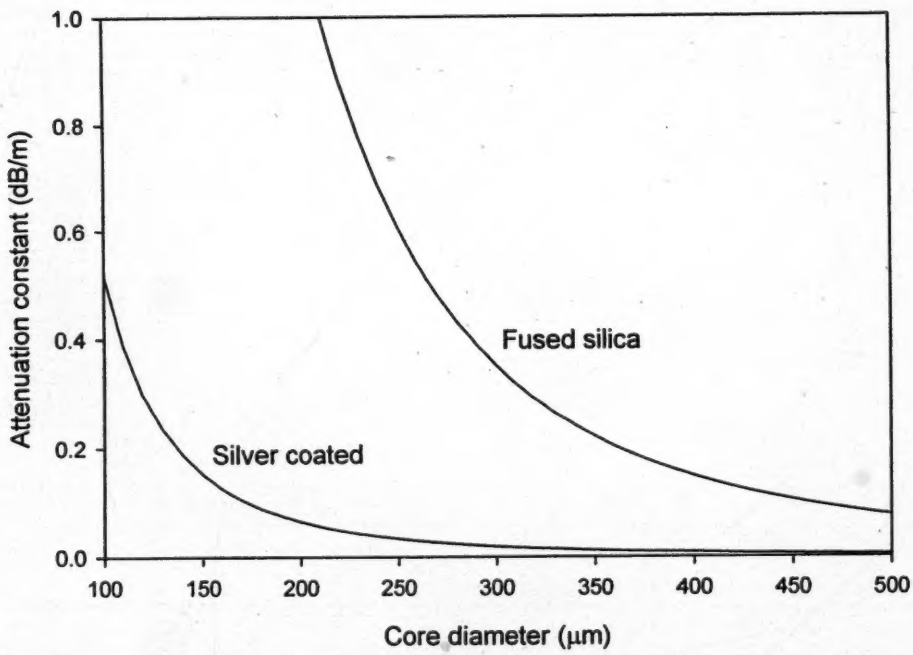

Fig. 2.8 Attenuation constant of the HE_{11} mode as a function of core diameter for a fused silica hollow waveguide and a silver coated hollow glass waveguide at 800 nm. The attenuation constant is inversely proportional to the cube of the core radius. Losses of the silver coated hollow fiber are much less for smaller values of core diameter.

2.3 Attenuation of bent hollow waveguide

The effect of mild bending on the attenuation constants of the modes in a hollow cylindrical waveguide has been evaluated in Ref. 5. This is accomplished by adding a perturbation correction term to the attenuation constant of a straight hollow waveguide. The field components are obtained by solving the Maxwell's equations in the toroidal coordinate system with origin at the center of the waveguide and a distance R from the center of curvature, where R is the radius of bending. The field components and the propagation constant of the curved waveguide are determined as functions of the field components and the propagation constant of the straight waveguide using a first order

perturbation technique. As the radius of bending approaches infinity, the bent waveguide degenerates into a straight waveguide with a cylindrical coordinate system.

The attenuation constants for a bent hollow cylindrical waveguide are obtained by using the approximation that the wavelength is much smaller than the core radius and also assuming that the radius of curvature is large compared to the core radius. A parameter $\sigma = 2(2\pi a/u_{nm}\lambda)^2 a/R$ is introduced and the field vectors and the attenuation constants are found by assuming that $\sigma << 1$. The attenuation constant $\alpha_{11}(R)$ of the HE_{11} mode for a bent hollow waveguide with radius of curvature R is given by [5]

$$\alpha_{11}(R) = \alpha_{11}(\infty)\left[1+\frac{4}{3}\left(\frac{2\pi a}{u_{11}\lambda}\right)^4\left(\frac{a}{R}\right)^2\left(1+\frac{1}{u_{11}^{\ 2}}+\frac{3}{4}\frac{\mathrm{Re}\sqrt{\nu^2-1}}{\mathrm{Re}\dfrac{\nu^2+1}{\sqrt{\nu^2-1}}}\cos 2\theta\right)\right] \qquad (2.14)$$

where $\alpha_{11}(\infty)$ is the attenuation constant of the HE_{11} mode for a straight hollow waveguide with $R = \infty$, $u_{11} = 2.405$ is the first zero of the Bessel function $J_0(x)$, and θ is an angle specifying the direction of the electric field relative to the plane of bending. The attenuation constant is minimum for an electric field perpendicular to the plane of bending ($\theta = \pm 90^\circ$) and maximum for an electric field with parallel polarization ($\theta = 0^\circ$). Therefore, the attenuation constant for the bent waveguide consists of two parts, the attenuation constant of the straight waveguide which is independent of polarization plus an additional term due to curvature of the waveguide which depends on polarization. In finding the attenuation constants of the modes for the bent waveguide mode conversion to higher order modes is not taken into account. Such an assumption is only valid in the limit of very large radii of curvature.

The attenuation of a bent hollow waveguide has also been studied in Ref. 20. Again, it is assumed that the core radius a is much larger than the free space wavelength λ and the radius of bending R is large compared to the core radius a. A scalar wave equation is used to determine the transverse electric field of the linearly polarized dominant mode of a bent cylindrical hollow waveguide. Maxwell's equations are used in the toroidal coordinate system and an equation is obtained for the transverse field component by using the assumption that the bending radius is large and neglecting terms of R^{-2} and also terms of R^{-1} which are not multiplied by the propagation constant. The attenuation constant of the HE_{11} mode is obtained as the ratio of the power radiated from the core region to the cladding to the power transmitted in the core region. The attenuation constants, with the direction of the field perpendicular or parallel to the plane of curvature, are given by [20]

$$\alpha_{per} = \frac{1}{R}\left[c_1 \operatorname{Re}(z_{TE}) + c_2 \operatorname{Re}(y_{TM})\right] \tag{2.15}$$

$$\alpha_{par} = \frac{1}{R}\left[c_2 \operatorname{Re}(z_{TE}) + c_1 \operatorname{Re}(y_{TM})\right] \tag{2.16}$$

where c_1 and c_2 are integral functions of the transverse electric field which are evaluated numerically at the boundary between the core and the cladding. The quantities z_{TE} and y_{TM} are surface impedance and admittance defined at the interface between the core and the cladding. For a hollow waveguide with complex refractive index of the cladding ν, z_{TE} and y_{TM} are defined by

$$z_{TE} = \frac{1}{\sqrt{\nu^2 - 1}} \tag{2.17}$$

$$y_{TM} = \frac{v^2}{\sqrt{v^2 - 1}} \tag{2.18}$$

Explicit expression for the parameters c_1 and c_2 can be obtained by approximating the numerical curves using a method of least squares. The results can be written in terms of a parameter defined by $b = (2\pi a)^2 a/\lambda^2 R$, yielding

$$c_1 = 1 - 0.23b^{-0.5} - 1.98b^{-1} + 5.2b^{-1.5} \tag{2.19}$$

$$c_2 = 0.57b^{-0.5} + 1.12b^{-1} + 1.45b^{-1.5} \tag{2.20}$$

The values calculated for c_1 and c_2 from the above equations are very close to the numerical results.

2.4 Dispersion

When a pulse of light propagates through a dispersive medium it spreads out in time. A signal or a light pulse that is carried by a wave propagates at the group velocity v_g given by

$$v_g = \frac{d\omega}{d\beta} = \frac{1}{d\beta/d\omega} \tag{2.21}$$

where β is the propagation constant and ω is the frequency of the wave. Therefore, the time it takes for an optical signal to travel a distance L is

$$\tau = \frac{L}{v_g} = L\frac{d\beta}{d\omega} \tag{2.22}$$

If the optical signal contains a range of frequencies $\Delta\omega$, then the amount of spread is given by

$$\Delta\tau = \frac{d\tau}{d\omega}\Delta\omega = L\frac{d^2\beta}{d\omega^2}\Delta\omega = L\beta_2\Delta\omega \tag{2.23}$$

where β_2 is called the group velocity dispersion.

The dispersion of a mode is due to the fact that the group velocity is a function of the wavelength λ (or frequency ω). There are two causes for this dispersion: 1. material dispersion and 2. waveguide dispersion. Material dispersion occurs because the refractive index of the core material is a function of wavelength. Waveguide dispersion occurs because the propagation constant of any given mode varies with the wavelength. The propagation constant is also a function of the refractive index of the core material and the core radius a. Therefore, material and waveguide dispersions must be considered together in calculating the dispersion of the hollow waveguide.

Let's assume that the hollow fiber is filled with air. The refractive index of air as a function of the wavelength λ is given by [21]

$$n(\lambda) = 1 + 10^{-6}\left(64.328 + \frac{29498.1\lambda^2}{146\lambda^2 - 1} + \frac{255.4\lambda^2}{41\lambda^2 - 1}\right) \tag{2.24}$$

where λ is in μm. Using the refractive index of air and the equation for the propagation constant β, the group velocity dispersion parameter β_2 and the third order dispersion parameter β_3 can be calculated as

$$\beta_2 = \frac{d^2\beta}{d\omega^2} \tag{2.25}$$

$$\beta_3 = \frac{d^3\beta}{d\omega^3} \tag{2.26}$$

Figure 2.9 shows the GVD of a fused silica hollow fiber filled with air as a function of the core radius. The GVD is calculated for a wavelength of 800 nm. The material dispersion of air is also plotted for comparison. It is seen that as the core radius increases the GVD of the hollow fiber approaches the material dispersion of air. The TOD of a

fused silica hollow fiber filled with air as a function of the core radius is shown in Fig. 2.10, at a wavelength of 800 nm. The third order material dispersion of air has also been plotted. We can see that as the core radius increases, the TOD of the fused silica hollow fiber decreases and approaches the third order material dispersion of air. In chapter 5 the second and third order dispersions of silver coated and fused silica hollow fibers are calculated and compared which is important for nonlinear applications such as optical pulse compression.

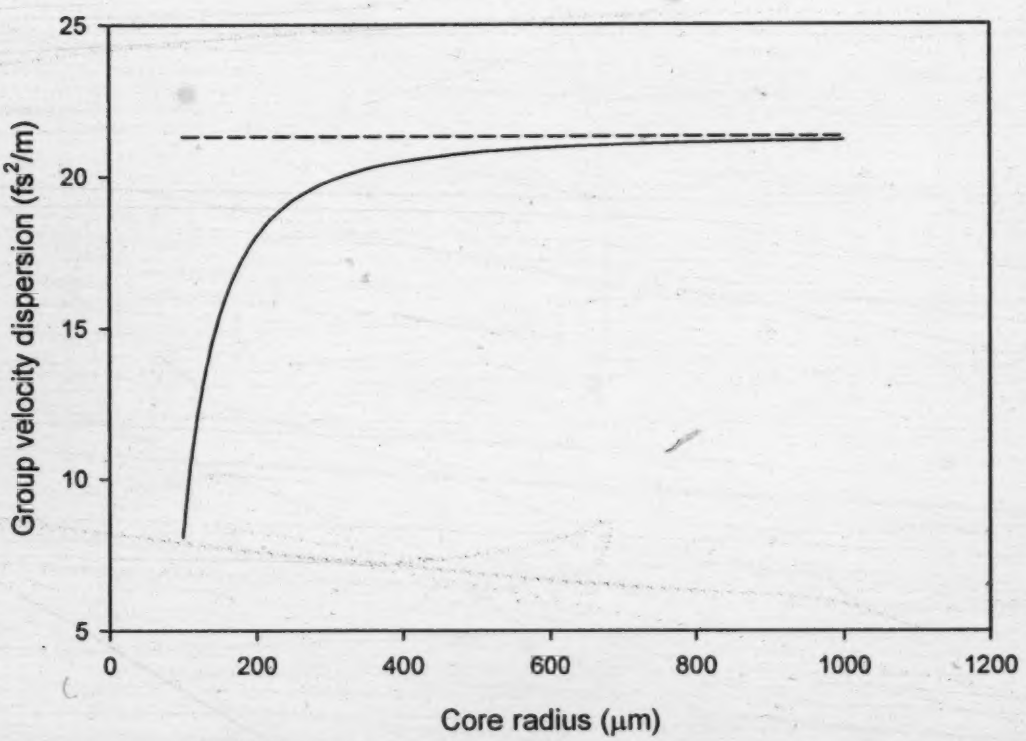

Fig. 2.9 Group velocity dispersion of a fused silica hollow fiber filled with air as a function of core radius at a wavelength of 800 nm (solid line). The GVD parameter for a core radius of 125 μm is β_2=12.8 fs^2/m. The material dispersion of air is also shown (dashed line).

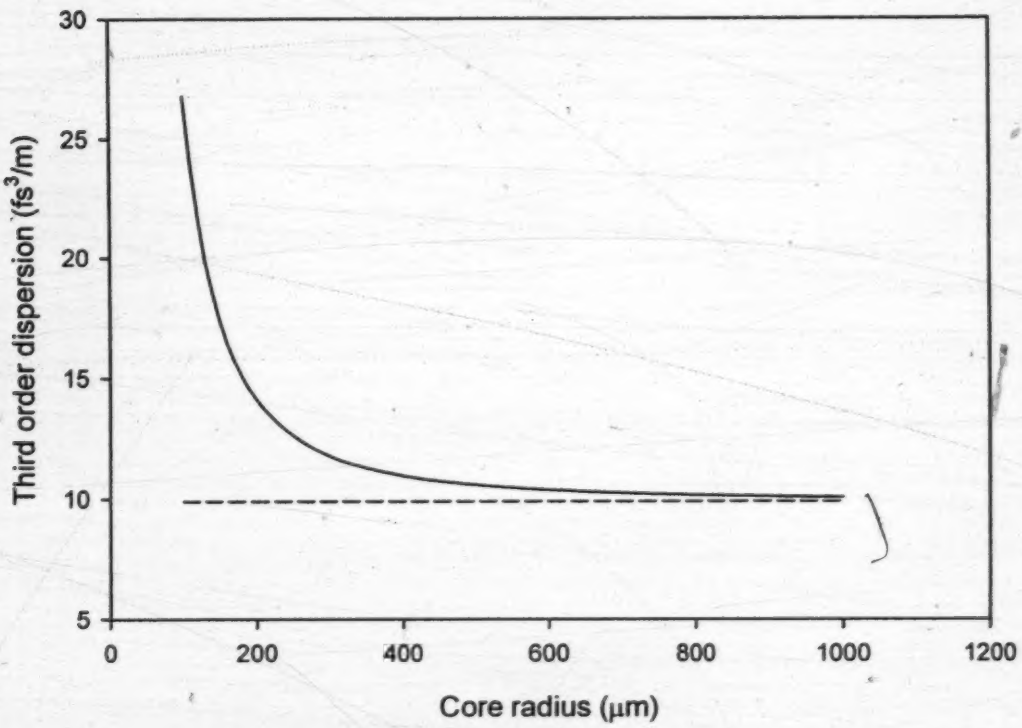

Fig. 2.10 Third order dispersion of a fused silica hollow fiber filled with air as a function of core radius at a wavelength of 800 nm (solid line). The TOD parameter for a core radius of 125 μm is β_3=20.7 fs^2/m. The third order material dispersion of air is also shown (dashed line).

Chapter 3

Beam transport experimental results

3.1 Introduction

In this chapter experimental results obtained using silver coated and uncoated hollow glass waveguides are presented. These experiments consist of transmission and beam profile measurements of straight hollow waveguides and transmission measurements for bent hollow waveguides. A 50 cm long uncoated fused silica hollow fiber and a 50 cm long silver coated hollow fiber with inner diameter of 250 μm were used for optical transmission measurements. The experimental setup for transmission measurements, shown in Fig. 3.1, consists of a Ti:sapphire laser, a half wave plate, a polarizer, a coupling lens, and a power meter. A CCD detector is used to take images of the output beam at various distances from the output end of the hollow fibers. These images are used to obtain the spatial output intensity profile of the beam and to measure the beam diameters. The Ti:sapphire laser (Spectra Physics MaiTai) produces optical pulses with a duration of 80 fs, a repetition rate of 80 MHz, and an average output power of 700 mW. This laser operates at a wavelength of 800 nm.

The half wave plate and polarizer combination is used to attenuate the laser output. A lens is used to couple the laser beam into the hollow fiber. First, the problem of coupling a free space TEM_{00} Gaussian mode to the fundamental HE_{11} mode of a hollow cylindrical waveguide is addressed. A condition is given for calculating the focal length of the coupling lens for maximum coupling of the free space TEM_{00} mode to the HE_{11} mode of a hollow fiber. Next, the experimental results obtained for a fused silica hollow

fiber are reported. For the silver coated hollow glass fiber, fabrication of the metallic coating is described and the experimental results are presented.

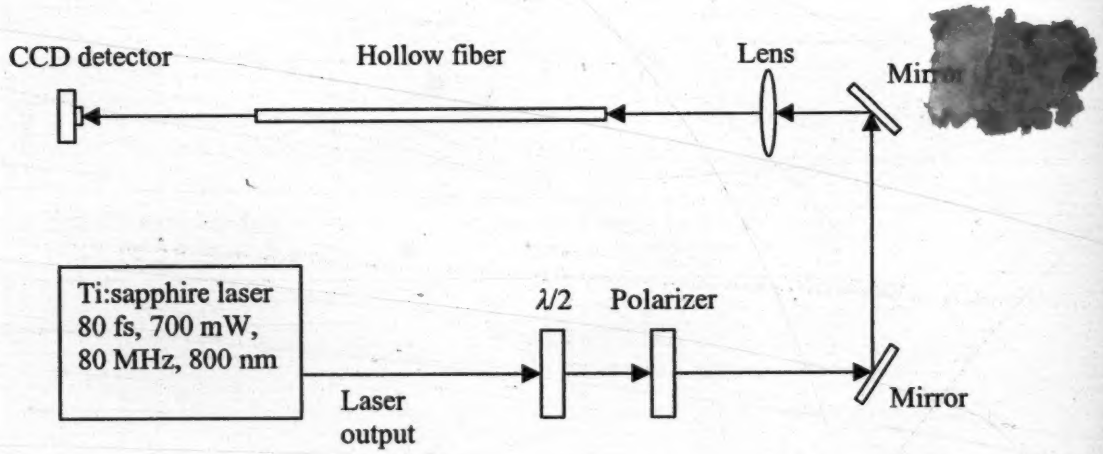

Fig. 3.1 The experimental setup for transmission and beam diameter measurements. The laser beam is attenuated by the half wave plate and polarizer combination. A lens is used to couple the laser beam into the hollow fiber. Images of the output beam are taken by a CCD detector, which are then used to measure the beam diameters at different distances from the exit of the hollow fiber.

3.2 Mode coupling

It has been found that by choosing the beam waist of the laser pulses at the entrance of the hollow fiber equal to $0.64a$ the coupling is maximized, where a is the inner radius of the waveguide. The condition for optimum coupling into the waveguide can be found by calculating the power coupling efficiency of the free space TEM_{00} Gaussian mode to the HE_{11} mode of the hollow fiber. The spatial profile of the HE_{11}

mode in a hollow waveguide with large inner core diameter is given by the Bessel function of the first kind and zero order

$$E(r) = E_0 J_0\left(2.405\frac{r}{a}\right) \tag{3.1}$$

where a is the core radius and E_0 is an arbitrary amplitude. The fundamental Gaussian mode, TEM_{00}, with beam radius of w is given by

$$E(r) = E_0 \exp\left(-\frac{r^2}{w^2}\right) \tag{3.2}$$

The power coupling efficiency of the free space TEM_{00} Gaussian mode to the HE_{11} mode of the hollow fiber is given by the following integral equation

$$\eta(w) = \frac{\left[\int_0^a \exp\left(-\frac{r^2}{w^2}\right) J_0\left(2.405\frac{r}{a}\right) r dr\right]^2}{\left[\int_0^\infty \exp\left(-\frac{2r^2}{w^2}\right) r dr\right]\left[\int_0^a J_0{}^2\left(2.405\frac{r}{a}\right) r dr\right]} \tag{3.3}$$

We can plot this equation as a function of normalized beam waist w/a. Fig. 3.2 shows the coupling efficiency as a function of normalized beam waist. The maximum coupling efficiency is 98% and it happens for w/a=0.64. By using this beam waist the coupling efficiency for HE_{12}, HE_{13}, and HE_{14} modes are 0.55%, 0.15%, and 0.5% respectively.

The required focal length of the coupling lens is found using the relation between the beam waist at a lens and the beam waist at the focal point of the lens given by

$$w_2 = \frac{f\lambda}{\pi w_1} \tag{3.4}$$

where w_1 is the beam radius at the lens, w_2 is the beam waist at the focal point of the lens, f is the focal length of the lens, and λ is the wavelength. By using w_2=0.64a in equation

(3.4), we can find the focal length of the lens for maximum coupling of the fundamental Gaussian mode to the HE_{11} mode of a hollow waveguide given by

$$f = 0.64\frac{\pi aD}{2\lambda} \tag{3.5}$$

where $D=2w_1$ is the $1/e^2$ intensity diameter of the Gaussian beam at the lens.

The problem of coupling the free space TEM_{00} mode to the HE_{11} mode of a hollow cylindrical waveguide has also been studied by Abrams [22]. In that work the HE_{11} mode of a hollow fiber is expanded into the free space Laguerre-Gaussian modes and the same condition is obtained by maximizing the fraction of power contained in the fundamental free space mode. For the optimum beam waist parameter $w_0 = 0.64a$ at the input of a hollow fiber, the coupling of the HE_{11} mode to the fundamental free space Gaussian mode at the output of the hollow fiber is also maximized. The fraction of power coupled from the HE_{11} mode at the output of a hollow fiber to the six lowest order Laguerre-Gaussian free space modes is given in Table 3.1.

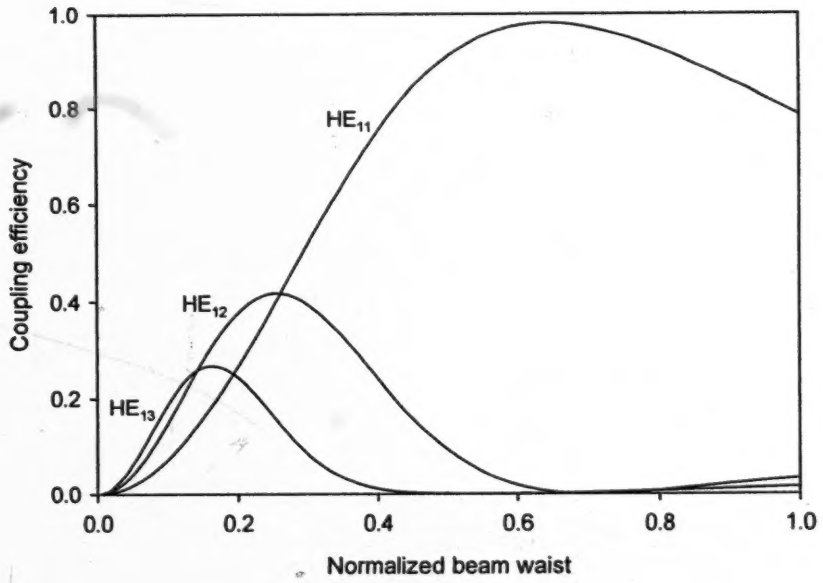

Fig. 3.2 Coupling efficiency of the fundamental free space mode to the HE_{11} mode of a hollow cylindrical waveguide as a function of normalized beam waist. Maximum coupling efficiency of 98% occurs for a normalized beam waist of 0.64.

Table 3.1 Fraction of power contained in the first six free space Laguerre-Gaussian modes in the expansion of the HE_{11} mode.

Mode number	Fraction of power
0	0.980673
1	0
2	0.014518
3	0.001852
4	0.000384
5	0.001165

3.3 Fused silica hollow fiber

A 50 cm fused silica hollow fiber was used for the transmission measurement. The inner diameter of the waveguide is 250 μm. The horizontal spatial intensity profile of the input beam at the coupling lens, located 82 cm from the exit of the laser, is shown in Fig. 3.3. The measured $1/e^2$ input beam diameter was 1.7 mm. A 25 cm focal length lens was used to couple the beam into the hollow fiber. This is close to the optimum focal length of 27 cm calculated by using equation (3.5). The transmission, output energy over input energy, was measured to be 80%, which is equivalent to an attenuation of 1.94 dB/m. The measured transmission includes the input coupling losses which may account for part of the losses observed.

Measurements of transmission were made using a Spectra Physics power meter (Model 407A) placed before and after the waveguide. This power meter is a thermal detector that converts light into heat and then converts heat into an electric signal. Light is converted to heat through absorption of the incident radiation by the front surface of a thermopile, which is an organized collection of thermocouple junctions connected electrically in series. A thermocouple consists of a junction of two dissimilar metals, with the property that the electric potential difference across the junction is temperature dependent. By measuring the voltage difference between the signal junction and a reference junction, the power of the incident radiation is measured. The power meter can be used over a wavelength range of 250 nm to 11 μm and can measure powers from 5 mW to 20 W.

For comparison, in Ref. 23 a typical transmission of 60% is reported for an 85 cm hollow glass fiber with inner diameter of 260 μm (2.61 dB/m), and in Ref. 24 the

transmission is 70% for a 50 cm hollow glass fiber with inner diameter of 250 μm (3.1 dB/m). Thus, the present measured transmission exceeds those reported in the literature for fused silica hollow fibers. This may be due to the extra care taken here to achieve optimum coupling from the free space mode to the hollow fiber mode. It may also be related to the straightness and inner wall quality of the hollow fibers.

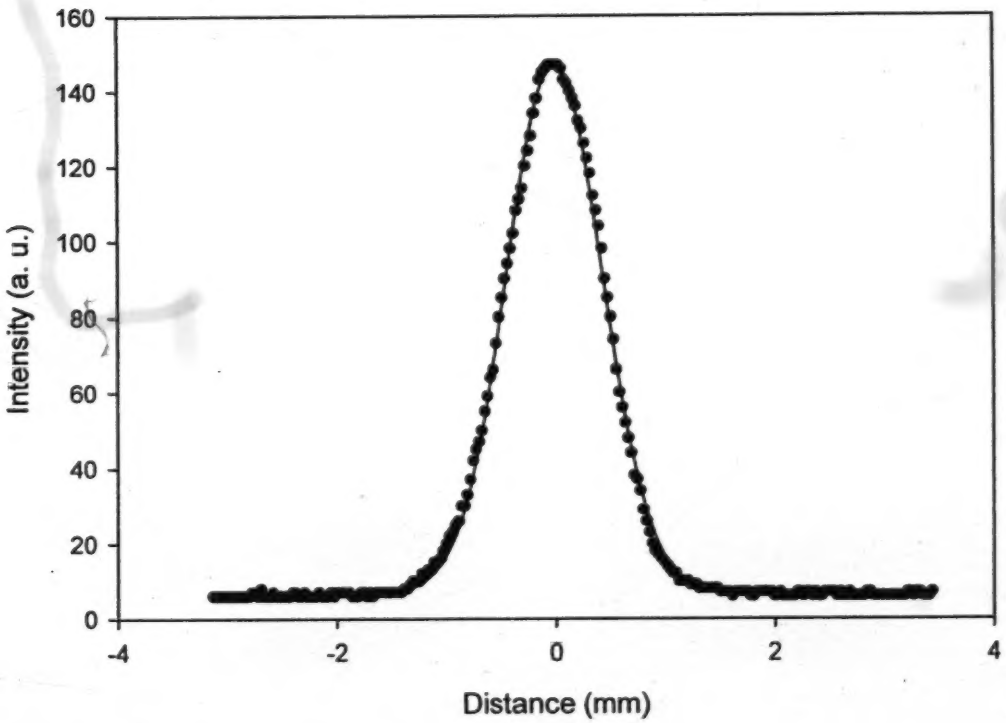

Fig. 3.3 The horizontal spatial intensity of the input beam. There is a small intensity offset due to dark current in the CCD detector.

Figure 3.4 shows the output of the fused silica hollow fiber at a distance of 20 cm from the output end of the fiber. An Electrim CCD detector (Model EDC-1000HR) was used for this measurement. The CCD detector consists of an array of semiconductor detectors cells, with each cell having a size of 27 by 11.5 μm. Each detector is connected

to a voltage source that produces a potential well inside the semiconductor material. Absorption of light generates electron hole pairs and the electrons are attracted into the potential well. When the desired signal has been accumulated in each pixel, each column of cells is transferred into a shift register. The data is read out sequentially and digitized using an 8 bit A/D converter, which is then sent to a computer.

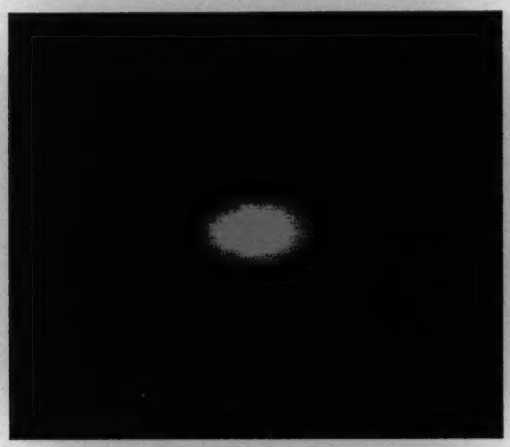

Fig. 3.4 Output image of the beam from the fused silica hollow fiber at 20 cm from output end of the fiber. The actual beam is circular. The image was taken using a CCD detector with pixel size of 27 μm by 11.5 μm, which results in an elliptically appearing image. The image is 5.5 mm by 3.7 mm in the vertical and horizontal directions respectively.

The spatial output intensity profile in the horizontal direction is shown in Fig. 3.5. The beam diameter of the output optical pulse can be calculated theoretically by expanding the electric field amplitude of the HE_{11} mode into free space Gaussian modes. By choosing the 1/e radius of the mode amplitude $w_0=0.64a$, the coefficient of the lowest Gaussian mode is maximized and 98% of the energy will be contained in this mode [22].

By using the first six expansion terms, almost all the energy (over 99%) contained in the HE_{11} mode is accounted for. The calculated beam diameters, using the first six Gaussian modes, are compared with the experimental values in Fig. 3.6. As can be seen there is good agreement between the theoretical and experimental results.

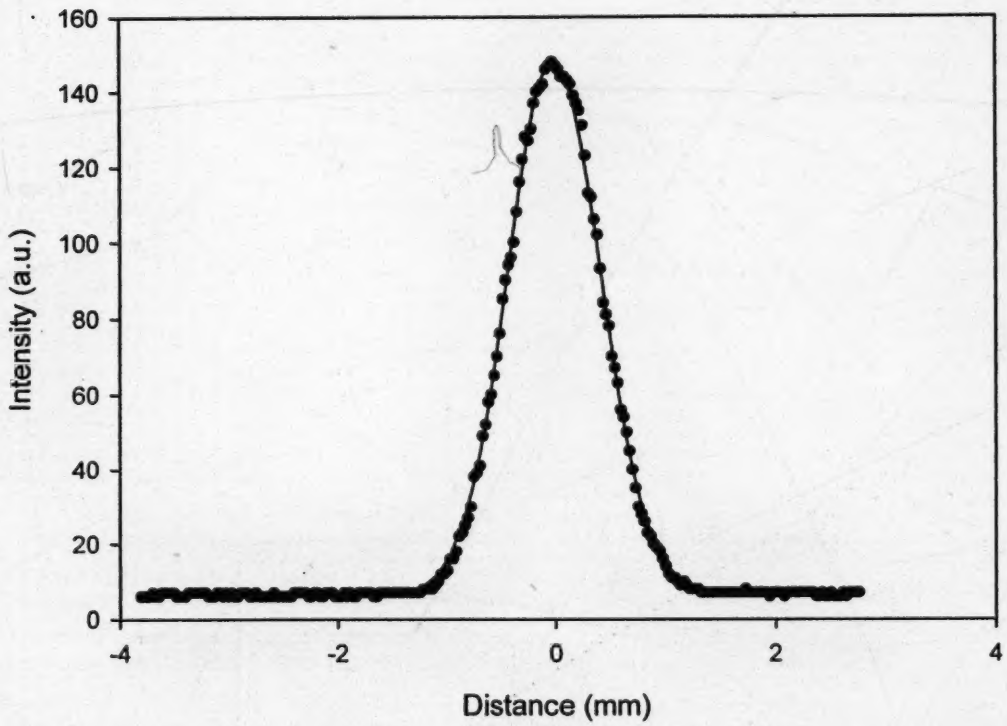

Fig. 3.5 Spatial output intensity of the fused silica hollow fiber at 20 cm from output end of the fiber and a Gaussian fit to the data (line). The data is taken from a horizontal line through the center of the image shown in Fig. 3.4. There is a small intensity offset due to the dark current in the CCD detector.

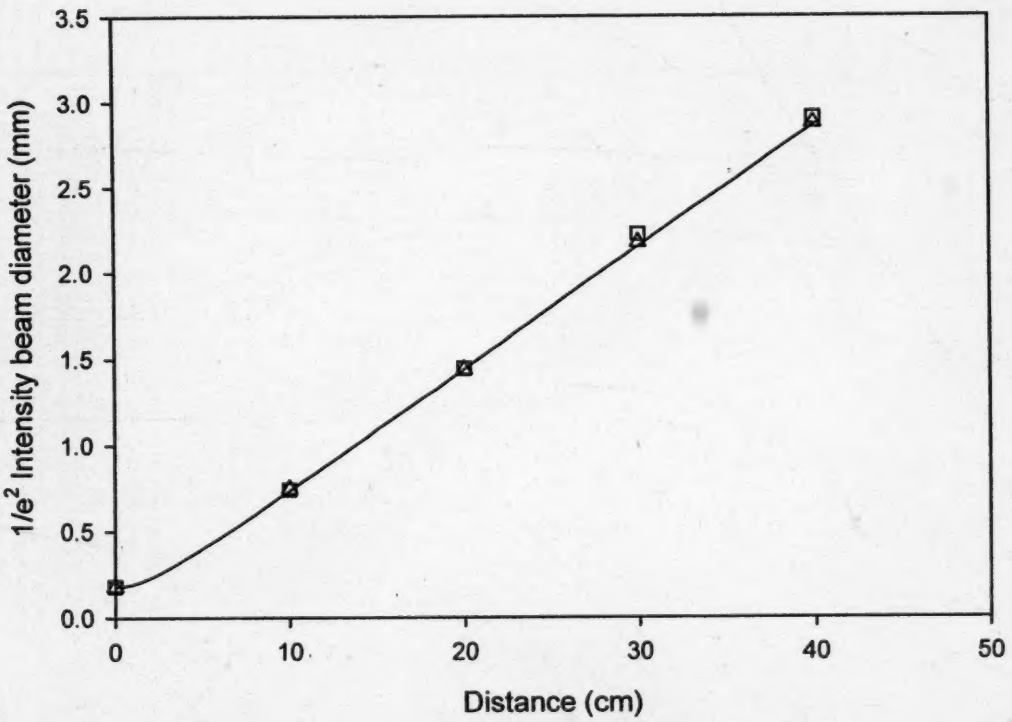

Fig. 3.6 Comparison of theoretical and experimental beam diameters for output beam of the fused silica hollow fiber as a function of distance from output end of the fiber. The line represents the calculated values. Squares are the horizontal beam diameters and triangles are the vertical beam diameters measured experimentally. The measurement error bars are smaller than the size of the symbols.

3.4 Silver coated hollow fiber

3.4.1 Fabrication

To reduce the loss of a hollow glass fiber, the inner surface of the glass tubing can be coated with a thin film of metal such as silver [25]. The metal thin film must have high reflectivity and a smooth surface. The silver film is deposited inside the hollow silica waveguide by a liquid phase deposition process. The silver thin film deposition is an autocatalytic process.

The basis for this chemical reaction is the reduction of the silver ions in solution. The deposition solutions are all prepared in distilled and deionized water: Solution A contains 3 g/l of silver nitrate, Solution B contains 2.2 g/l of sodium hydroxide, and Solution C contains 0.55 g/l of dextrose and 0.08 g/l of sodium salt of ethylenediaminetetraceticacid (EDTA). Solution A is titrated with 10% ammonia solution. The solution first turns brown owing to the formation of insoluble silver oxide precipitate and then clears up on further titration owing to the formation of soluble silver nitrate ammonia complex. Then one part by volume of solution B is added to four parts of the titrated solution A. The resultant solution turns cloudy again and will become clear by titrating it with ammonia solution. This is the final silver solution and it is photosensitive. The addition of sodium hydroxide facilitates the adhesion of the silver film to the silica substrate. The reducer solution is solution C.

Equal volumes of the silver solution and the reducer solution are pumped through Tygon tubing and the hollow glass waveguide with a peristaltic pump. The solutions are mixed in a Y connector in the Tygon tubing and the resultant solution is pumped into the hollow glass waveguide. The two solutions react to yield metallic silver on the inner surface of the hollow glass waveguide. The thickness of the silver film is controlled by varying the reaction time, the flow rate, the temperature, and the concentration of the reacting solutions. The thickness of the silver film must be sufficient to prevent the interaction of light with the glass tubing.

There is an additional scattering loss due to surface roughness of the silver film that is deposited on the inner glass surface. The interaction of light with this rough inner surface results in scattering of light into higher order modes in hollow waveguides. The

scattering loss depends on the dimension of the scattering features relative to the wavelength and the index difference between the scattering feature and the surrounding medium. At short wavelengths, scattering losses become more important. Therefore, it is desirable to use the smoothest bore possible. Fused silica is used as the substrate material. The losses that result from inner surface roughness are due to the silver films. The film thickness and roughness increase with the silvering time.

In Ref. 10 the effect of silvering time on the film thickness and roughness has been studied. It was found that short silvering times produce the lowest loss at short wavelengths. This has been verified through spectral loss measurements as well as an attenuation measurement of the waveguides measured at 0.63, 1.06, 3, and 10 μm. The dependence of attenuation on the silvering time (the thickness and roughness of silver) holds true at shorter wavelengths. This effect is not observed at the CO_2 wavelength of 10 μm. Long silvering times produces a thicker silver film with greater surface roughness, resulting in higher losses. Recent roughness measurements for silver films deposited on a flat glass substrate for 20 minutes is approximately 25 nm. The thickness of the silver layer of the hollow waveguide fabricated for the 800 nm wavelength and used in the present experiments is 200 nm. The hollow waveguide was fabricated at room temperature with a flow rate of 100 ml/min for the combined solution. An AFM scan of the silver film is shown in Fig. 3.7. The roughness of these films can be reduced further by lowering the temperature of the reacting solutions or by reducing the temperature of the substrates [26]. A decrease in processing temperature increases the nucleation sites thereby leading to a finer grain size distribution and hence smoother films for the same

reaction time. The silver coated hollow waveguide used in the present experiments were prepared by the research group of Prof. Harrington at Rutgers University.

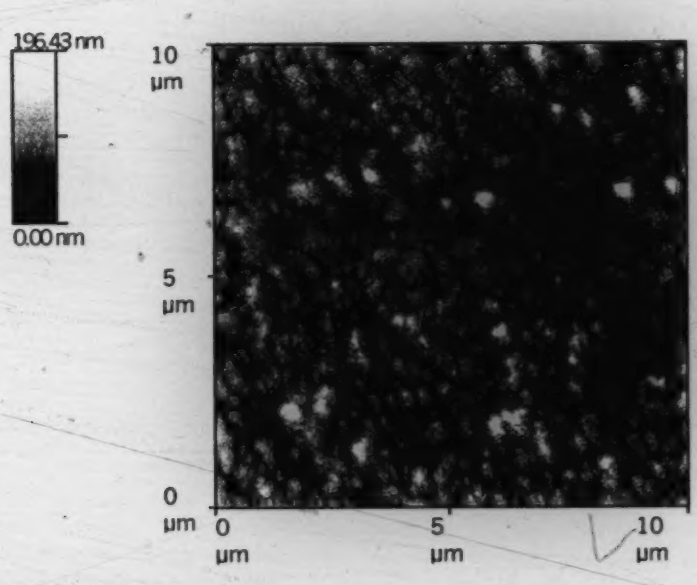

Fig. 3.7 AFM image of the silver thin film deposited on a glass slide for 20 minutes. Image was provided by Prof. Harrington's research group at Rutgers University.

3.4.2 Transmission measurements

A 50 cm silver coated hollow fiber with inner diameter 250 μm was used for transmission measurement. The inner diameter of the hollow waveguide was measured with an optical microscope giving a value of 250 μm (±5 μm). The waveguide was mounted in a precisely machined straight V groove in an aluminum bar. The same coupling lens with focal length of 25 cm was used in order to ensure that the 1/e radius of the mode amplitude is equal to $w_0=0.64a$ at the entrance of the hollow fiber. Thus, coupling 98% of the energy contained in the lowest Gaussian mode of the input beam,

TEM_{00}, to the HE_{11} mode of the hollow fiber. The total transmission (output energy over input energy) of the silver coated hollow fiber was measured to be 95% (equivalent to an attenuation of 0.44 dB/m).

Images were taken at different distances from the output of the hollow fiber, which indicated a single HE_{11} mode exiting from the output of the hollow fiber and coupling to the free space modes. Fig. 3.8 shows the output of the silver coated hollow fiber at a distance of 20 cm from the output end of the fiber. The spatial output intensity profile is shown in Fig. 3.9.

Fig. 3.8 Output image of the beam from the silver coated hollow fiber at 20 cm from output end of the fiber. The actual beam is circular. The image was taken using a CCD detector with pixel size of 27 μm by 11.5 μm, which results in an elliptically appearing image. The image is 5.5 mm by 3.7 mm in the vertical and horizontal directions respectively.

The beam diameter of the output optical pulse was calculated theoretically as before. The calculated beam diameters, using the first six Gaussian modes, are compared

with the experimental values in Fig. 3.10. As can be seen they agree very well indicating that the output of the hollow fiber is an HE_{11} mode. This single mode propagation of the silver coated hollow fiber is important for nonlinear applications in the 800 nm region, in addition to beam delivery of femtosecond optical pulses.

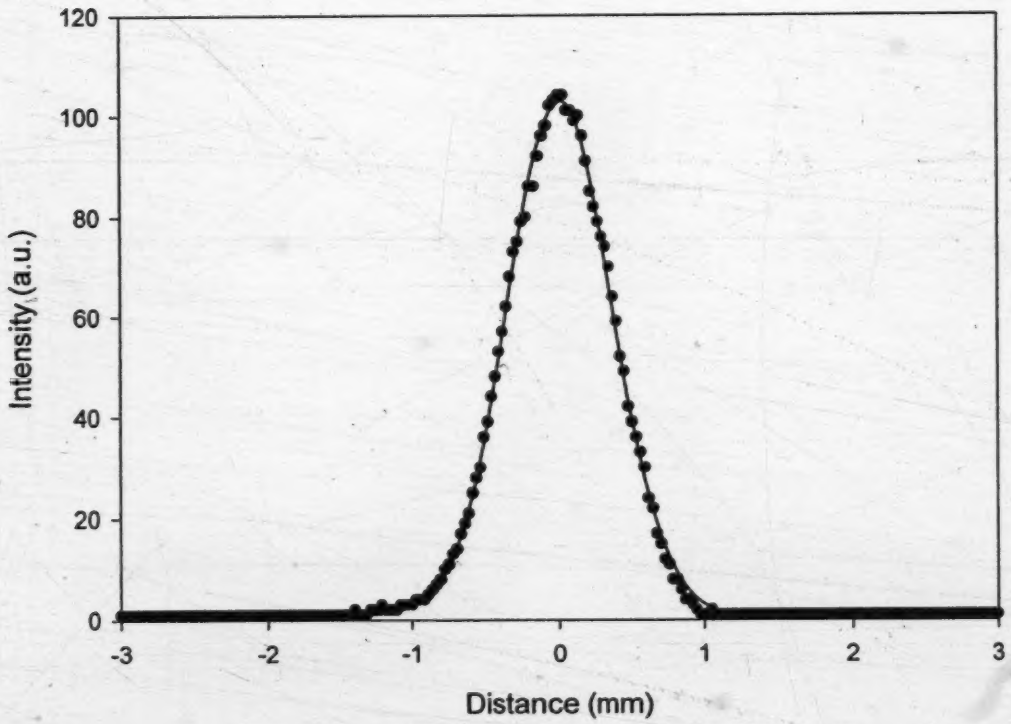

Fig. 3.9 Horizontal spatial output intensity (dots) at 20 cm from output end of the silver coated hollow fiber and a Gaussian fit to the data (line). The data is taken from a horizontal line through the center of the image shown in Fig. 3.8.

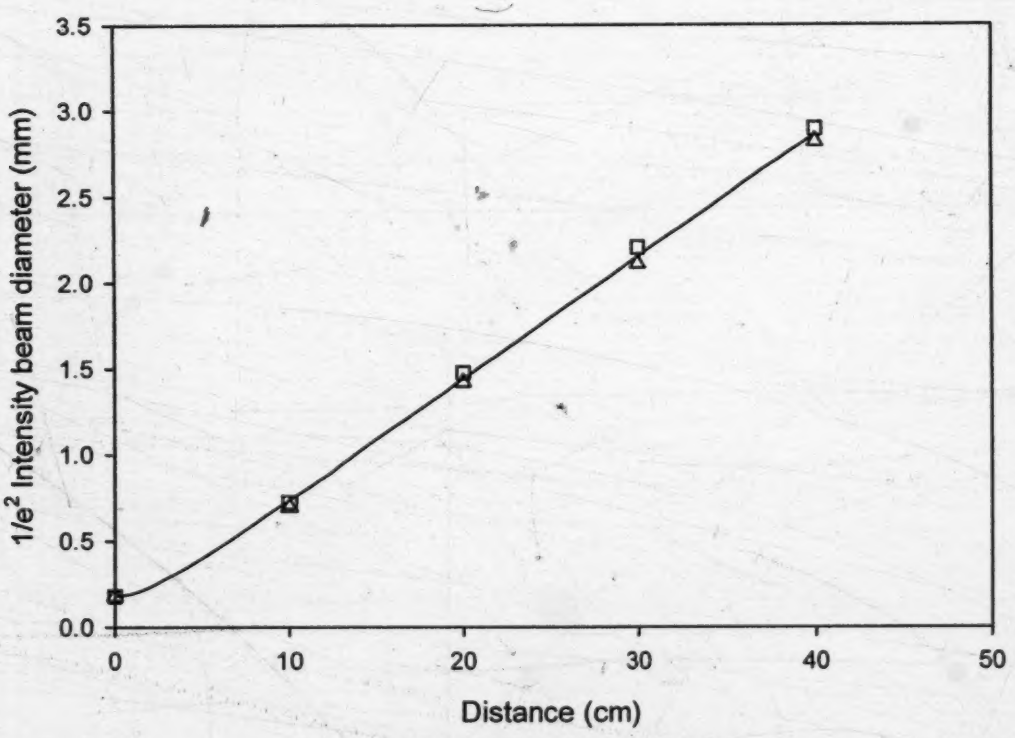

Fig. 3.10 Comparison of theoretical and experimental beam diameters for output beam of the silver coated hollow fiber as a function of distance from output end of the fiber. The line represents the calculated values. Triangles are the horizontal beam diameters and squares are the vertical beam diameters measured experimentally.

3.4.3 Bending loss

When a waveguide is bent the loss is increased. In order to find the bending loss, the silver coated hollow waveguide was bent by different radii of curvature. A V groove was made in curved aluminum bars with radii of 30, 50, and 100 cm. The waveguide had a straight section of 5 cm followed by a bent section of 10 cm. The attenuation constant for a straight silver coated hollow waveguide was used to subtract the loss of the straight section from the total measured loss. The experimental setup shown in Fig. 3.1 was used

for the measurements. A half wave plate was inserted before the lens in order to change the polarization of the input laser pulses. The transmission was measured for perpendicular and parallel polarizations relative to the bending plane. The bending loss measurements for the perpendicular polarization are shown in Table 3.2. The theoretical results calculated using the equations of Ref. 5 and Ref. 20 given in chapter 2 are shown for comparison. The theoretical and measured losses for the parallel polarization are shown in Table 3.3.

Table 3.2 Bending loss of the silver coated hollow fiber for perpendicular polarization.

Bending Radius (cm)	Measured Loss (dB/m)	Theoretical Loss (dB/m) (Ref. 5)	Theoretical Loss (dB/m) (Ref. 20)
30	4.6 ± 0.5	99.49	0.283
50	2.3 ± 0.4	35.84	0.197
100	1.1 ± 0.4	8.98	0.125

Table 3.3 Bending loss of the silver coated hollow fiber for parallel polarization.

Bending Radius (cm)	Measured Loss (dB/m)	Theoretical Loss (dB/m) (Ref. 5)	Theoretical Loss (dB/m) (Ref. 20)
30	13.9 ± 0.8	396	4.35
50	7.7 ± 0.6	143	2.60
100	4.6 ± 0.5	36	1.28

3.5 Discussion

In summary, the overall transmission loss of the straight silver coated hollow glass waveguide is 0.44 dB/m, which is significantly less than the overall transmission loss of 1.94 dB/m for the uncoated fused silica hollow waveguide. The measured transmission of the 50 cm silver coated hollow fiber was 95%, which is still less than the theoretical value of 99.6%. The difference is most likely due to an additional scattering loss caused by the surface roughness of the silver coating as discussed earlier. The scattering loss could be reduced by depositing a smoother silver coating. Another reason for this discrepancy is that about 2% of the input beam energy is coupled to the higher order modes, which have higher attenuations than the HE_{11} mode.

There was close agreement between the theoretical and experimental beam diameters of the output beam propagating into free space for both the silver coated and fused silica hollow fibers. This indicated that a single mode output can be obtained from the silver coated hollow fiber. This can be accomplished by choosing the correct focal length for the coupling lens, by keeping the hollow fiber straight, and by careful alignment of the input beam into the hollow fiber. Otherwise, higher order modes can propagate inside the hollow fiber which will result in a multimode output. In order to align the waveguide, the laser beam is first adjusted so that its height from the optical table remains approximately the same, as it propagates. Next, the input and output ends of the waveguide are moved in vertical direction and sideways until a good mode is seen at the output. Finally, a power meter is used to maximize the output power by adjusting the coupling lens.

The bending loss of the silver coated hollow fiber was measured for bending radii of 30, 50, and 100 cm. The measured values were compared with the theoretical results calculated for the HE_{11} mode using the attenuation constants given in Ref. 5 and Ref. 20. The expression for the bending attenuation constant from Ref. 5, equation (2.14) in Chapter 2, gives values that are much higher than the measured losses. They obtained the attenuation constants by introducing a perturbation parameter $\sigma = 2(2\pi a/u_{nm}\lambda)^2 a/R$ and using a perturbation technique with the assumption that $\sigma << 1$. However, for the wavelength and core radius considered in this thesis and a curvature radius of $R = 1\,\mathrm{m}$, we get $\sigma = 42$ which does not meet the above requirement. Therefore, the bending attenuation constant given in Ref. 5 may only be used for very large radii of curvature. This conclusion also agrees with previous results from bending loss measurements of hollow fibers at 10.6 μm [6, 27]. The measured bending losses of hollow silica waveguides with a core diameter of 1.04 mm and a bending radius of 1 m [27] were found to be much smaller (8 dB/m) than predicted by the theory of Ref. 5 (129 dB/m). A hollow nickel waveguide with a core radius of 1.5 mm and a bending radius of 1 m [6] had much lower bending losses (3 dB/m) than the calculated values (449 dB/m) using the bending attenuation constant of Ref. 5.

The theoretical losses calculated using the theory of Ref. 20, equations (2.15) and (2.16) in Chapter 2, are less than the measured bending losses. The difference between the theoretical and measured losses may be due to mode mixing in the bent section of the hollow fiber, which leads to propagation of higher order modes and extra losses. The theoretical results of Ref. 20 are for the linearly polarized HE_{11} mode and do not include higher order mode conversion. The roughness of the silver coating also adds to the total

bending loss of the hollow fiber. The measured bending losses of dielectric and silver coated hollow waveguides fabricated for 10.6 μm [28] with a core diameter of 250 μm and bending radius of 1 m were larger (3 dB/m) than the theoretically predicted losses of Ref. 20 (0.15 dB/m).

Recently a hollow glass waveguide coated with silver and a dielectric layer has been investigated for the delivery of femtosecond pulses in multiple spatial modes in the 800 nm region [29]. They report a straight loss as low as 0.13 dB/m for a hollow waveguide with bore diameter of 1000 μm. The loss of hollow fibers is inversely proportional to the cube of the core radius. Therefore, the loss of such a waveguide with an equivalent bore diameter of 250 μm would be 8.32 dB/m which is much higher than the transmission loss of the silver coated hollow fiber investigated in this thesis. They also report a bending loss of 0.86 dB/m for a 90° bend with a radius of curvature of 50 cm. Since the bending loss for hollow fibers scales as powers of the inverse of the core radius, one would expect higher losses for a smaller core radius.

Chapter 4

Theory of optical pulse compression

4.1 Nonlinear Wave propagation

The propagation of optical pulses in a single mode fiber or a hollow fiber can be described by using the electromagnetic wave equation. An optical pulse propagating inside a waveguide is affected by dispersive and nonlinear optical properties of the medium. Maxwell's equations are used to derive a wave equation that includes both dispersive and nonlinear optical effects. This is accomplished by considering a frequency dependent dielectric constant consisting of linear and nonlinear parts. In deriving the wave equation, the slowly varying envelope approximation is used. The nonlinear part of the refractive index is intensity dependent and leads to the phenomenon of self phase modulation. The effect of SPM on an optical pulse propagating in a waveguide is to broaden the spectrum.

4.1.1 Nonlinear refractive index

The response of materials to very intense electromagnetic fields becomes nonlinear and the induced polarization $\vec{P}$ is no longer linear in the electric field $\vec{E}$ and is given by the general relation [30]

$$\vec{P} = \varepsilon_0[\chi^{(1)} \cdot \vec{E} + \chi^{(2)} : \vec{E}\vec{E} + \chi^{(3)} \vdots \vec{E}\vec{E}\vec{E} + \cdots] \qquad (4.1)$$

where ε_0 is the permittivity of free space and $\chi^{(j)}$ (j=1,2,...) is a tensor of rank j+1 and represents the jth order susceptibility. $\chi^{(1)}$ is the linear susceptibility which is used to find the value of the linear refractive index. Effects such as second-harmonic generation and

sum-frequency generation are due to the second-order susceptibility $\chi^{(2)}$ which is zero for isotropic materials with inversion symmetry. The third-order susceptibility causes nonlinear refraction. This adds an intensity dependent nonlinear part to the refractive index of the material. The refractive index is then given by

$$n = n_0 + n_2 I \tag{4.2}$$

where n_0 is the linear index of refraction, n_2 is the nonlinear index of refraction, and I is the intensity. The nonlinear refractive index n_2 is related to $\chi^{(3)}$ by

$$n_2 = \frac{3}{8n_0}\mathrm{Re}[\chi^{(3)}_{xxxx}] \tag{4.3}$$

where it has been assumed that the electric field has linear polarization so that only one component of $\chi^{(3)}$ contributes to the refractive index. The electric field is defined by

$$\vec{E}(\vec{r},t) = \frac{1}{2}\hat{x}[E(\vec{r},t)\exp(-\omega_0 t) + c.c.] \tag{4.4}$$

where $\hat{x}$ is the unit vector in the direction of the electric field, ω_0 is the center frequency, $E(\vec{r},t)$ is the slowly varying envelope of the electric field, $\vec{r}$ is the position vector of a point in space, t is time, and c.c. is complex conjugate. One of the nonlinear effects that results from the intensity dependence of the refractive index is self phase modulation (SPM). In this phenomenon, the phase of the optical field changes as it propagates inside an optical fiber or a hollow fiber. This phase is a function of the nonlinear refractive index and the intensity of the optical field and results in spectral broadening.

4.1.2 Nonlinear wave equation

By using Maxwell's equations we can obtain a wave equation that describes the propagation of light inside a single mode optical fiber or a hollow fiber. The wave equation in its general form is given by

$$\nabla \times \nabla \times \vec{E} = -\frac{1}{c^2}\frac{\partial^2 \vec{E}}{\partial t^2} - \mu_0 \frac{\partial^2 \vec{P}}{\partial t^2} \tag{4.5}$$

where $c = 1/\sqrt{\mu_0 \varepsilon_0}$ is the speed of light in vacuum. The induced polarization $\vec{P}$ is given by

$$\vec{P} = \vec{P}_L + \vec{P}_{NL} \tag{4.6}$$

where $\vec{P}_L$ is the linear polarization and $\vec{P}_{NL}$ is the nonlinear polarization. In solving equation (4.5), the nonlinear polarization is considered as a small perturbation to the total induced polarization. By setting $\vec{P}_{NL} = 0$, the wave equation can be written in the frequency domain as

$$\nabla \times \nabla \times \vec{E}(\vec{r}, \omega) - \varepsilon(\omega)\frac{\omega^2}{c^2}\vec{E}(\vec{r}, \omega) = 0 \tag{4.7}$$

where the frequency dependent electric field $\vec{E}(\vec{r}, \omega)$ is the Fourier transform of $\vec{E}(\vec{r}, t)$ defined by

$$\vec{E}(\vec{r}, \omega) = \int_{-\infty}^{\infty} \vec{E}(\vec{r}, t) \exp(-i\omega t) dt \tag{4.8}$$

The frequency dependent dielectric constant $\varepsilon(\omega)$ is given by

$$\varepsilon(\omega) = 1 + \chi^{(1)}(\omega) \tag{4.9}$$

where $\chi^{(1)}(\omega)$ is the Fourier transform of the linear susceptibility $\chi^{(1)}(t)$ and is in general a matrix with complex numbers. For an isotropic medium, all three components

of $\chi^{(1)}(\omega)$ are equal. By assuming that $\varepsilon(\omega)$ is independent of the spatial coordinates and using the relation $\nabla \cdot \vec{D} = \varepsilon \nabla \cdot \vec{E} = 0$, the wave equation is written as

$$\nabla^2 \vec{E}(\vec{r},\omega) - \varepsilon(\omega)\frac{\omega^2}{c^2}\vec{E}(\vec{r},\omega) = 0 \tag{4.10}$$

The nonlinear effects are included in the wave equation by treating $\vec{P}_{NL}$ as a small perturbation to $\vec{P}_L$. Assuming that the nonlinear response is instantaneous, the nonlinear polarization $\vec{P}_{NL}$ is given by

$$P_{NL}(\vec{r},t) = \varepsilon_0 \chi^{(3)} \vdots \vec{E}(\vec{r},t)\vec{E}(\vec{r},t)\vec{E}(\vec{r},t) \tag{4.11}$$

We can also write the electric field in terms of a slowly varying envelope and a rapidly varying part. By using separation of variables, the Fourier transform of the electric field is then defined as

$$\vec{E}(\vec{r},\omega-\omega_0) = \frac{1}{2}\hat{x}F(x,y)A(z,\omega-\omega_0)\exp(-i\beta_0 z) + c.c. \tag{4.12}$$

where $F(x,y)$ is the transverse modal distribution, $A(z,\omega-\omega_0)$ is the slowly varying envelope, and β_0 is the wave number. In the slowly varying envelope approximation $\partial^2 A/\partial z^2$ is neglected. By substituting equation (4.12) in the wave equation and using the above approximation, the following two equations are obtained

$$\frac{\partial^2 F}{\partial x^2} + \frac{\partial^2 F}{\partial y^2} + [\varepsilon(\omega)k_0{}^2 - \tilde{\beta}^2]F = 0 \tag{4.13}$$

$$2i\beta_0 \frac{\partial A}{\partial z} + (\tilde{\beta}^2 - \beta_0{}^2)A = 0 \tag{4.14}$$

The wave number $\tilde{\beta}$ is found by solving equation (4.13). The dielectric constant $\varepsilon(\omega)$ in equation (4.13) also includes the nonlinear effects and is defined by

$$\varepsilon = \left(n - i\frac{\alpha}{2k_0} \right)^2 \tag{4.15}$$

where n includes the nonlinear refractive index and is defined by equation (4.2) and α is given by

$$\alpha = \alpha_0 + \alpha_2 I \tag{4.16}$$

where α_0 is the linear attenuation constant and α_2 is the intensity dependent loss. The dielectric constant $\varepsilon(\omega)$ can be written in terms of the liner refractive index n_0 and a small perturbation Δn, giving

$$\varepsilon = (n_0 + \Delta n)^2 \approx {n_0}^2 + 2n_0 \Delta n \tag{4.17}$$

where Δn is given by

$$\Delta n = n_2 I - \frac{i\alpha}{2k_0} \tag{4.18}$$

The wave equation is solved by first replacing $\varepsilon(\omega)$ with ${n_0}^2$ in equation (4.13) and obtaining the modal distribution $F(x,y)$ and the corresponding wave number $\beta(\omega)$. Next, the effect of Δn is taken into account and the wave number $\tilde{\beta}$ is found as

$$\tilde{\beta}(\omega) = \beta(\omega) + \Delta\beta \tag{4.19}$$

where $\Delta\beta$ is given by

$$\Delta\beta = \frac{k_0 \int_{-\infty}^{\infty}\int \Delta n |F(x,y)|^2 \, dxdy}{\int_{-\infty}^{\infty}\int |F(x,y)|^2 \, dxdy} \tag{4.20}$$

By substituting the wave number $\tilde{\beta}(\omega) = \beta(\omega) + \Delta\beta$ in equation (4.14), this equation is written as

$$\frac{\partial A}{\partial z} = i[\beta(\omega) + \Delta\beta - \beta_0] \tag{4.21}$$

where $\tilde{\beta}^2 - \beta_0^2$ has been approximated by $2\beta_0(\tilde{\beta} - \beta_0)$. This equation indicates that different spectral components of the pulse envelope obtain a frequency and intensity dependent phase shift as a result of propagation in the z direction. The wave number $\beta(\omega)$ can be expanded in a Taylor series about the carrier frequency ω_0, giving

$$\beta(\omega) = \beta_0 + (\omega - \omega_0)\beta_1 + \frac{1}{2}(\omega - \omega_0)^2\beta_2 + \frac{1}{6}(\omega - \omega_0)^3\beta_3 + \cdots \tag{4.22}$$

where

$$\beta_m = \left(\frac{d^m\beta}{d\omega^m}\right)_{\omega=\omega_0} \quad (m = 1,2,3,\cdots) \tag{4.23}$$

By using the Taylor expansion of $\beta(\omega)$ up to the cubic term, equation (4.21) can be written as

$$\frac{\partial A}{\partial z} = -\beta_1\frac{\partial A}{\partial t} - \frac{i\beta_2}{2}\frac{\partial^2 A}{\partial t^2} + \frac{1}{6}\beta_3\frac{\partial^3 A}{\partial t^3} + i\Delta\beta A \tag{4.24}$$

where this equation was obtained by taking the inverse Fourier transform and replacing $\omega - \omega_0$ by the operator $i\partial/\partial t$. The quantity $\Delta\beta$ can be evaluated using equation (4.20) and substituted in the above equation, yielding

$$\frac{\partial A}{\partial z} + \beta_1\frac{\partial A}{\partial t} + \frac{i\beta_2}{2}\frac{\partial^2 A}{\partial t^2} - \frac{\beta_3}{6}\frac{\partial^3 A}{\partial t^3} + \frac{\alpha}{2}A = i\gamma|A|^2 A \tag{4.25}$$

where γ is a nonlinear parameter defined by

$$\gamma = \frac{n_2\omega_0}{cA_{eff}} \tag{4.26}$$

In equation (4.25), $|A|^2$ is in units of optical power, W, and n_2 has units of m^2/W. The parameter A_{eff} is called the effective area of the core and is defined as

$$A_{eff} = \frac{\left(\int\int_{-\infty}^{\infty} |F(x,y)|^2 \, dxdy \right)^2}{\int\int_{-\infty}^{\infty} |F(x,y)|^4 \, dxdy} \tag{4.27}$$

For a hollow waveguide, A_{eff} is evaluated by using the modal distribution $F(x,y)$ of the fundamental hybrid mode HE_{11} given by $J_0(2.405r/a)$.

For ultrashort optical pulses, equation (4.25) should be modified in order to include the nonlinear effect of self steepening. In deriving this wave equation, we cannot use the nonlinear polarization given by equation (4.11). Instead, one must use the general form of the nonlinear polarization given by

$$\vec{P}_{NL} = \varepsilon_0 \int\int\int_{-\infty}^{\infty} \chi^{(3)}(t-t_1, t-t_2, t-t_3) \vdots \vec{E}(\vec{r},t_1)\vec{E}(\vec{r},t_2)\vec{E}(\vec{r},t_3) dt_1 dt_2 dt_3 \tag{4.28}$$

This equation describes various nonlinear effects such as third harmonic generation, four wave mixing, and nonlinear refraction. However, third harmonic generation and four wave mixing require phase matching and are not likely to occur. Nonresonant intensity dependent nonlinear effects are included by assuming that the third order susceptibility has the form [31]

$$\chi^{(3)}(t-t_1, t-t_2, t-t_3) = \chi^{(3)} R(t-t_1)\delta(t-t_2)\delta(t-t_3) \tag{4.29}$$

where $R(t-t_1)$ is the nonlinear response. The nonlinear polarization is found by substituting equation (4.29) in equation (4.28), yielding

$$\vec{P}_{NL}(\vec{r},t) = \varepsilon_0 \chi^{(3)} \vec{E}(\vec{r},t) \int_{-\infty}^{t} R(t-t_1) \left|\vec{E}(\vec{r},t_1)\right|^2 dt_1 \qquad (4.30)$$

where it is assumed that the induced polarization and the electric field have the same direction. The analysis that led to equation (4.25) can still be used with the nonlinear polarization now given by equation (4.30). The effect of nonlinear polarization is again treated as a small perturbation which changes the propagation constant by $\Delta\beta$ as given in equation (4.19). By using the slowly varying amplitude $A(z,t)$ defined as before, the resulting nonlinear wave equation becomes [32]

$$\frac{\partial A}{\partial z} + \beta_1 \frac{\partial A}{\partial t} + \frac{i\beta_2}{2}\frac{\partial^2 A}{\partial t^2} - \frac{\beta_3}{6}\frac{\partial^3 A}{\partial t^3} + \frac{\alpha}{2}A = i\gamma\left(1 + \frac{i}{\omega_0}\frac{\partial}{\partial t}\right)\left[A(z,t)\int_{-\infty}^{\infty} R(t')\left|A(z,t-t')\right|^2 dt'\right] \qquad (4.31)$$

The time derivative on the right hand side is responsible for self steepening of an optical pulse propagating inside a single mode fiber or a hollow fiber. The nonlinear response $R(t)$ includes electronic and vibrational effects. For a gas filled hollow fiber the fractional contribution of the vibrational response to the nonlinear polarization is zero and equation (4.31) simplifies to

$$\frac{\partial A}{\partial z} + \beta_1 \frac{\partial A}{\partial t} + \frac{i\beta_2}{2}\frac{\partial^2 A}{\partial t^2} - \frac{\beta_3}{6}\frac{\partial^3 A}{\partial t^3} + \frac{\alpha}{2}A = i\gamma\left[\left|A\right|^2 A + \frac{i}{\omega_0}\frac{\partial}{\partial t}\left(\left|A\right|^2 A\right)\right] \qquad (4.32)$$

This equation includes the effects of group velocity dispersion, third order dispersion, loss, self phase modulation, and self steepening.

The effect of SPM is included in the term $\gamma\left|A\right|^2 A$ of equation (4.32). This results from the intensity dependence of the refractive index and leads to spectral broadening of an optical pulse. SPM causes the phase shift of the optical pulse to become intensity

dependent. A time dependent phase shift means that the instantaneous frequency is not constant across the pulse and differs from the central frequency ω_0. Therefore, SPM imposes a frequency chirp on the pulse. As the pulse propagates, new frequency components are generated which broaden the spectrum.

4.2 Prism compressor

One of the applications of hollow fibers is in optical pulse compression, which is based on spectral broadening and chirping an optical pulse in a hollow fiber and propagating the output pulse through a compressor. A compressor is a dispersion delay line consisting of a grating pair, a prism pair, or chirped mirrors.

In this section the general aspects of optical compression is described and a prism compressor is explained in detail. Pulses propagating through a prism are broadened by angular dispersion. Angular dispersion depends on the geometry of an optical element. The equations for group velocity dispersion and third order dispersion of an optical element are given. By using the geometry of a prism, the GVD and TOD of a prism pair are obtained. The GVD of a prism pair, due to angular dispersion, is negative and can be adjusted by changing the distance between the prisms. Brewster angle prisms are used in order to reduce the losses.

4.2.1 General description of optical pulse compression

In general two kinds of compressors are used for compression of optical pulses [33]. In one technique a fiber or a gas filled hollow fiber with positive group velocity dispersion is used followed by a compressor consisting of a grating pair, a prism pair, or a

chirped mirror. In another technique a fiber is used in the negative dispersion region in order to form higher order solitons by combining the effects of group velocity dispersion and self phase modulation.

When an optical pulse propagates in a dispersive medium it broadens in time and becomes chirped. This means that the instantaneous frequency across the pulse is different from the central frequency ω_0. The frequency chirp depends on the sign of the GVD parameter β_2. If β_2 is positive (normal dispersion), the chirp is linear and positive across the pulse. Therefore, the frequency shift is negative at the leading edge of the pulse and consequently the leading edge becomes red-shifted. The frequency shift will be positive at the trailing edge of the pulse and, thus, the trailing edge becomes blue-shifted. Now, if this pulse propagates in a medium with negative GVD the red-shifted frequency components travel slower than the blue-shifted components. Since the leading edge of the pulse is red-shifted it travels slower than the trailing edge which is blue-shifted and the optical pulse is compressed.

If the dispersion parameter β_2 is negative (anomalous dispersion), the chirp is linear and negative across the pulse. In this case the frequency shift is positive at the leading edge of the pulse which results in the leading edge becoming blue-shifted. The frequency shift will be negative at the trailing edge of the pulse and, therefore, the trailing edge becomes red-shifted. If we apply positive GVD the red-shifted frequency components travel faster than the blue-shifted components. Since the trailing edge of the pulse is red-shifted it travels faster than the leading edge which is blue-shifted and the optical pulse is compressed.

In the early pulse compression experiments a grating pair was used to provide negative GVD and compress pulses that had been positively chirped in a medium with positive dispersion ($\beta_2>0$) [34]. In these early works the nonlinear effect of SPM was not used. As optical fibers were used as a nonlinear medium in different studies [35], optical pulse compression experiments based on the nonlinear process of SPM was also performed extensively [36]. In one experiment that was performed in 1987 optical pulses as short as 6 fs were generated at wavelength of 620 nm [37].

The nonlinear effect can be used in the following way for optical pulse compression. In optical compressors that use a grating pair, the optical pulse propagates in a fiber or a hollow fiber that has positive dispersion. The fiber is used in order to impose a positive chirp on the pulse by using the combined effect of SPM and GVD [38]. SPM also leads to spectral broadening of the pulse. The positively chirped pulses require negative GVD in order to compress. The optical pulse exiting the fiber is compressed by a grating pair which provides negative GVD [39]. The amount of compression is determined by the pulse and fiber parameters (peak power of the pulse, pulse width, fiber GVD parameter β_2, and fiber nonlinear parameter γ).

An optical fiber can support solitons which are created by a combination of SPM and negative GVD. As higher order solitons propagate inside a fiber, they first become narrowed before regaining the original shape after one soliton period. SPM provides a positive frequency chirp. Therefore, the leading edge of the optical pulse is red-shifted and the trailing edge is blue-shifted. If we only consider the effect of SPM, the pulse shape does not change. However, negative GVD of the fiber leads to compression of the positively chirped pulses. The chirp induced by SPM is linear only in the central portion

of the pulse. Therefore, the central portion of the pulse is compressed. Since soliton-effect compressors require fibers with negative GVD, they are used for wavelengths greater than 1.3 μm. Compressors that use fiber gratings require fibers that have positive GVD. Therefore, these compressors are useful for wavelengths less than 1.3 μm.

4.2.2 Angular dispersion

Consider a sequence of four prisms which have been arranged as shown in Fig. 4.1. As light travels through the prisms, different spectral components propagate along different optical paths. This causes an optical pulse to disperse temporally and spatially. The first two prisms produce negative GVD. But, they also change the cross section of the beam from circular to elliptic. This beam deformation is not desirable and is corrected by adding two more prisms which are placed symmetrically with respect to the first two prisms. At the output of the fourth prism, the spectral components are recombined and will have the original transverse distribution in the beam. Therefore, the effect of the four prisms on a light pulse is to introduce a negative GVD which causes an unchirped input pulse to broaden without changing the spatial distribution of the beam.

This GVD is a result of angular dispersion in the prisms [40, 41]. When different spectral components pass through a prism they are spatially distributed. Angular dispersion can be used to obtain a tunable GVD, as described below. This was first shown for optical compression using diffraction gratings [34]. This was also demonstrated by using prisms in an experiment which was reported in 1982 [42]. To find the GVD of a sequence of prisms, the optical path is calculated as a function of frequency. The phase delay is related to the optical path by

$$\phi = \frac{\omega}{c} p \tag{4.33}$$

where ϕ is the phase, p is the optical path length, c is the speed of light, and ω is the frequency. The group velocity dispersion is related to the second derivative of the phase ϕ with respect to frequency ω, which is defined by [43]

$$\frac{d^2\phi}{d\omega^2} = \frac{1}{c}\left(2\frac{dp}{d\omega} + \omega\frac{d^2p}{d\omega^2}\right) = \frac{1}{2\pi}\frac{\lambda^3}{c^2}\frac{d^2p}{d\lambda^2} \tag{4.34}$$

where λ is the wavelength in vacuum. In order to show the relationship between angular dispersion and GVD, consider the situation shown in Fig. 4.2. When a ray of light is diffracted or refracted by an optical element, different spectral components propagate at different angles. Two rays are shown, one with the center frequency ω_0 and one with frequency ω. Wavefronts are planes that are perpendicular to the direction of each light ray.

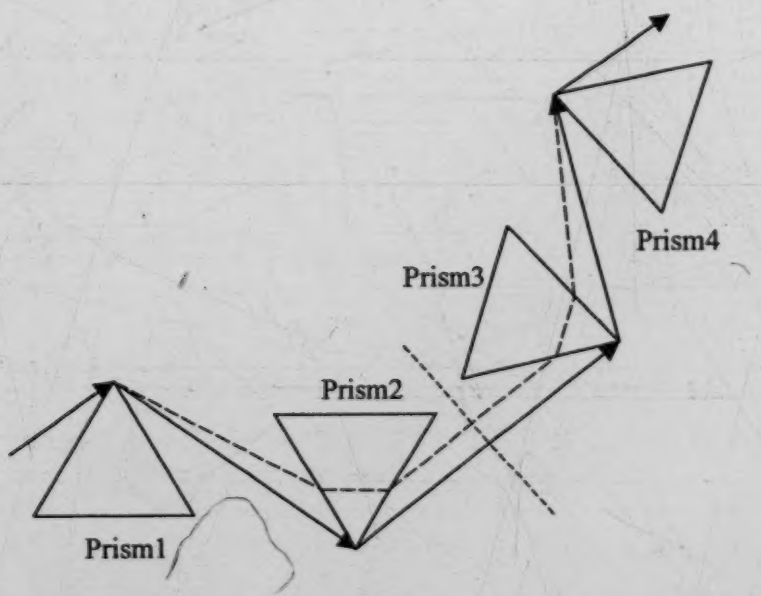

Fig. 4.1 A sequence of four prisms producing negative GVD. Prisms 1 and 2 are used to obtain the GVD. Prisms 3 and 4 correct the beam deformation.

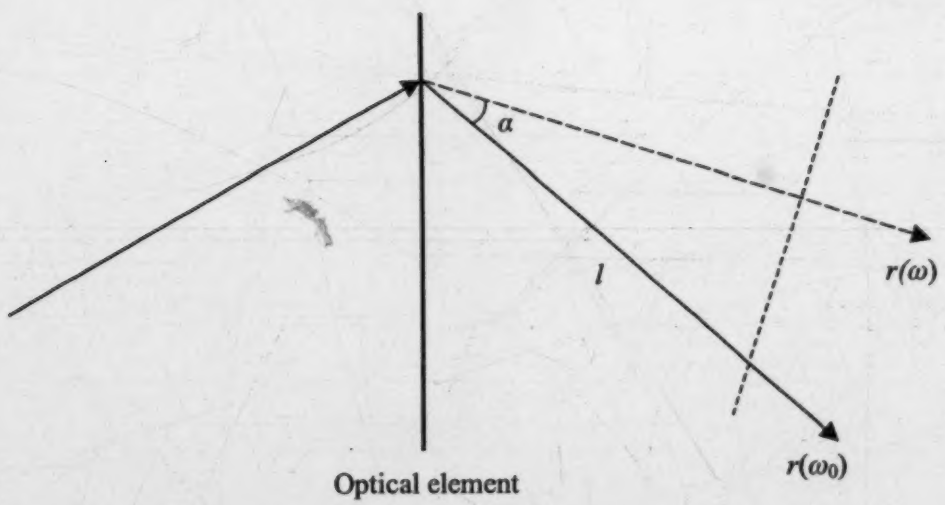

Fig. 4.2 Angular dispersion by an optical element. Rays of light are diffracted by the optical element and different spectral components propagate at different angles.

Using the ray with frequency ω_0 as the reference, the optical distance for the ray with frequency ω is given by [44]

$$p(\omega) = p(\omega_0)\cos\alpha = l\cos\alpha \tag{4.35}$$

where α is the angle between the two light rays. Therefore, the phase delay ϕ is found to be

$$\phi = \frac{\omega}{c} l\cos\alpha \tag{4.36}$$

The angle α is a function of frequency. When an optical pulse is diffracted by an optical element, different frequency components travel along different paths. Therefore, the time delays for these components are different. It takes less time for the blue-shifted frequency components to arrive at the output of a prism than the red-shifted components. If optical pulses are propagated through a fiber with positive GVD, the pulses exiting the fiber are

positively chirped. The trailing edge of the output pulse is blue-shifted and the leading edge is red-shifted. Thus, if these positively chirped pulses travel through a prism pair, the trailing edge travels faster than the leading edge and the pulse is compressed [45, 46].

The dispersion parameter which specifies the GVD is found by taking the second derivative of ϕ with respect to ω, yielding

$$\left.\frac{d^2\phi}{d\omega^2}\right|_{\omega_0} = -\frac{l}{c}\left[\sin\alpha\left(2\frac{d\alpha}{d\omega}+\omega\frac{d^2\alpha}{d\omega^2}\right)+\omega\cos\alpha\left(\frac{d\alpha}{d\omega}\right)^2\right]_{\omega_0}$$

$$\approx -\frac{l\omega_0}{c}\left(\left.\frac{d\alpha}{d\omega}\right|_{\omega_0}\right)^2 \qquad (4.37)$$

This expression is evaluated at the center frequency ω_0 for which sin α<<1. The quantity $d\alpha/d\omega$ causes angular dispersion and is a characteristic of the optical element under consideration. It can be seen that the dispersion parameter is always negative and does not depend on the sign of $d\alpha/d\omega$. It can also be seen that by increasing the distance l from the optical element dispersion increases. Therefore, it is concluded that angular dispersion produces an adjustable negative GVD. By differentiating equation (4.37), the third order dispersion can be obtained, giving

$$\left.\frac{d^3\phi}{d\omega^3}\right|_{\omega_0} \approx -\frac{3l}{c}\left[\left(\frac{d\alpha}{d\omega}\right)^2+\omega\frac{d\alpha}{d\omega}\frac{d^2\alpha}{d\omega^2}\right]_{\omega_0} \qquad (4.38)$$

Equations (4.37) and (4.38) represent the dispersion parameters for a general optical element. In the next section the geometry of a prism is used in order to evaluate the derivatives appearing in the above equations and to obtain the dispersion parameters for a prism pair.

4.2.3 Prism dispersion

In order to find expressions for the GVD and the third order dispersion (TOD) of a prism pair shown in Fig. 4.3, we need to specify $d\alpha/d\omega$ and $d^2\alpha/d\omega^2$. By using the chain rule we get

$$\frac{d\alpha}{d\omega} = \frac{d\alpha}{dn}\frac{dn}{d\omega} \tag{4.39}$$

where n is the refractive index of the prism material. The quantity $dn/d\omega$ which specifies the material dispersion can be written in terms of wavelength, giving

$$\frac{dn}{d\omega} = -\frac{1}{2\pi}\frac{\lambda^2}{c}\frac{dn}{d\lambda} \tag{4.40}$$

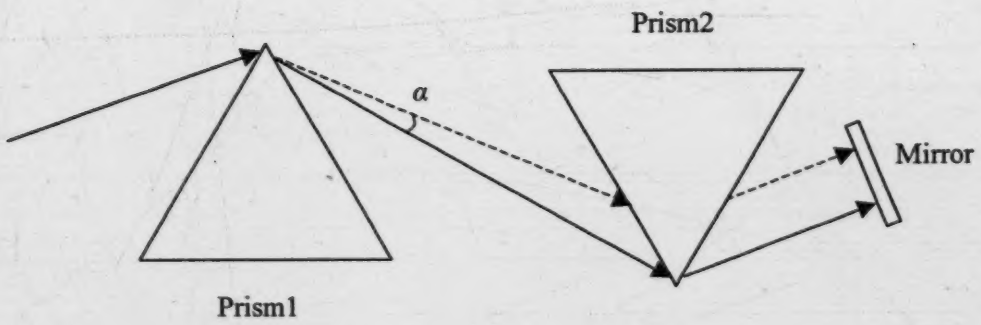

Fig. 4.3 Geometry of a prism pair used to find the GVD and TOD parameters. The mirror is used to reflect the beam back along the same path through the prism pair. The reflected beam can be separated from the input beam by slight adjustment of this mirror.

The prism geometry, such as apex angle and angle of incidence, can be used to find the quantity $d\alpha/dn$. For an angle of incidence resulting in symmetrical beam path parallel to

the base through the prism, minimum deviation, and a prism apex angle satisfying the Brewster condition, minimum reflection losses, the first and second derivatives of angle α with respect to the refractive index of prism material can be found, yielding [47, 48]

$$\frac{d\alpha}{dn} = -2 \tag{4.41}$$

$$\frac{d^2\alpha}{dn^2} = \frac{2}{n^3} - 4n \tag{4.42}$$

By using these identities in equation (4.37), we obtain the GVD in terms of frequency and wavelength

$$\begin{aligned} \left.\frac{d^2\phi}{d\omega^2}\right|_{\omega_0} &\approx -4\frac{\omega_0}{c} l \left(\left.\frac{dn}{d\omega}\right|_{\omega_0}\right)^2 \\ &\approx -4l\frac{\lambda_0^3}{2\pi c^2}\left(\left.\frac{dn}{d\lambda}\right|_{\lambda_0}\right)^2 \end{aligned} \tag{4.43}$$

Similarly, we can find an equation for the third order dispersion parameter by using the above identities in equation (4.38) giving

$$\left.\frac{d^3\phi}{d\omega^3}\right|_{\omega_0} \approx \frac{12l\lambda^4}{(2\pi)^2 c^3}\left\{\left(\frac{dn}{d\lambda}\right)^2\left[1-\lambda\frac{dn}{d\lambda}\left(n^{-3}-2n\right)\right]+\lambda\left(\frac{dn}{d\lambda}\frac{d^2n}{d\lambda^2}\right)\right\}\Bigg|_{\lambda_0} \tag{4.44}$$

In order to avoid transverse displacement of the spectral components, a sequence of four prisms is used as shown in Fig. 4.1. We can also use a mirror after the second prism and reflect the beam back along the same path through the prisms as shown in Fig. 4.3. The reflected beam is separated from the input beam vertically by slight adjustment of this mirror. This double-pass configuration has the added advantage of doubling the amount of negative GVD provided by the prism pair and effectively reducing the necessary separation between the prisms by a factor of two.

There is also an additional contribution to the dispersion by the prism material. The beam passes through a certain length of glass in each prism, which gives rise to material dispersion. In the visible and near infrared region of the spectrum, the material dispersion of fused silica is positive. Therefore, the amount of GVD can be adjusted by changing the total glass path length L in the prisms. The second and third order material dispersion parameters are given by

$$\left.\frac{d^2\phi}{d\omega^2}\right|_{mat} = \frac{\lambda^3}{2\pi c^2} L \frac{d^2 n}{d\lambda^2} \tag{4.45}$$

$$\left.\frac{d^3\phi}{d\omega^3}\right|_{mat} = -\frac{\lambda^2}{(2\pi)^2 c^3}\left(3\lambda^2 \frac{d^2 n}{d\lambda^2} + \lambda^3 \frac{d^3 n}{d\lambda^3}\right) L \tag{4.46}$$

The total dispersion of the prism sequence is found by adding the angular and material dispersions, giving

$$\left.\frac{d^2\phi}{d\omega^2}\right|_{total} = \left.\frac{d^2\phi}{d\omega^2}\right|_{ang} + \left.\frac{d^2\phi}{d\omega^2}\right|_{mat} \tag{4.47}$$

$$\left.\frac{d^3\phi}{d\omega^3}\right|_{total} = \left.\frac{d^3\phi}{d\omega^3}\right|_{ang} + \left.\frac{d^3\phi}{d\omega^3}\right|_{mat} \tag{4.48}$$

The prisms used in this project are made of fused silica with an apex angle of 69.08°. The refractive index of fused silica is given by [49]

$$n(\lambda) = \left(1 + \frac{0.6961663\lambda^2}{\lambda^2 - 0.0684043^2} + \frac{0.4079426\lambda^2}{\lambda^2 - 0.1162414^2} + \frac{0.8974794\lambda^2}{\lambda^2 - 9.896161^2}\right)^{\frac{1}{2}} \tag{4.49}$$

where λ is wavelength in μm. The refractive index and material dispersion of fused silica as a function of wavelength are shown in Fig. 4.4 and Fig. 4.5. The value of material dispersion at wavelength of 0.8 μm is 361 fs^2/cm.

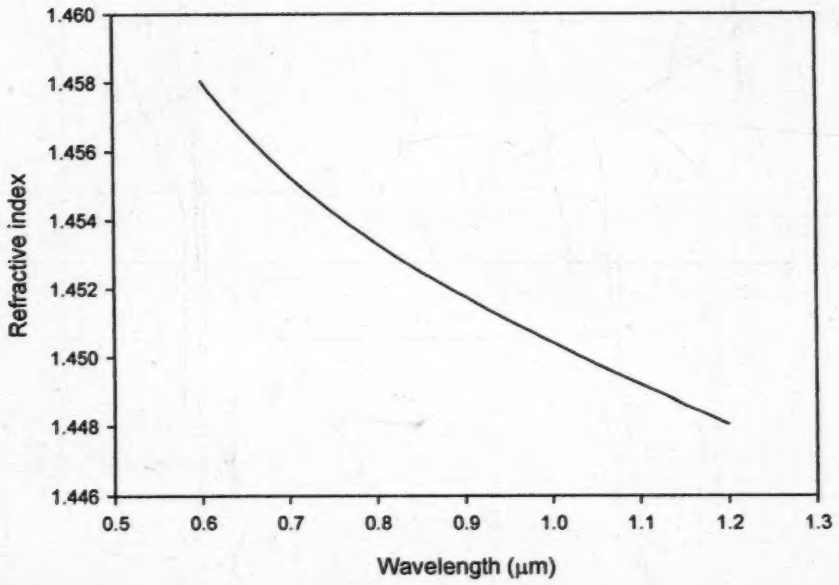

Fig. 4.4 Refractive index of fused silica as a function of wavelength. The refractive index of fused silica at 0.8 μm is 1.4533.

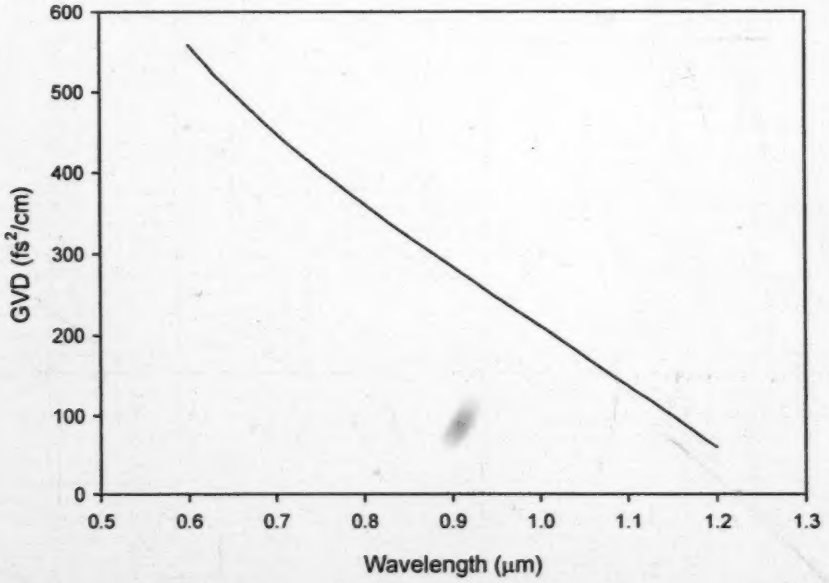

Fig. 4.5 GVD of fused silica as a function of wavelength. The material dispersion of fused silica at 0.8μm is 361 fs^2/cm.

The GVD and TOD of a fused silica prism pair can be obtained as a function of wavelength by using values for the refractive index of fused silica and its first and second derivatives with respect to wavelength in equations (4.47) and (4.48). Fig. 4.6 shows the GVD of a fused silica prism pair. A glass length of 0.5 cm in each prism was considered. It can be seen that the GVD is always negative for the range of wavelengths shown. The TOD of a fused silica prism pair has been plotted in Fig. 4.7. The GVD and TOD parameters at a wavelength of 0.8 μm are found to be β_2= 9.6 fs^2/cm and β_3= 14.2 fs^3/cm respectively.

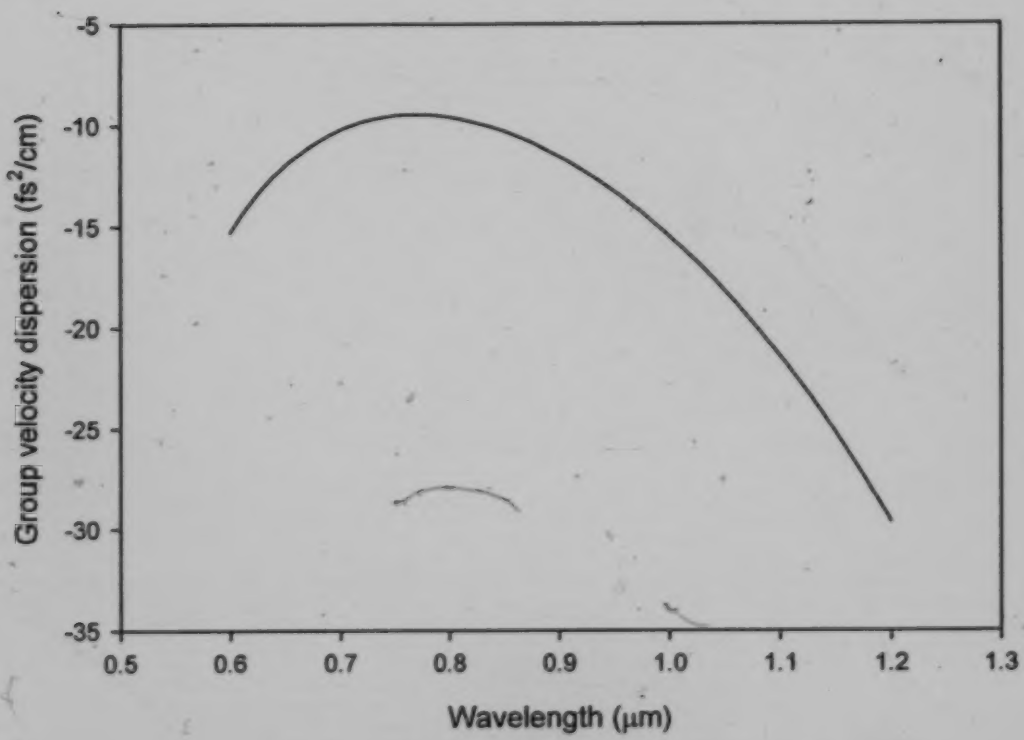

Fig. 4.6 GVD of a double-pass fused silica prism pair with apex angle of 69.08 degrees. Prism separation is 60 cm. The GVD parameter at 0.8 μm is β_2= 9.6 fs^2/cm.

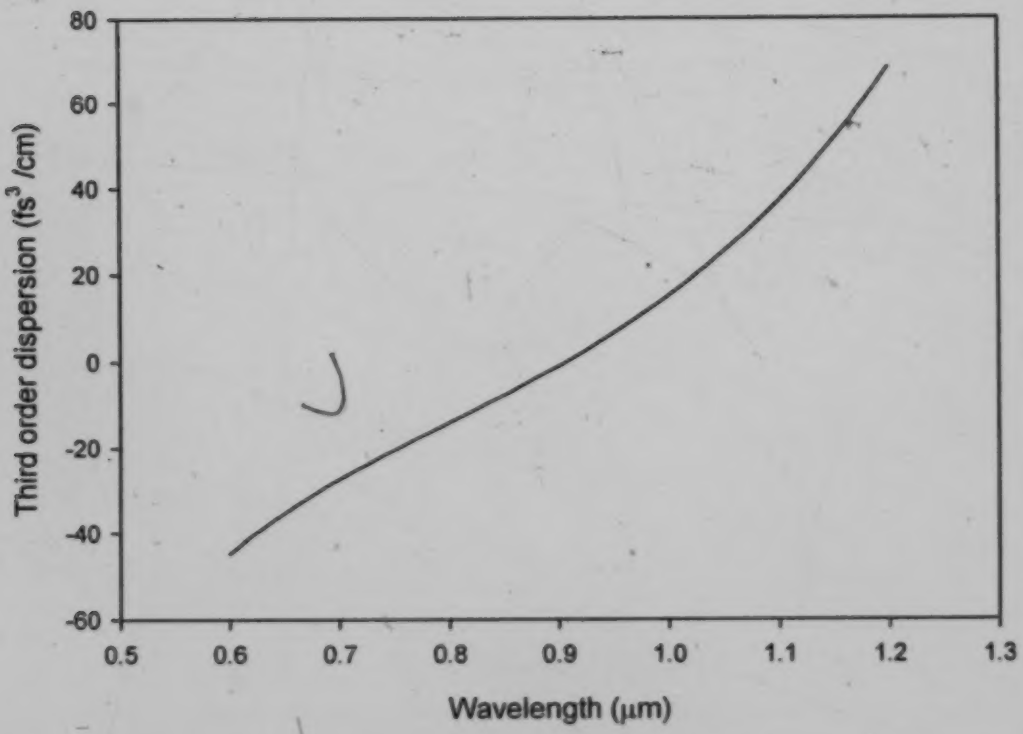

Fig. 4.7 TOD of a double-pass fused silica prism pair with apex angle of 69.08 degrees. Prism separation is 60 cm. The TOD parameter at 0.8 μm is β_3= 14.2 fs^3/cm.

Chapter 5

Optical pulse compression using silver coated hollow fiber

5.1 Introduction

Fused silica hollow fibers filled with a noble gas have been used for optical pulse compression at high energies [15, 50] and high harmonic generation [51]. The use of a waveguide results in good mode quality and the use of a noble gas yields high multiphoton ionization thresholds [52]. However, hollow glass fibers have high losses which limit the efficiency of the optical pulse compressor. It was shown in chapter 3 that the silver coated hollow fiber has low losses and its output mode has high purity and is as good as that obtained from a fused silica hollow fiber.

In this chapter modeling and experimental results for optical pulse compression of femtosecond pulses using a silver coated hollow fiber filled with argon gas are presented. The 50 cm long silver coated hollow waveguide with inner diameter of 250 μm, characterized in chapter 3, and filled with argon is used to compress optical pulses from a Ti:sapphire laser at 800 nm. This waveguide has a transmission of 95% as reported in chapter 3. Input pulses with energy of 250μJ and duration of 110 fs are used. The output optical pulses are compressed to 20 fs by using a prism compressor. Numerical and experimental results are presented and compared for argon gas pressures of 2.4 and 1.5 atm. The image of the output beam taken at different distances from the silver coated hollow fiber output shows that a single HE_{11} mode couples to free space modes from the exit of the fiber. A 50 cm long fused silica hollow fiber is also used for optical pulse compression which has a measured transmission of 80%. The experimental results for

optical pulse compression using the fused silica hollow fiber are compared for pulse energies of 250 and 300 μJ and pressures of 2.4 and 2 atm.

5.2 Numerical modeling

In this numerical study optical pulses with energy of 250 μJ, pulse width of 110 fs, and wavelength of 800 nm are considered. We assume that the silver coated hollow waveguide is filled with argon and the pressure is set at 2.4 atm. The generalized nonlinear Schrödinger equation, which was derived in chapter 4, is used to study the propagation of optical pulses inside the hollow fiber, given by

$$\frac{\partial A}{\partial z} = -\frac{i}{2}\beta_2 \frac{\partial^2 A}{\partial T^2} + \frac{1}{6}\beta_3 \frac{\partial^3 A}{\partial T^3} - \frac{\alpha}{2}A + i\gamma\left[|A|^2 A + \frac{i}{\omega_0}\frac{\partial}{\partial T}(|A|^2 A)\right] \tag{5.1}$$

The difference between equation (5.1) and equation (4.32) is that we have introduced the reduced time T defined by

$$T = t - \frac{z}{v_g} \tag{5.2}$$

where t is time, z is propagation distance, and v_g is the group velocity of the optical pulse. The reduced time T is now measured in the reference frame moving with the pulse envelope $A(z,T)$. The dispersion parameters, β_2 and β_3, and the intensity attenuation constant α have already been defined in chapter 2. The nonlinear coefficient γ is given by equation (4.26). Equation (5.1) can be written in normalized form, giving

$$\frac{\partial U}{\partial z} = -\frac{i\,\mathrm{sgn}(\beta_2)}{2L_D}\frac{\partial^2 U}{\partial \tau^2} + \frac{\mathrm{sgn}(\beta_3)}{6L_D'}\frac{\partial^3 U}{\partial \tau^3} - \frac{\alpha}{2}U + \frac{i}{L_{NL}}\left[|U|^2 U + \frac{i}{\omega_0 T_0}\frac{\partial}{\partial \tau}(|U|^2 U)\right] \tag{5.3}$$

where $\tau = T/T_0$ is the normalized time, T_0 is the 1/e intensity half width of the pulse, and $U(z,\tau)$ is the normalized pulse amplitude. The terms $\mathrm{sgn}(\beta_2)$ and $\mathrm{sgn}(\beta_3)$ can be ±1,

depending on the sign of each dispersion parameter. By normalizing the wave equation new parameters are defined. L_D and L_D' are the second order and third order dispersion lengths given by

$$L_D = \frac{T_0^2}{|\beta_2|} \tag{5.4}$$

$$L_D' = \frac{T_0^3}{|\beta_3|} \tag{5.5}$$

The nonlinear length parameter L_{NL} is defined by

$$L_{NL} = \frac{1}{\gamma P_0} = \frac{cA_{eff}}{n_2 \omega_0 P_0} \tag{5.6}$$

where p_0 is the peak power of the pulse, n_2 is the nonlinear refractive index, c is the speed of light, and A_{eff} is the effective area of the mode as given in chapter 4.

In order to find the dispersion lengths, we need to evaluate the group velocity and third order dispersions of the hollow fiber filled with argon. The dispersion parameters β_2 and β_3 for a hollow fiber can be calculated using the phase constant of the HE_{11} mode given by

$$\beta = \frac{2\pi}{\lambda}\left\{1 - \frac{1}{2}\left(\frac{2.405\lambda}{2\pi a}\right)^2\left[1 + \frac{\lambda}{\pi a}\mathrm{Im}\left(\frac{1}{2}\frac{\nu^2+1}{\sqrt{\nu^2-1}}\right)\right]\right\} \tag{5.7}$$

The refractive index of fused silica is a real number. Thus, the Im term in equation (5.7) is zero for a fused silica hollow fiber and the phase constant reduces to

$$\beta = \frac{2\pi}{\lambda}\left[1 - \frac{1}{2}\left(\frac{2.405\lambda}{2\pi a}\right)^2\right] \tag{5.8}$$

This equation was used in chapter 2 to find the dispersion parameters for the fused silica hollow fiber in air as a function of core diameter. In order to use the silver coated hollow fiber for optical pulse compression, we must find the dispersion parameters β_2 and β_3 and compare them to dispersion parameters for a fused silica hollow fiber. Then, it can be decided whether a silver coated hollow fiber is suitable for pulse compression. For optical pulse compression using a prism pair, the GVD of the hollow fiber must be positive in order to induce a positive chirp on the propagating optical pulses.

We can look at this problem in two ways. The Im term in the phase constant of equation (5.7) is multiplied by the factor $\lambda/\pi a$. The propagation constants of the hollow fiber have been obtained assuming $\lambda << a$. Using the values for wavelength and core radius, λ=800 nm, a=125 μm, we obtain $\lambda/\pi a \approx 0.002$. Since this value is much less than unity and $(\lambda/\pi a)\,\mathrm{Im}[(\nu^2+1)/2(\nu^2-1)^{1/2}] \approx -0.005$, the Im term in equation (5.7) can effectively be neglected. This is the only term in which the refractive index of the cladding material appears. The remaining dispersion effects only depend on the waveguide radius and the refractive index of the gas inside the hollow core. Therefore, we can conclude that the dispersion parameters are essentially the same for silver coated and fused silica hollow fibers.

The dispersion parameters for the silver coated hollow fiber can also be calculated by using the refractive index of silver in equation (5.7). The GVD is shown in Fig. 5.1 for argon gas pressure of 2.4 atm. At a wavelength of 800 nm, the GVD dispersion parameter is found to be β_2=39.24 fs^2/m. The material and waveguide dispersions are also shown. The material dispersion of argon was calculated using the refractive index of argon given by [53]

$$n^2(\lambda)-1=5.547\times10^{-4}\left[1+\frac{5.15\times10^{5}}{\lambda^2}+\frac{4.19\times10^{11}}{\lambda^4}+\frac{4.09\times10^{17}}{\lambda^6}+\frac{4.32\times10^{23}}{\lambda^8}\right] \quad (5.9)$$

where λ is in angstroms. The waveguide dispersion was calculated by assuming that the hollow core consists of free space or the index of refraction of the material filling the core does not vary with wavelength. It can be seen that adding the material and waveguide dispersions results in the total dispersion of the hollow fiber filled with argon, which was obtained by taking the second derivative of the propagation constant given by equation (5.7) with respect to the frequency ω.

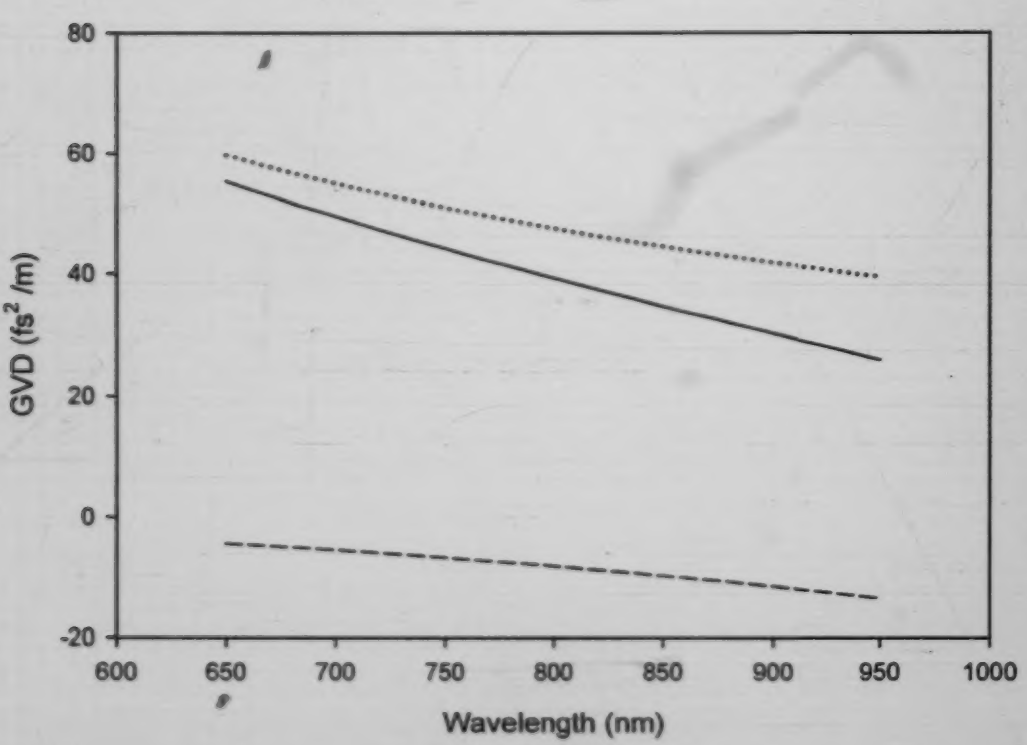

Fig. 5.1 GVD of the HE_{11} mode for the silver coated hollow fiber filled with argon at 2.4 atm (solid line). The core radius of the hollow fiber is 125 μm. The GVD parameter β_2=39.24 fs^2/m at 800 nm. The material (dotted line) and waveguide (dashed line) dispersions are shown for comparison.

The group velocity dispersions of silver coated and fused silica hollow fibers are compared in Fig. 5.2. At a wavelength of 800 nm, the GVD parameter for a fused silica hollow fiber filled with argon at a pressure of 2.4 atm is calculated to be β_2=38.94 fs^2/m using equation (5.8). This compares well with the value obtained for the GVD parameter of silver coated hollow fiber using equation (5.7).

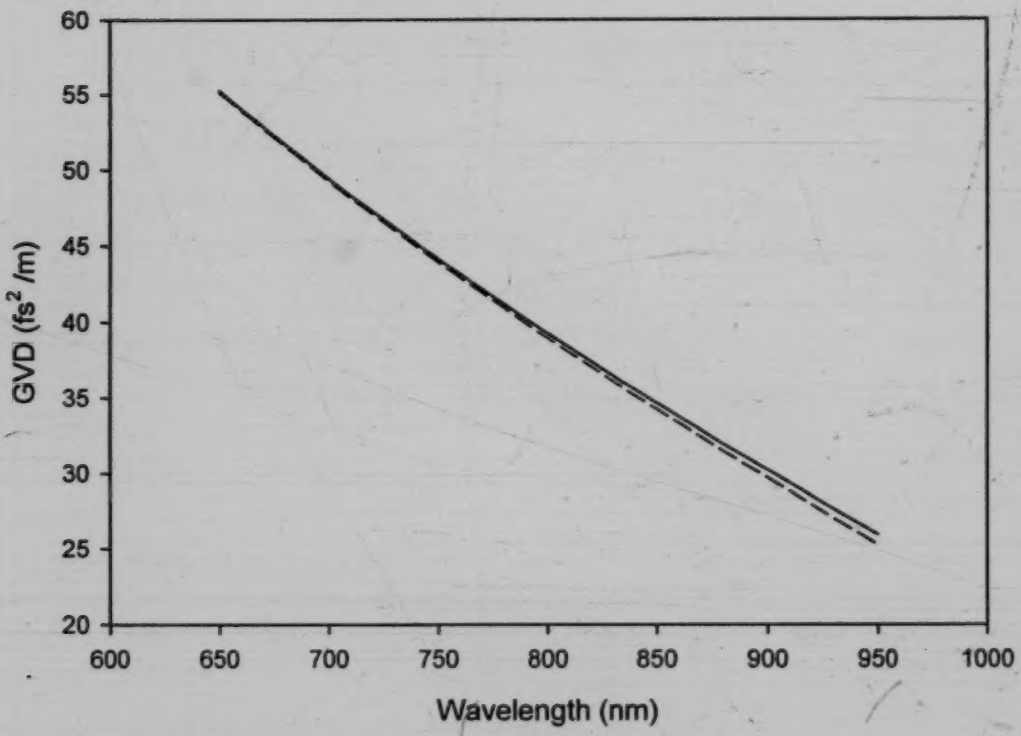

Fig. 5.2 Comparison of GVD for the silver coated (solid line) and fused silica (dashed line) hollow fibers filled with argon at 2.4 atm.

The TOD for the silver coated hollow fiber calculated assuming an argon gas pressure of 2.4 atm is shown in Fig. 5.3. A value of β_3=32.04 fs^3/m is calculated for the third order dispersion parameter at a wavelength of 800 nm. The third order material and

waveguide dispersions are also shown in Fig. 5.3. Again, the refractive index of argon was used to find the third order material dispersion and the waveguide dispersion was calculated by assuming that the index of refraction of the core material does not vary with wavelength. Adding the third order material and waveguide dispersions in this case also results in the total third order dispersion of the hollow fiber filled with argon, which was obtained by taking the third derivative of equation (5.7) with respect to the frequency ω. Therefore, calculation of the dispersion parameters by adding the material and waveguide dispersions is an excellent approximation to the total dispersion parameters obtained using equation (5.7).

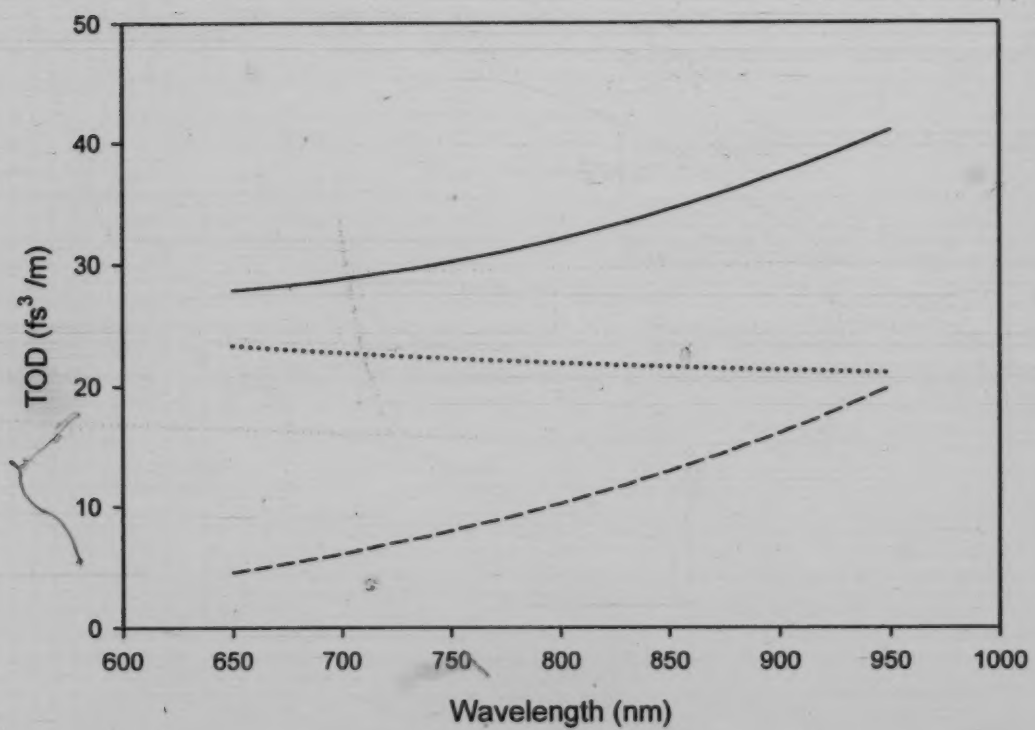

Fig. 5.3 Third order dispersion (TOD) of the HE_{11} mode for the silver coated hollow fiber filled with argon at 2.4 atm (solid line). The TOD parameter β_3=32.04 fs^3/m at 800 nm. The third order material (dotted line) and waveguide (dashed line) dispersions are shown for comparison.

The third order dispersions of silver coated and fused silica hollow fibers are compared in Fig. 5.4. At a wavelength of 800 nm, the TOD parameter for a fused silica hollow fiber filled with argon at a pressure of 2.4 atm is calculated to be β_3=32.67 fs^3/m using equation (5.8). This compares well with the value obtained for the TOD parameter of silver coated hollow fiber using equation (5.7).

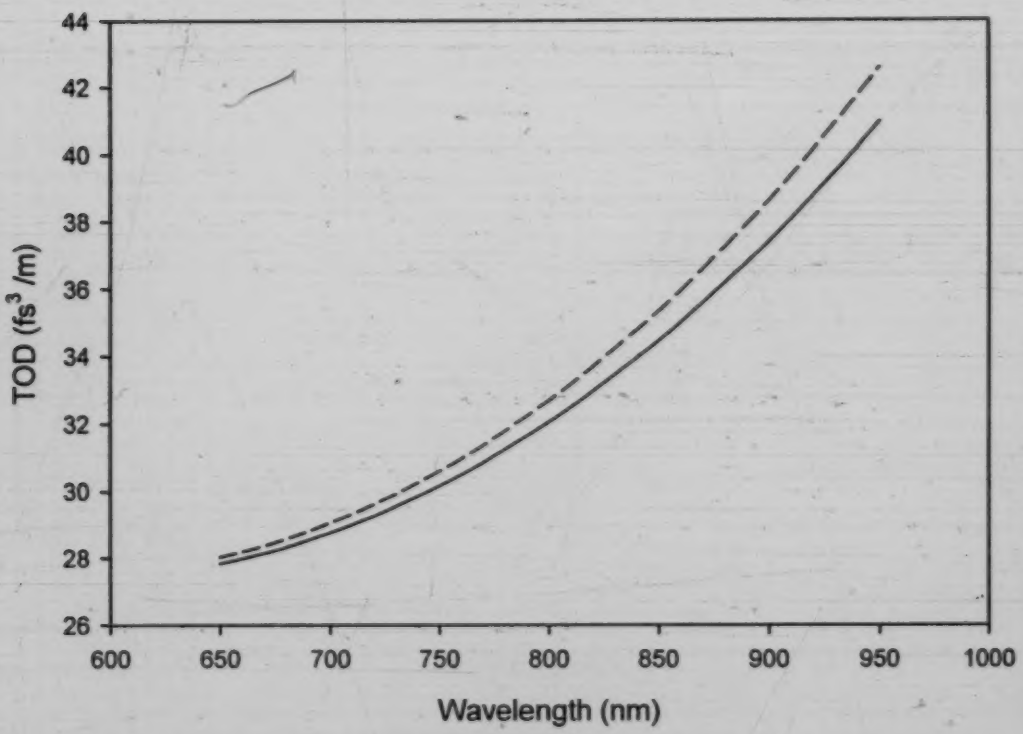

Fig. 5.4 Comparison of TOD for the silver coated (solid line) and fused silica (dashed line) hollow fibers filled with argon at 2.4 atm.

Comparison of the dispersion parameters for the silver coated and fused silica hollow fibers filled with argon shows that an optical pulse propagating in each waveguide will effectively have the same dispersion. Therefore, the silver coated hollow fiber can

be used for optical pulse compression in essentially the same way as a fused silica hollow fiber. Since the silver coated hollow fiber has much higher transmission, as shown in chapter 3, compressed pulses with higher energy can be obtained.

The input pulse is considered to be an unchirped hyperbolic secant pulse for which the normalized optical field amplitude is given by

$$U(0,T) = \sec h\left(\frac{T}{T_0}\right) \tag{5.10}$$

where T_0 is the 1/e intensity half width of the pulse equal to $T_{FWHM}/1.76$. The theoretical intensity attenuation constant for the HE_{11} mode propagating in a silver coated hollow waveguide is 0.0076 m^{-1}, at a wavelength of 800 nm. The second and third order dispersion lengths are found using the values for dispersion parameters β_2 and β_3 of the HE_{11} mode, yielding L_D = 100 m and L_D' = 7620 m. The nonlinear coefficient and the nonlinear length are calculated to be $\gamma = 7.9\times10^{-9}$ $W^{-1}m^{-1}$ and $L_{NL} = 6.3$ cm, using the nonlinear refractive index of argon $n_2 = 9.8\times10^{-24}$ m^2/Watm [15, 54] and the effective area of the mode $A_{eff} = 2.34\times10^{-4}$ cm^2. The effective area of the mode is evaluated for the fundamental hybrid mode HE_{11}, whose modal distribution is given by the Bessel function $J_0(2.405r/a)$. It is clear that dispersion does not play an important role and the output pulse shape should be very similar to the input pulse shape with very little pulse broadening.

Using the above values in the nonlinear Schrödinger equation the output pulse is obtained which is shown in Fig. 5.5. As can be seen the output pulse has not broadened and has some distortion which is due to the self steepening term in equation (5.3). Because the nonlinear refractive index is intensity dependent, the group velocity of the

pulse also becomes intensity dependent and the peak moves at a lower speed than the low intensity wings. Thus, the trailing edge of the pulse becomes steeper as the propagation distance z increases and the pulse shape becomes asymmetric.

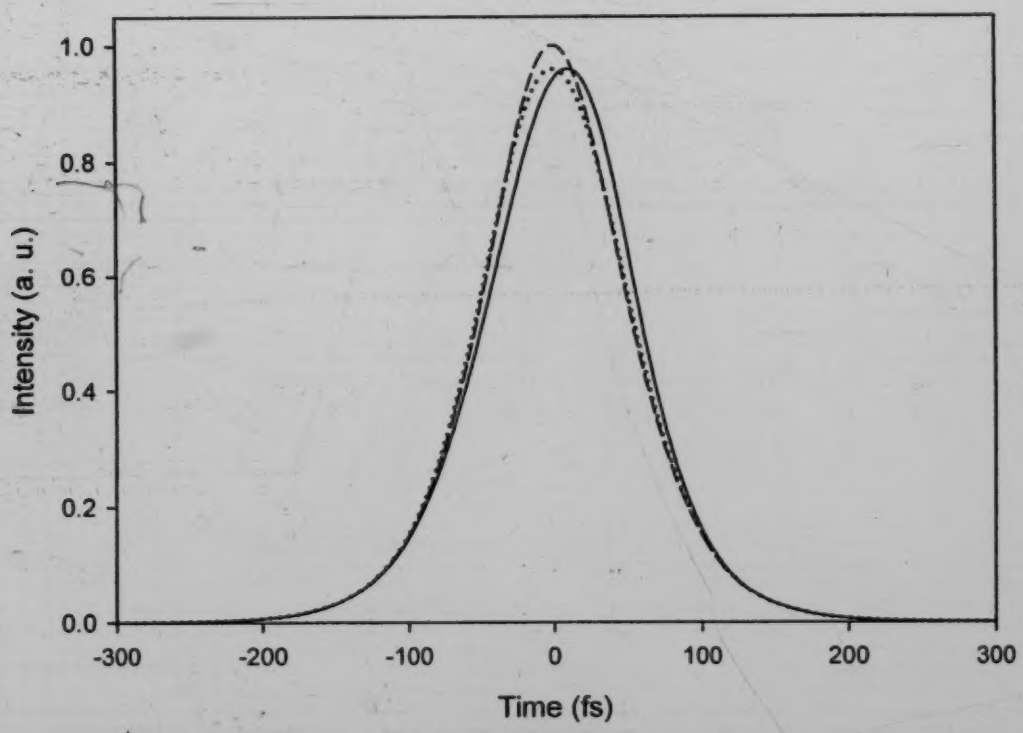

Fig. 5.5 Input (dashed line) and output (solid line) pulse shapes obtained from simulating the propagation of hyperbolic secant optical pulses through the silver coated hollow fiber for an argon pressure of 2.4 atm. The propagation distance is 50 cm. The distortion of the output pulse is due to the nonlinear effects. Because of large value of the dispersion length (100 m), the output pulse has broadened very little. The output pulse without the self steepening effect is also shown (dotted line).

The frequency chirp of the output pulse is shown in Fig. 5.6. It can be seen that the chirp is asymmetric and larger near the trailing edge of the pulse due to the self steepening effect. Since the chip is positive, the trailing edge becomes blue-shifted with larger spectral broadening compared to the leading edge. It also has a linear part in the

central portion of the pulse. Therefore, a prism pair with negative chirp can be used to compress the output optical pulse. Because the chirp is linear only in the central portion of the pulse and changes sign near the edges, some of the energy in the wings will not be compressed.

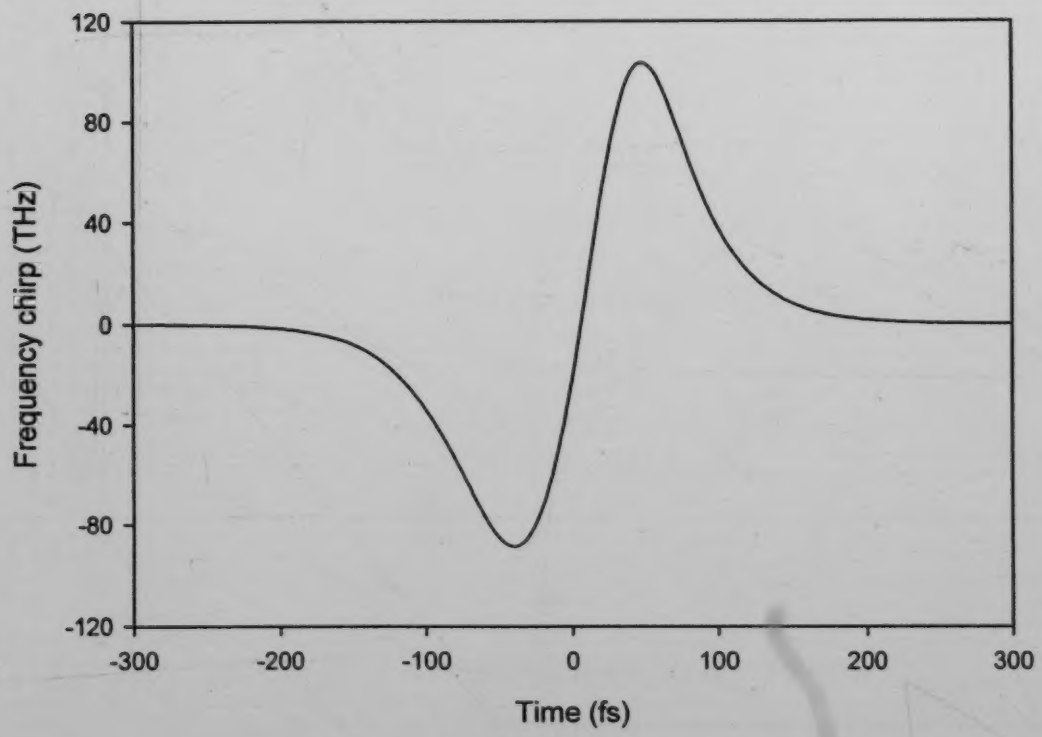

Fig. 5.6 Frequency chirp of the output pulse (shown in Fig. 5.5) for argon pressure of 2.4 atm. It shows a linear positive chirp in the central portion of the pulse. The frequency chirp is asymmetric and is larger near the trailing edge. This leads to larger spectral broadening for the blue-shifted frequency components.

The output spectrum of the hollow waveguide is shown in Fig. 5.7. It has broadened considerably compared to the input spectrum. The full width at half maximum of the output spectrum is about 59 nm, which is more than seven times the FWHM of the input spectrum. We can see that the spectral broadening is larger for the blue-shifted

frequencies. Assuming a Gaussian pulse shape, we expect to compress the pulses to 16 fs using a compressor with negative GVD.

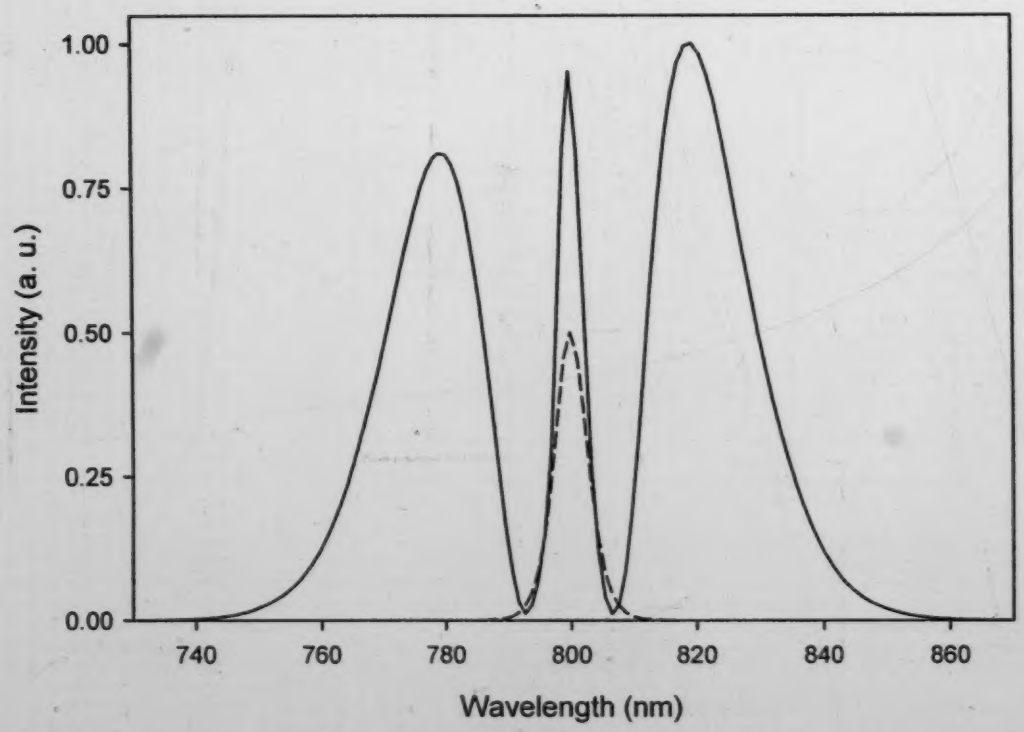

Fig. 5.7 Output spectrum (solid line) of the silver coated hollow fiber at argon pressure of 2.4 atm obtained from the simulation. The spectral broadening is larger on the high frequency side of the spectrum. The peaks are characteristic of SPM induced spectral broadening. The input spectrum (dashed line) is also shown.

The method used for the simulation is a split-step Fourier method [30]. In this method the nonlinear wave equation for the field amplitude is written in terms of a linear operator which includes the dispersion and loss effects and a nonlinear operator which includes the self phase modulation and self steepening effects. The dispersion and absorption effects are calculated in the frequency domain using the fast Fourier transform (FFT) and the nonlinear refractive index effects are calculated in the time domain. The

method is implemented by dividing the length of the hollow fiber into small segments with length h. Starting at the input of the first segment, the nonlinear operator is used in the time domain and the pulse envelope is calculated at $z = h$. Next, the FFT of the resulting pulse envelope is obtained and the linear operator is applied in the frequency domain. This completes the solution for the first segment. The same procedure is applied to the remaining segments by using the previous result as input and finding the pulse envelope at the output of each successive segment.

The program code was written in MATLAB. The length of the fiber was divided to fifty segments, each having a length of one cm, and 1024 points were used to represent the pulse envelope in the time domain. Because of the speed of the FFT, the program runs quickly and the results are obtained in less than one minute on a Pentium 4, 1.6 GHz computer. If the number of steps in space and the number of points in time are increased, the run time of the program can increase to several minutes. Error analysis shows that the method described above is accurate to second order in step size h. To improve the accuracy to third order in step size h, a different procedure called the symmetrized split step Fourier method can be used to propagate the optical pulse over one segment. The main difference is that within each segment the propagation of the optical field is carried out in three steps. The dispersion effect is used to propagate the optical field over a distance of $h/2$. The nonlinear effect is then used at the midpoint of the segment with a step size of h. The linear operator is used again with a step size of $h/2$ and the optical field at the output of the segment is obtained. This procedure was also implemented for simulating the nonlinear wave equation, but no difference in results was observed for the case considered here.

The dispersion equations for a Brewster angle prism pair made of fused silica, which were given in chapter 4, are used in order to simulate the pulse compression. The calculated dispersion parameters for the prism pair compressor are β_2= 9.6 fs^2/cm and β_3= 14.2 fs^3/cm. The shortest compressed pulse width of 20 fs is obtained for a prism separation of 60 cm. The compressed pulse for the silver coated hollow fiber is shown in Fig. 5.8. It can be seen that some of the energy contained in the wings has not been compressed. As explained earlier, this is due to the fact that the frequency chirp is only linear in the central part of the pulse.

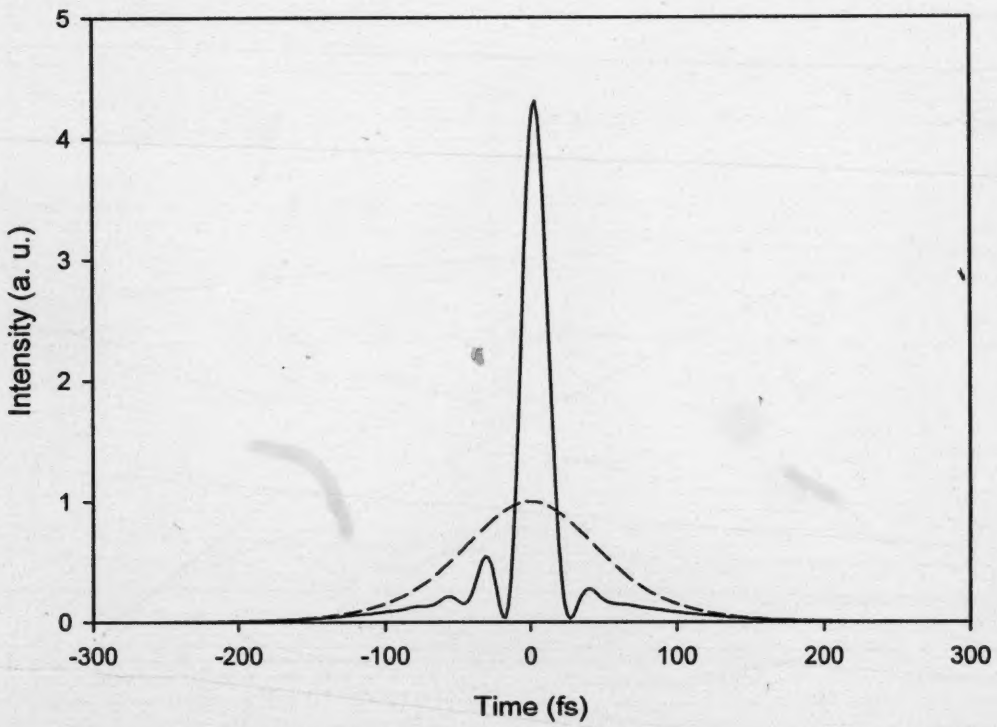

Fig. 5.8 Calculated compressed (solid line) and input (dashed line) pulses for the silver coated hollow fiber at argon pressure of 2.4 atm. A fused silica prism pair with spacing of 60 cm was used to compress the frequency broadened output pulses of the hollow fiber. Because the chirp is linear only in the central portion of the pulse, some of the energy in the wings is not compressed.

In order to examine the effect of prism spacing on the amount and quality of pulse compression, the propagation of an optical pulse through the compressor system was simulated by varying the prism separation. If the distance between the prisms is reduced to 50 cm, the amount of compression in the wings decreases as shown in Fig. 5.9. Thus, more energy in the wings remains uncompressed compared to the optimum case where the prism distance is 60 cm. The amount of compression in the central part of the pulse remains approximately the same. For prism separations below 50 cm, the compressed pulse width decreases and the amount of uncompressed energy at the wings of the pulse increases.

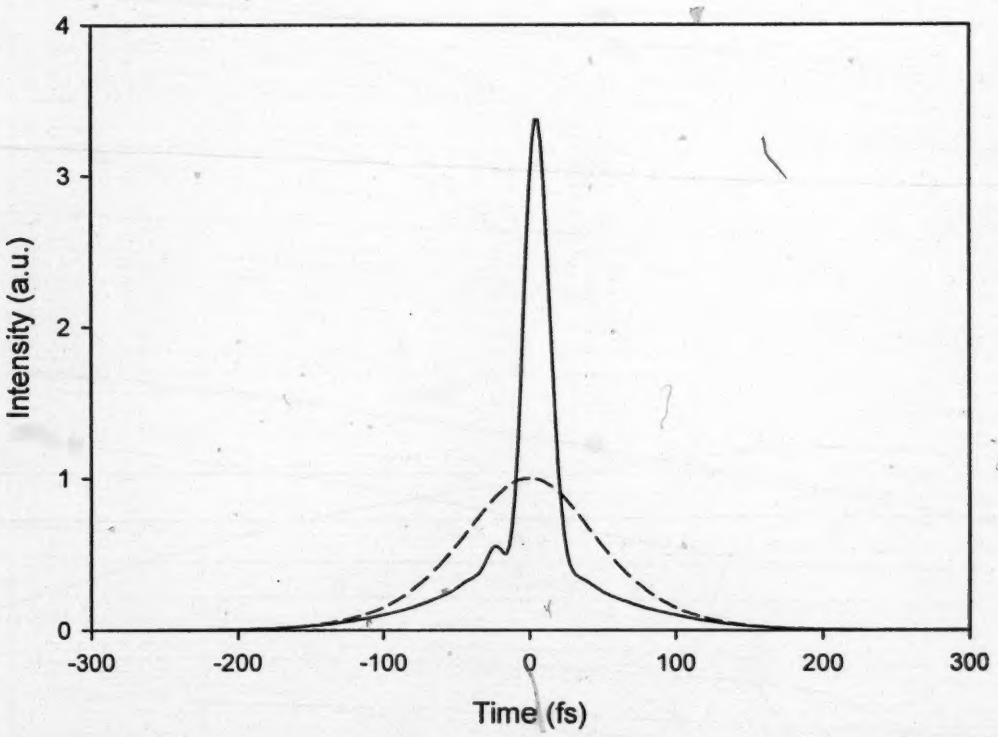

Fig. 5.9 Calculated compressed (solid line) and input (dashed line) pulses for prism separation of 50 cm. When the prism distance is reduced below the optimum value of 60 cm the amount of uncompressed energy in the wings increases.

The simulation of the compressor system shows that as the distance between the prisms is increased beyond 70 cm, the compressed pulse becomes oscillatory. The compressed pulses resulting from the simulation for prism separations of 70 and 80 cm are shown in Fig. 5.10 and Fig. 5.11. There is a slight decrease in the amount of compression for prism spacing of 80 cm. But, the amplitude of oscillations at the wings has grown compared to the optimum distance of 60 cm indicating that more uncompressed energy is contained in the wings. Increasing the prism separation above 80 cm causes the compressed pulse to become completely oscillatory.

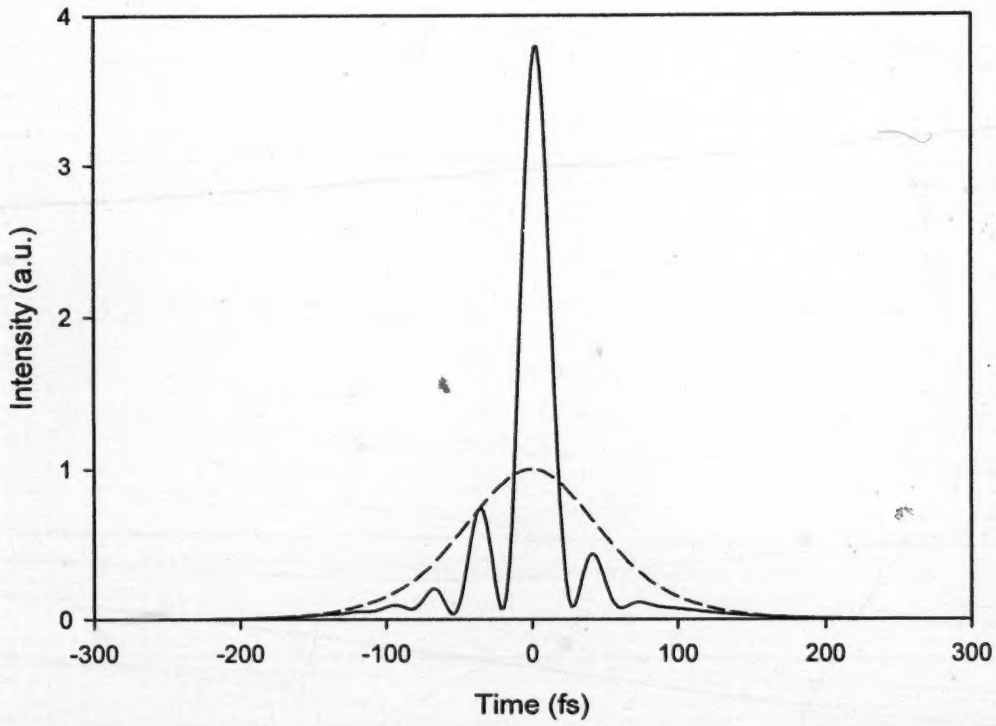

Fig. 5.10 Compressed (solid line) and input (dashed line) pulses for prism separation of 70 cm. By increasing the prism distance above the optimum value of 60 cm, there is a slight decrease in the amount of compression. The amplitude of oscillations at the wings also increases.

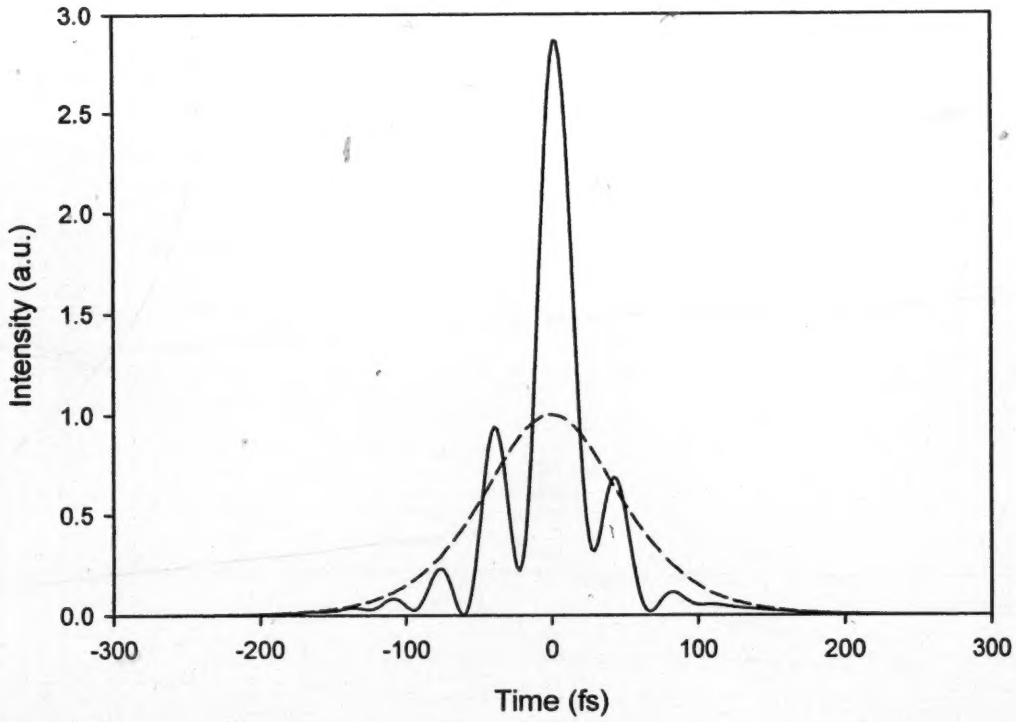

Fig. 5.11 Compressed (solid line) and input (dashed line) pulses for prism separation of 80 cm. By increasing the prism distance beyond 70 cm, the amount of compression decreases. The amplitude of oscillations at the wings has also grown indicating that more uncompressed energy is contained in the wings.

The propagation of the optical pulses inside the hollow fiber was also simulated using an unchirped Gaussian pulse for which the normalized optical field amplitude is given by

$$U(0,T) = \exp\left(-\frac{T^2}{2T_0^{\,2}}\right) \tag{5.11}$$

where T_0 is the 1/e intensity half width of the pulse equal to $T_{FWHM}/1.665$. Using the values for dispersion parameters β_2 and β_3 of the HE_{11} mode, the second and third order

dispersion lengths are found to be $L_D = 111$ m and $L'_D = 8973$ m. The nonlinear length is calculated to be $L_{NL} = 5.92$ cm, using the nonlinear refractive index of argon n_2 and the effective area of the mode A_{eff}. With these new values of the dispersion and nonlinear lengths, the nonlinear wave equation was simulated for a Gaussian input pulse. The output pulse is shown in Fig. 5.12. As can be seen, similar to the previous case, the output pulse has not broadened and has some distortion which is due to the self steepening effect.

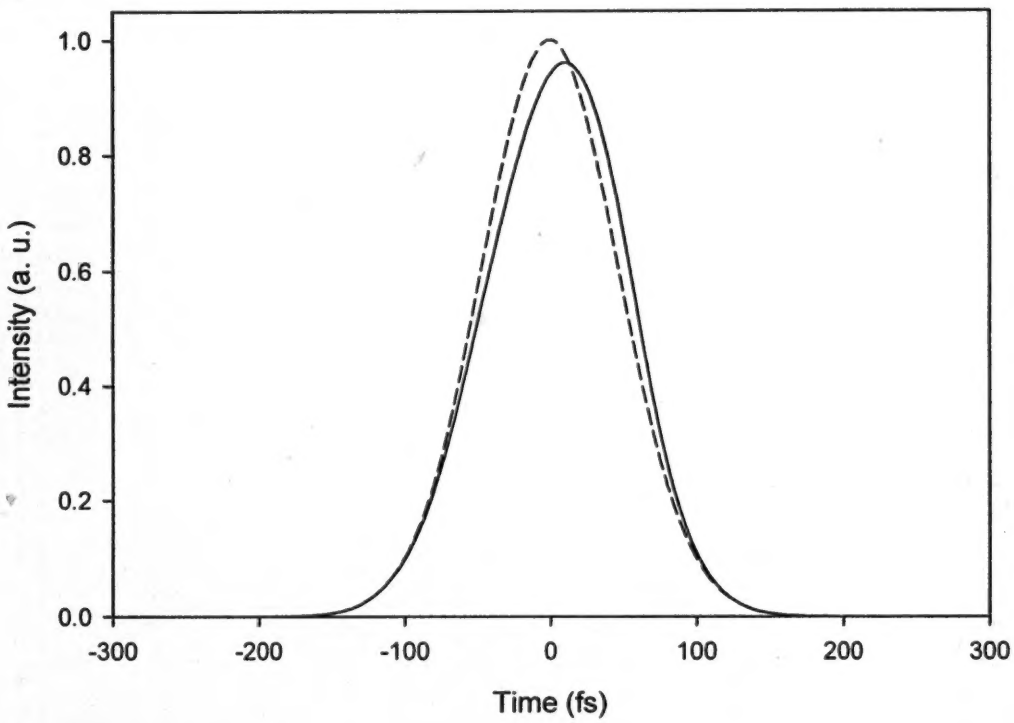

Fig. 5.12 Input (dashed line) and output (solid line) pulse shapes obtained from simulating the propagation of Gaussian optical pulses through the silver coated hollow fiber for an argon pressure of 2.4 atm.

The frequency chirp is shown in Fig. 5.13, which has a linear part in the central portion of the pulse. The amount of frequency chirp has increased compared to the

previous case where a hyperbolic secant input pulse was used, which leads to more spectral broadening and larger spectral width. Again, a prism pair with negative chirp can be used to compress the output optical pulse.

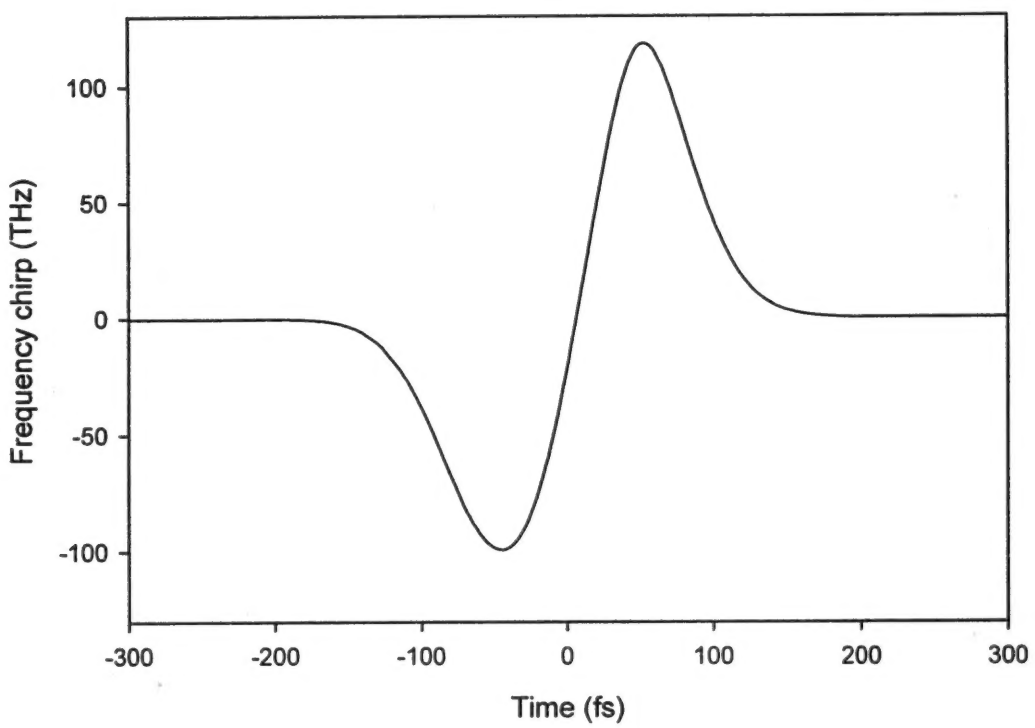

Fig. 5.13 Frequency chirp of the output pulse (shown in Fig. 5.12) for argon pressure of 2.4 atm, assuming a Gaussian input pulse.

The output spectrum of the hollow waveguide is shown in Fig. 5.14, with the full width at half maximum of the output spectrum equal to about 69 nm. The spectral width has increased by 10 nm compared to the spectral width of 59 nm obtained when the input pulse was assumed to be hyperbolic secant. Assuming a Gaussian pulse shape, we expect to compress the pulses to 14 fs. Using the same dispersion equations for a fused silica

prism pair, the shortest compressed pulse width of 19 fs was obtained for a prism separation of 55 cm. The compressed pulse is shown in Fig. 5.15.

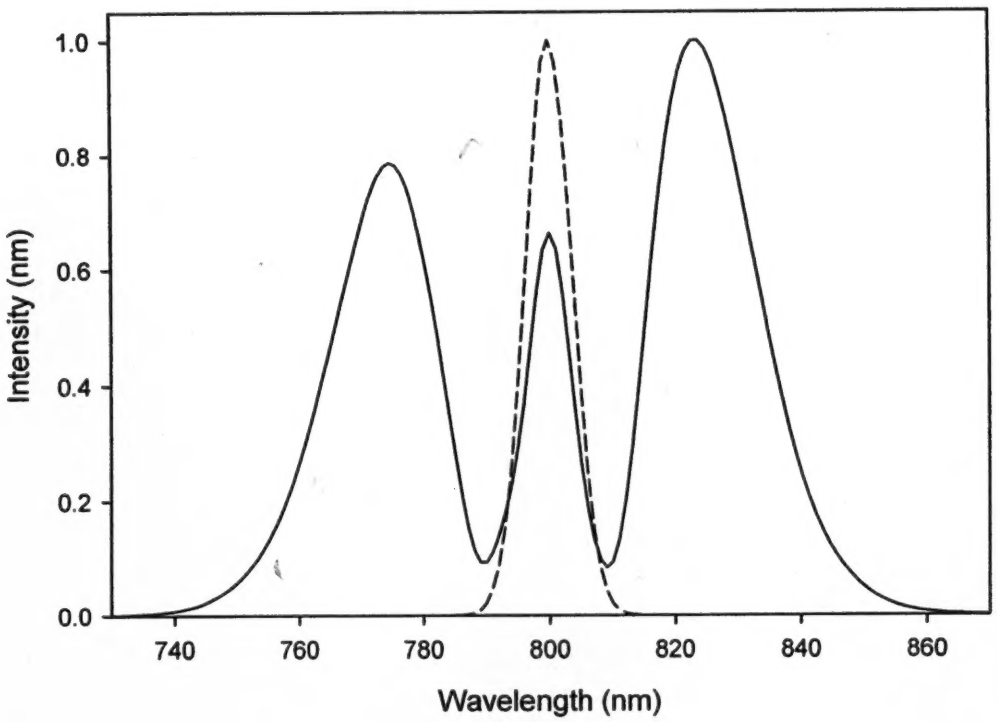

Fig. 5.14 Output spectrum (solid line) of the silver coated hollow fiber at argon pressure of 2.4 atm, obtained from the simulation for Gaussian input pulses. The input spectrum (dashed line) is shown for comparison.

Another optical pulse compression simulation was also performed using the silver coated hollow fiber at argon gas pressure of 1.5 atm. The dispersion values for the hollow fiber filled with argon at 1.5 atm are β_2=21.46 fs^2/m and β_3=23.85 fs^3/m. The values for the dispersion length and the nonlinear length are calculated to be L_D=182 m and L_{NL}=10 cm. As we can see the dispersion length is very large compared to the nonlinear length and the hollow fiber length. Therefore, the dispersion does not play an important role and

the output pulse shape should be very similar to the input pulse shape with very little pulse broadening. The nonlinear length is still small compared to the dispersion length and the hollow fiber length. But, it is larger than the nonlinear length for gas pressure of 2.4 atm. Thus, the nonlinear effects are important and we expect spectral broadening of the output pulse. However, the amount of spectral broadening should be less than before where the argon gas pressure was 2.4 atm.

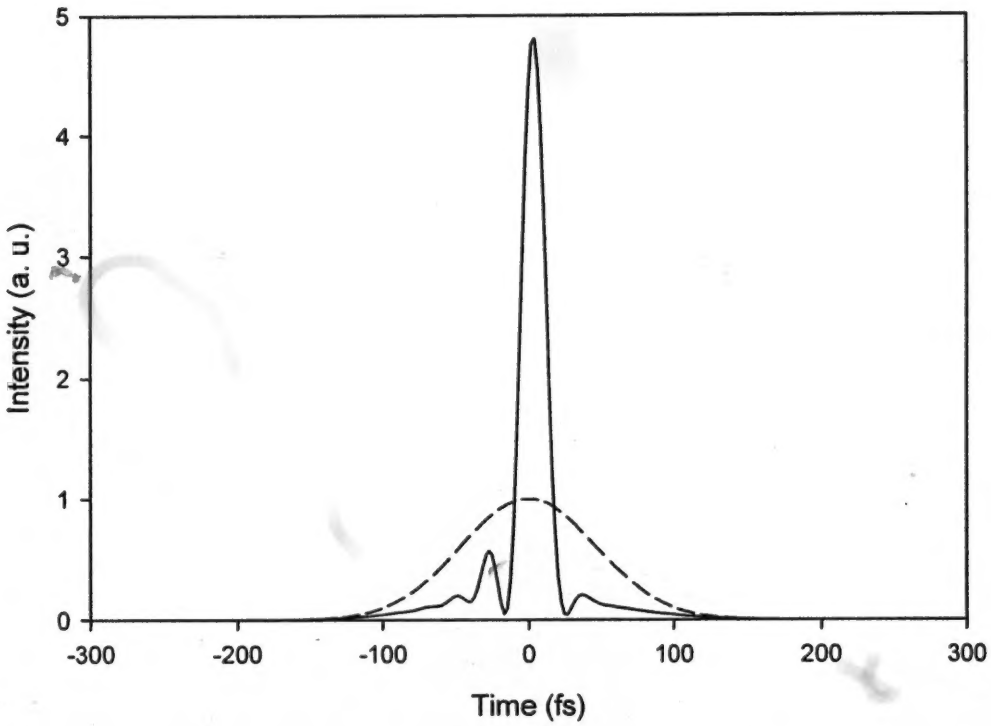

Fig. 5.15 Calculated compressed (solid line) and input (dashed line) pulses for the silver coated hollow fiber at argon pressure of 2.4 atm, using Gaussian input pulses. A fused silica prism pair with spacing of 55 cm was assumed for compression in the simulation.

The wave equation (5.3) was simulated with new values of the dispersion and nonlinear lengths. The calculated output pulse of the hollow fiber is shown in Fig. 5.16.

As can be seen the output pulse has not broadened which shows that the dispersion terms in the nonlinear wave equation are not very important. The output pulse has some distortion which is due to the self steepening term in equation (5.3), as explained earlier. The frequency chirp is shown in Fig. 5.17. It has a linear positive chirp in the central portion of the pulse. It can be seen that the amount of frequency chirp is less compared to the frequency chirp calculated for argon pressure of 2.4 atm. Therefore, the spectral width of the output spectrum will be less than before. The asymmetry in the frequency chirp is also apparent. Thus, the spectral broadening on the high frequency side of the spectrum will be slightly larger.

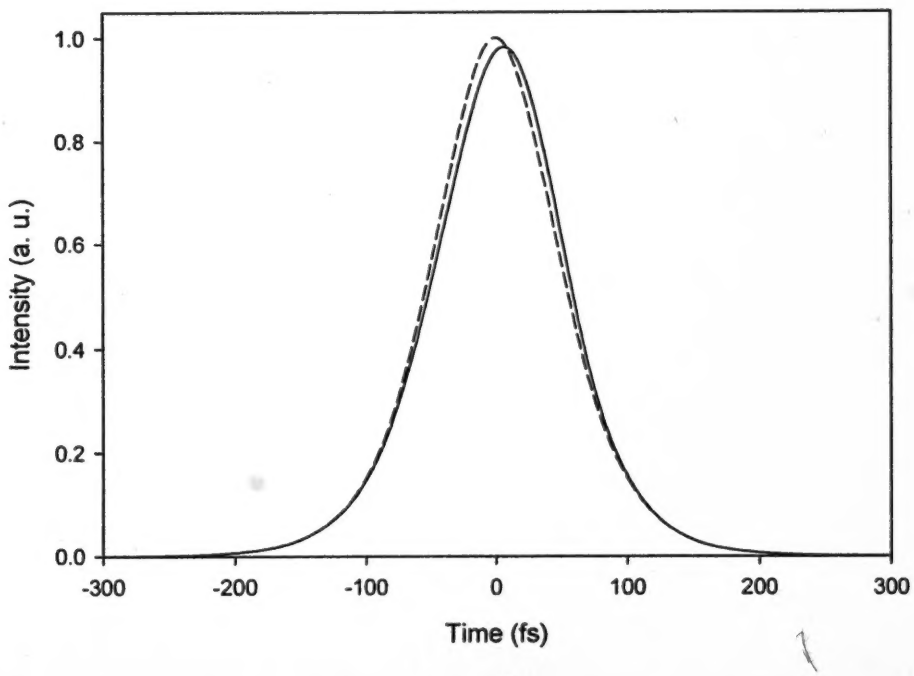

Fig. 5.16 Input (dashed line) and output (solid line) pulse shapes obtained from simulating the propagation of optical pulses through the silver coated hollow fiber for argon pressure of 1.5 atm. The propagation distance is 50 cm. The distortion of the output pulse is due to the nonlinear effects.

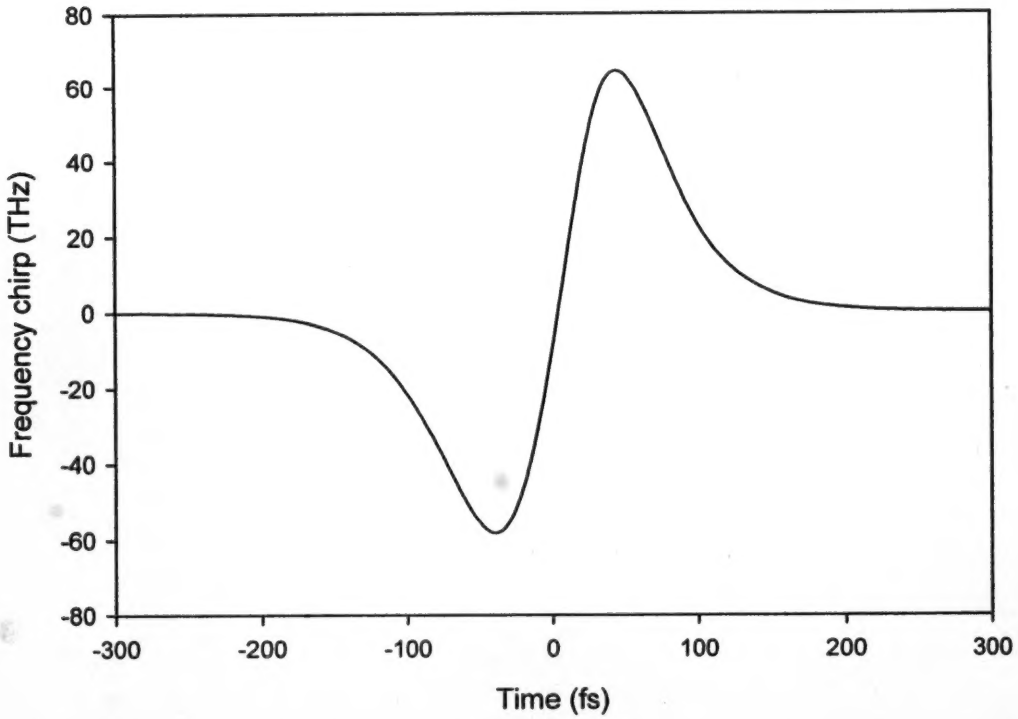

Fig. 5.17 Calculated frequency chirp of the output pulse for argon pressure of 1.5 atm. It shows a linear positive chirp in the central portion of the pulse. The frequency chirp is asymmetric and is larger near the trailing edge. The amount of frequency chirp is less compared to the frequency chirp for pressure of 2.4 atm.

The output spectrum of the hollow waveguide is shown in Fig. 5.18. The full width at half maximum of the output spectrum is about 36 nm. Reducing the pressure has lead to a decrease in the nonlinear effects and, thus, less spectral broadening. Assuming a Gaussian pulse shape, we expect to compress the frequency broadened pulses to 26 fs. The dispersion equations for a prism pair made of fused silica were used in the simulation. The shortest compressed pulse width of 30 fs was obtained for a prism separation of 70 cm. The compressed pulse is shown in Fig. 5.19.

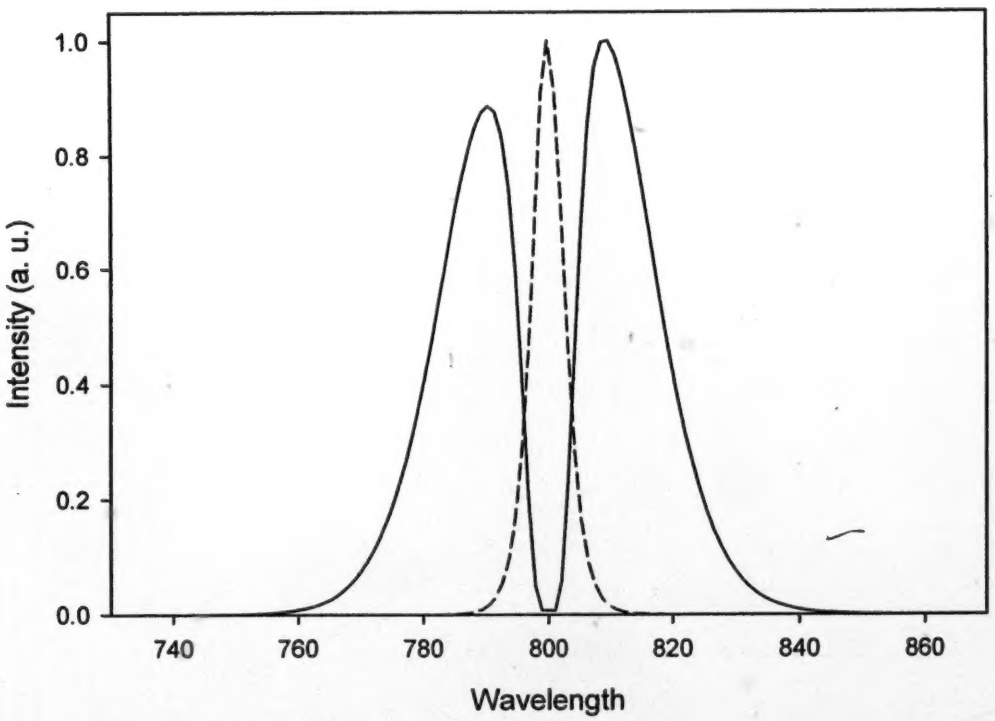

Fig. 5.18 Output spectrum (solid line) of the silver coated hollow fiber at argon pressure of 1.5 atm obtained from the simulation. The peaks are characteristic of SPM induced spectral broadening. The number of peaks has reduced which is due to larger value of the nonlinear length (10 cm) for 1.5 atm compared to its value (6.3 cm) for 2.4 atm. The input spectrum (dashed line) is also shown.

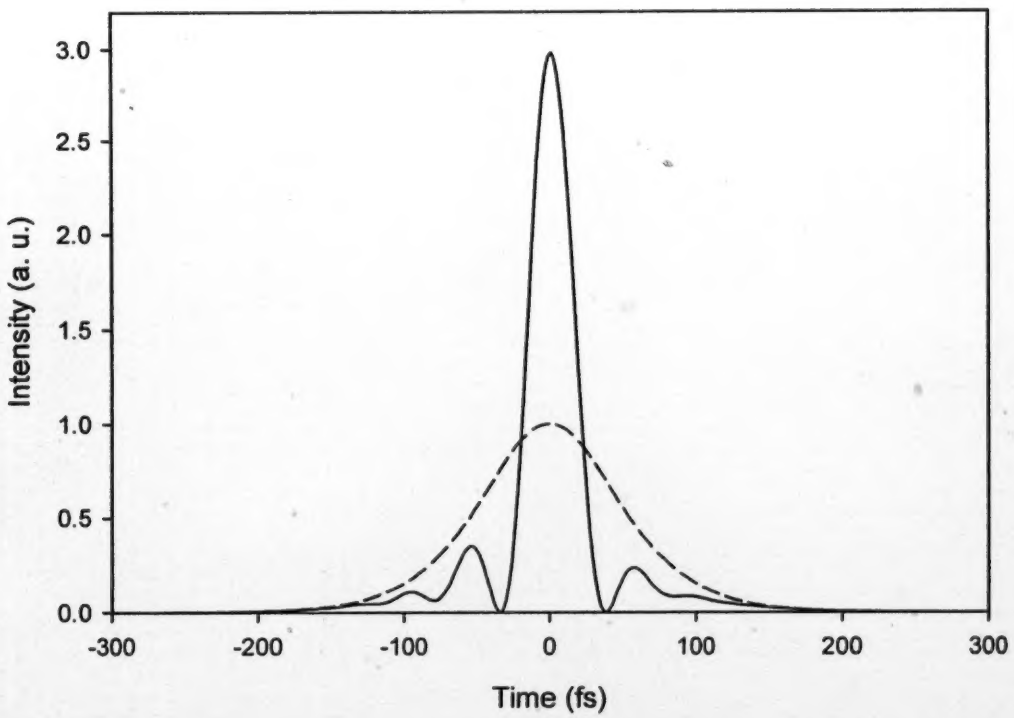

Fig. 5.19 Calculated compressed (solid line) and input (dashed line) pulses for the silver coated hollow fiber at argon pressure of 1.5 atm. A fused silica prism compressor was used to compress the frequency broadened output pulses of the hollow fiber. Because the chirp is linear only in the central portion of the pulse, some of the energy in the wings is not compressed. The compressed pulse width has increased to 30 fs for 1.5 atm compared to 20 fs for 2.4 atm.

5.3 Experimental results

The experiments were performed using a Ti:sapphire laser amplifier (Spectra Physics Hurricane). The pulse energy was set to 250 μJ using an attenuator consisting of a half wave plate and a polarizer. The pulse duration was 110 fs and the wavelength of the pulses was 800 nm. The silver coated hollow fiber with bore size of 250 μm and length of 50 cm was used to obtain spectral broadening of the optical pulses. As explained in chapter 3, the silver film is deposited inside a hollow silica waveguide in order to reduce the losses. The experimental setup is shown in Fig. 5.20.

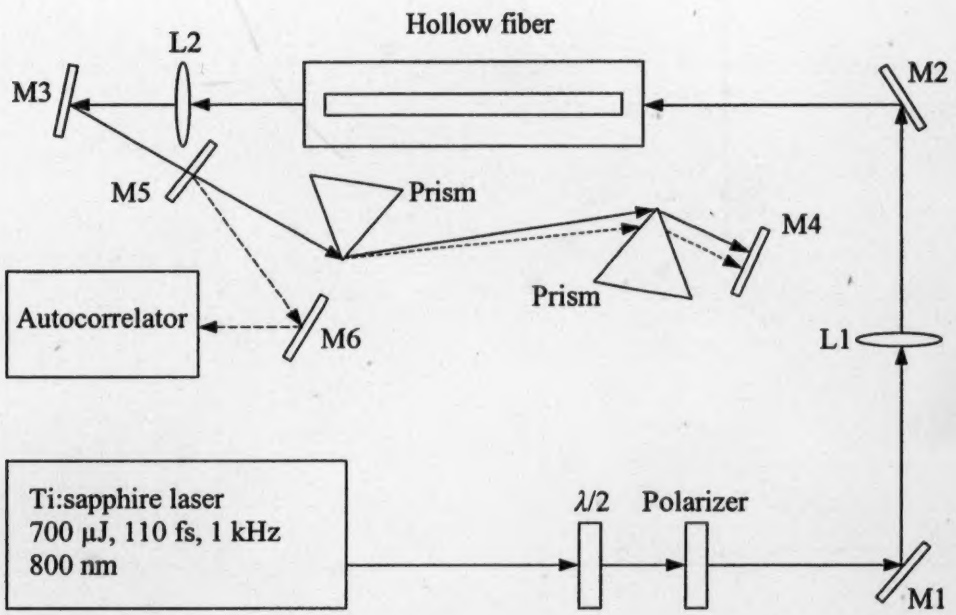

Fig. 5.20 The experimental setup used for optical pulse compression. The hollow fiber is in a tube filled with argon gas. The lenses are antireflection coated. A fused silica prism pair is used to obtain compression. The reflected beam is separated from the input beam vertically by adjusting mirror M4 and the output beam is obtained using mirror M5.

The hollow fiber was kept straight in a V groove in an aluminum bar and placed in a tube filled with argon gas. Antireflection coated windows made of fused silica with thickness of 0.5 mm were used to couple the laser beam in and out of the tube. The argon gas pressure was set to 2.4 atm. The half wave plate and polarizer are used to attenuate the 700 μJ pulse energy of the laser output beam to 250 μJ at the input of the hollow fiber. A 75 cm focal length lens (L1) was used to couple the laser pulses into the hollow fiber. The focal length of the lens was chosen to maximize the coupling of the free space TEM_{00} mode of the laser pulses to the HE_{11} mode of the hollow fiber. A transmission of 95% (0.44 dB/m) was measured for the silver coated hollow fiber as described in chapter 3. A transmission of 94% was measured from the entrance of the input window to the output of the exit window of the gas enclosure.

The output spectrum was measured using an Ocean Optics S2000 Fiber Optic Spectrometer. Light is transmitted into the spectrometer using a 200 μm diameter optical fiber with numerical aperture of 0.22. The light exiting the optical fiber is collimated by a spherical mirror. A grating with groove density of 600 lines/mm, wavelength coverage of 490 to 1100 nm, and blaze wavelength of 750 nm is used to diffract the light. A 25 μm slit is mounted at the input of the spectrometer channel. With the 600 lines/mm grating, this slit provides a resolution of approximately 1.25 nm. A second spherical mirror is used to focus the light and project an image of the spectrum onto a one dimensional CCD array. The data is transferred to a computer through an A/D converter.

The output spectrum is shown in Fig. 5.21. The spectrum has broadened considerably compared to the spectrum of input pulses and shows oscillations that are

characteristic of self phase modulation. The measured spectral width is approximately 55.6 nm which compares well with the simulation result of 59 nm. The spectrum obtained from simulation is compared with the spectrum obtained from experiment in Fig. 5.22, which shows good agreement. The difference between the calculated and experimental spectral widths is because the theoretical attenuation constant of the silver coated hollow fiber was used in the numerical calculations. The extra losses in the experiment leads to reduced spectral broadening.

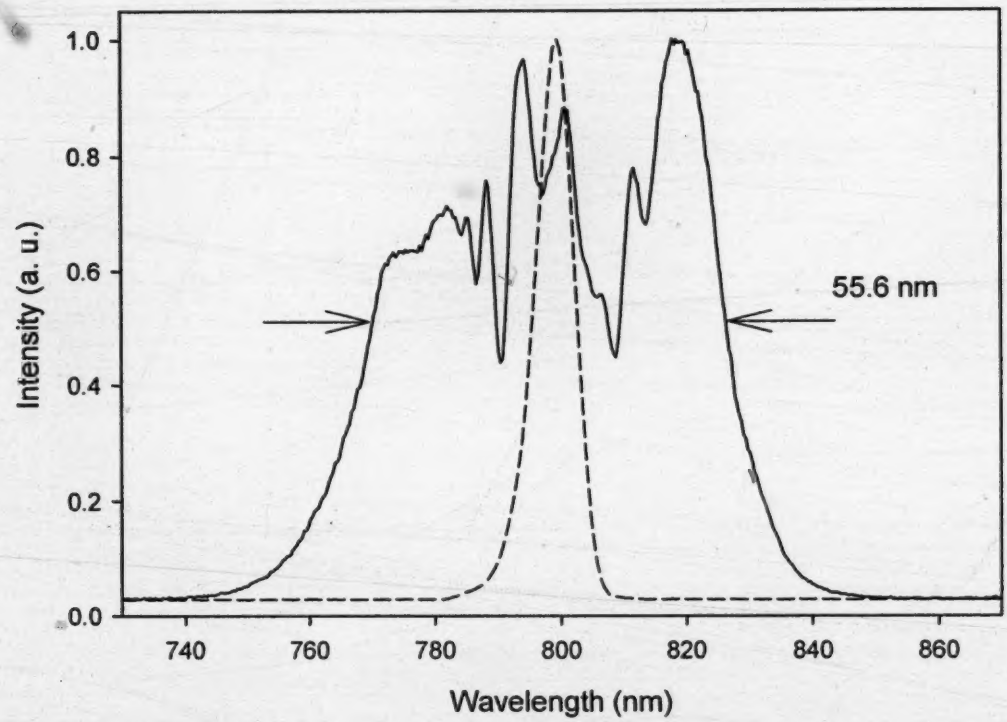

Fig. 5.21 Measured output spectrum (solid line) of the silver coated hollow fiber filled with argon at 2.4 atm. Input pulse energy is 250 μJ and input pulse width is 110 fs. Spectrum of the input pulse (dashed line) is shown for comparison. The spectral width is 55.6 nm.

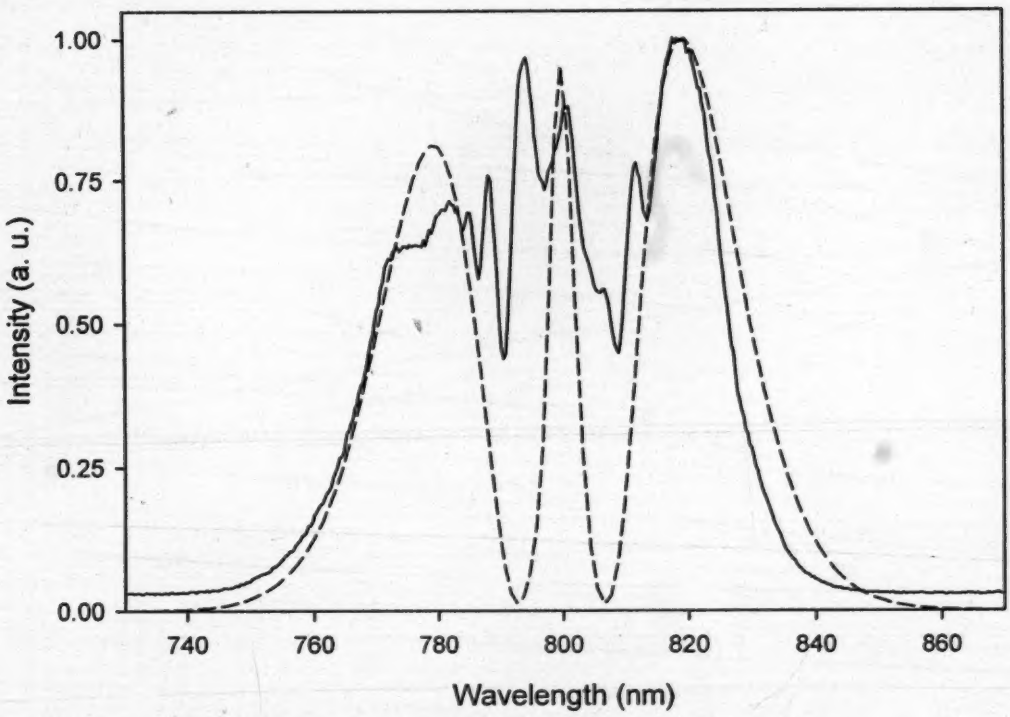

Fig. 5.22 Comparison of output spectrum measured from experiment (solid line) with output spectrum obtained from simulation (dashed line) for the silver coated hollow fiber. The input pulse energy is 250 μJ, the input pulse width is 110 fs, and the argon gas pressure is 2.4 atm. There is close agreement between the theoretical and experimental spectra.

The pulses exiting the silver coated hollow fiber were collimated and propagated through a prism pair. The pulses leaving the second prism were reflected back traveling along the same path through the prisms, displaced vertically to separate the beams. The distance between the prisms (apex to apex) was set to 60 cm which was the value obtained from the simulation for optimum pulse compression. The frequency broadened pulses were compressed to 20 fs. The autocorrelation trace of the compressed pulses is shown in Fig. 5.23. The autocorrelation trace of the compressed pulse obtained from simulation, shown in Fig. 5.8, is also plotted. We can see that there is good agreement

between the calculated and experimental results. The autocorrelation of a 20 fs Gaussian pulse is also shown for comparison. Using the spectral width of 55.6 nm and the pulse width of 20 fs, the time bandwidth product is calculated to be 0.52. Therefore, the compressed pulses are 1.18 times transform limited, assuming a Gaussian shape.

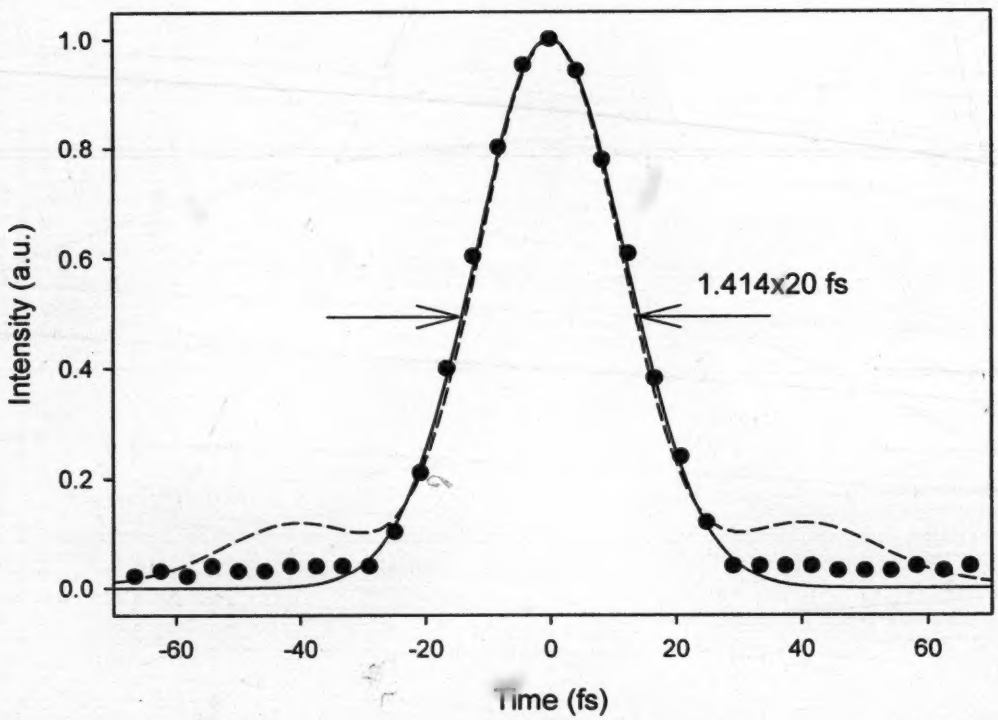

Fig. 5.23 Measured autocorrelation trace (dots) of the compressed pulses and calculated autocorrelation trace (solid line) assuming a Gaussian pulse shape. The argon pressure is 2.4 atm. The output pulses of the silver coated hollow fiber were compressed using a fused silica prism pair with separation of 60 cm. The autocorrelation of the compressed pulse of Fig. 5.8 is also shown (dashed line).

A single shot background free autocorrelator (Spectra Physics Positive Light, Model SSA) was used to measure the pulse width. The incoming laser pulses are split into two beams of equal intensity that are displaced from a common optical axis. The two

beams are then recombined noncollinearly in a nonlinear crystal (KDP) for frequency doubling. A micrometer is used to impart an adjustable delay on one of the beams. A CCD diode array is used to monitor the intensity of the second harmonic generation as a function of delay between the two pulses, which is then displayed on an oscilloscope. In order to determine the actual pulse width from the autocorrelation trace, it is necessary to assume a pulse shape. If a Gaussian pulse shape is assumed, the FWHM of the autocorrelation trace is divided by $\sqrt{2}$, and for a hyperbolic secant pulse shape it is divided by 1.54. In order to calibrate the autocorrelator, the delay micrometer was adjusted by a fixed amount in μm and the amount that the autocorrelation peak moved on the oscilloscope trace was measured in μs. By using the speed of light and converting the optical path length to optical delay and dividing it by the amount the peak moved on the oscilloscope, a calibration factor of 0.416 fs/μs was obtained. By assuming a Gaussian pulse shape and dividing by $\sqrt{2}$, the actual pulse duration is derived using the conversion factor of 0.294 fs/μs. Pulse widths of ≥ 20 fs can be measured with the autocorrelator.

In order to determine the spatial profile of the beam exiting the silver coated hollow fiber, images were taken at different distances from the output using a CCD detector. The spatial output intensity profile at a distance of 25 cm is shown in Fig. 5.24. We can see that there is close agreement between the experimental data and the Gaussian fit. The beam diameter of the output optical pulse can be calculated theoretically by expanding the electric field amplitude of the HE_{11} mode into free space Gaussian modes, as explained in chapter 3. When the silver coated hollow fiber is placed inside the tube filled with argon gas, the alignment of the input laser beam into the waveguide becomes more difficult. By calculating the beam diameters and comparing with the measured

values, we can get an indication of the output mode quality. The calculated beam diameters are compared with the experimental values in Fig. 5.25. As can be seen they agree very well indicating that the output of the hollow fiber is an HE_{11} mode.

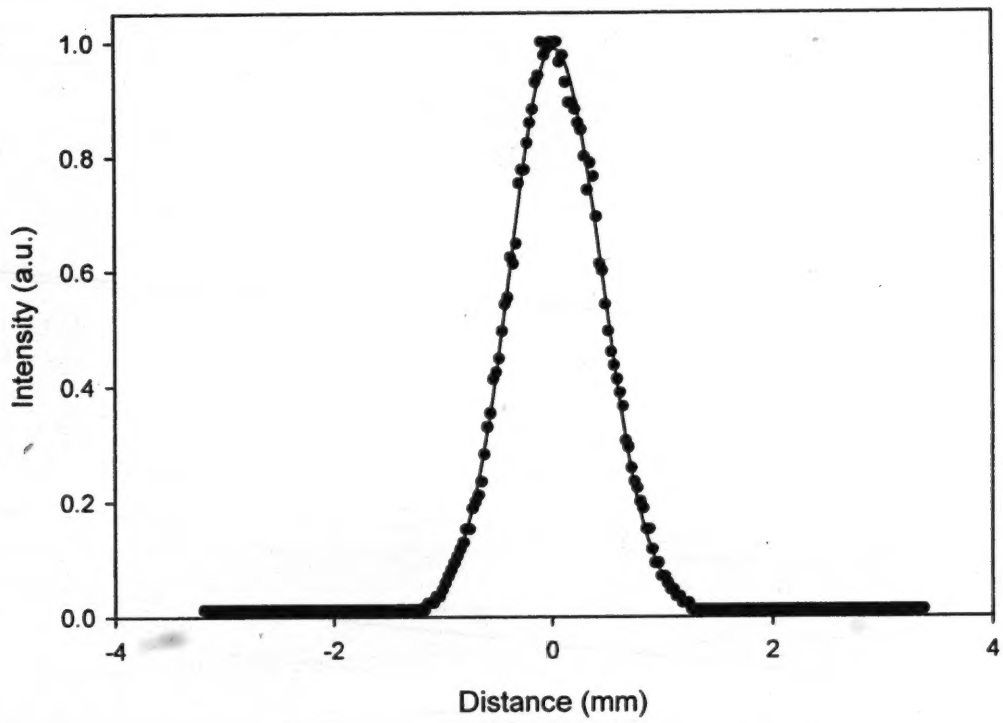

Fig. 5.24 Spatial output intensity of the silver coated hollow fiber at a distance of 25 cm from the output end of the fiber. Dots are the experimental data. The Gaussian fit (line) to the data is also shown.

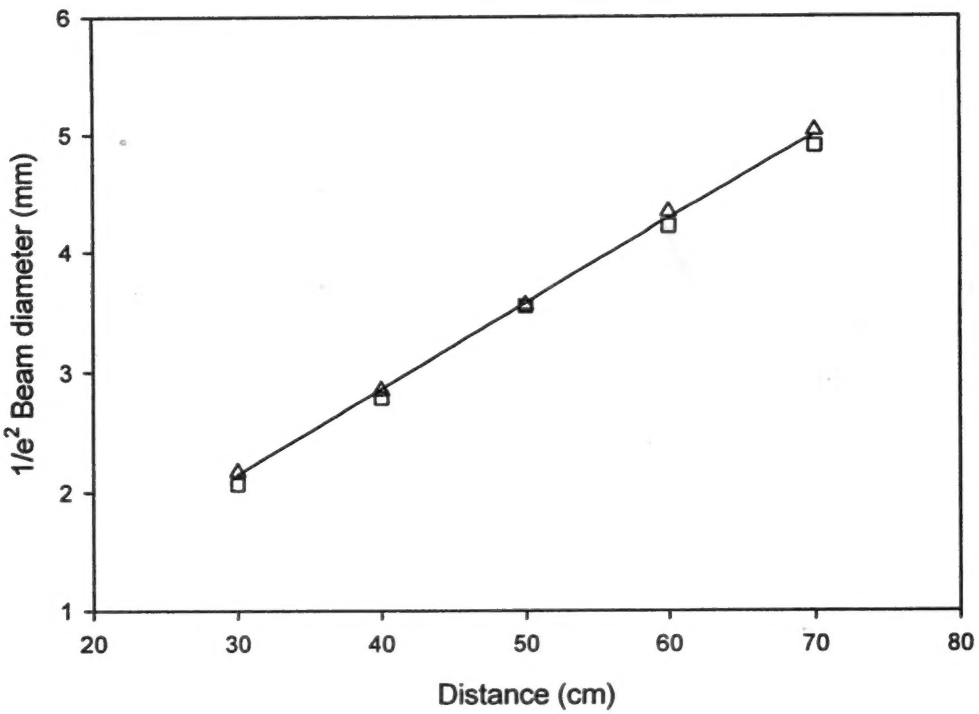

Fig. 5.25 Comparison of calculated (line) and experimental beam diameters as a function of distance for the output beam of the silver coated hollow fiber. Distance is measured from the output end of the hollow fiber. Triangles are the horizontal beam diameters and squares are the vertical beam diameters measured experimentally.

Another optical pulse compression experiment was also performed using the silver coated hollow fiber at argon gas pressure of 1.5 atm. The simulation results for argon pressure of 1.5 atm were presented in the previous section. The optical pulse compression experiment was performed with input pulse energy of 250 μJ, input pulse width of 110 fs, and argon gas pressure of 1.5 atm. The measured output spectrum is shown in Fig. 5.26. The spectrum has broadened considerably compared to the spectrum of input pulses. The spectral width is approximately 28 nm full width at half maximum. The output spectrum obtained from the simulation is compared with the experimental

output spectrum in Fig. 5.27. Again, the difference between the calculated and experimental spectral widths is due to the use of the theoretical attenuation constant of the silver coated hollow fiber in the numerical calculations. The experimental losses of the hollow fiber are larger which yields less spectral broadening compared to the calculations.

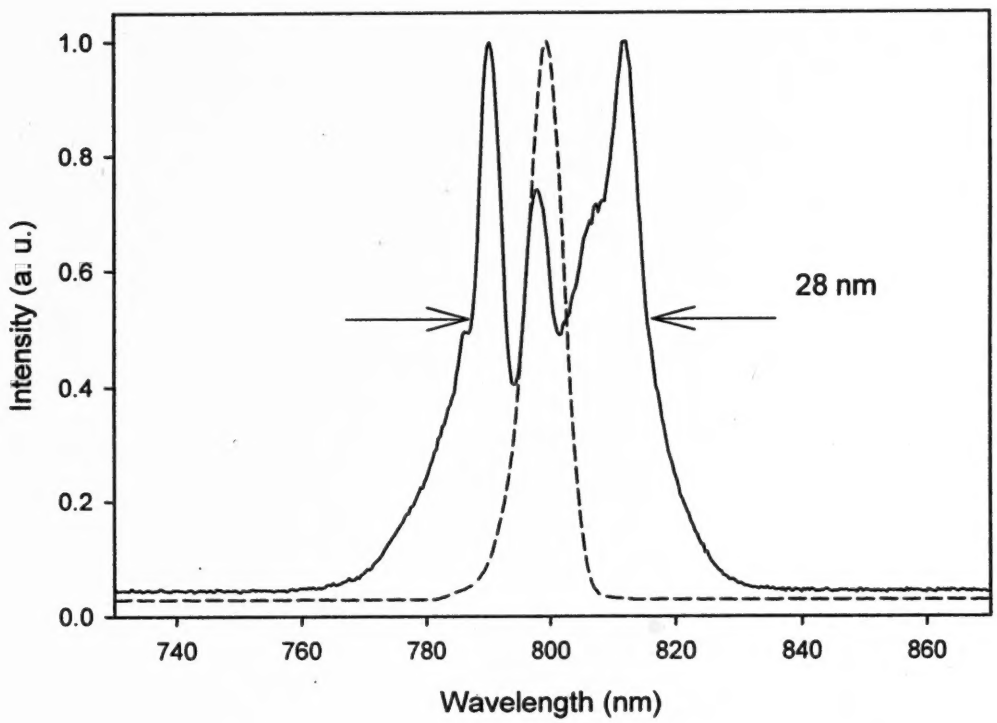

Fig. 5.26 Measured output spectrum (solid line) of the silver coated hollow fiber filled with argon at 1.5 atm. Input pulse energy is 250 μJ and input pulse width is 110 fs. Spectrum of the input pulse (dashed line) is shown for comparison. The spectral width is 28 nm.

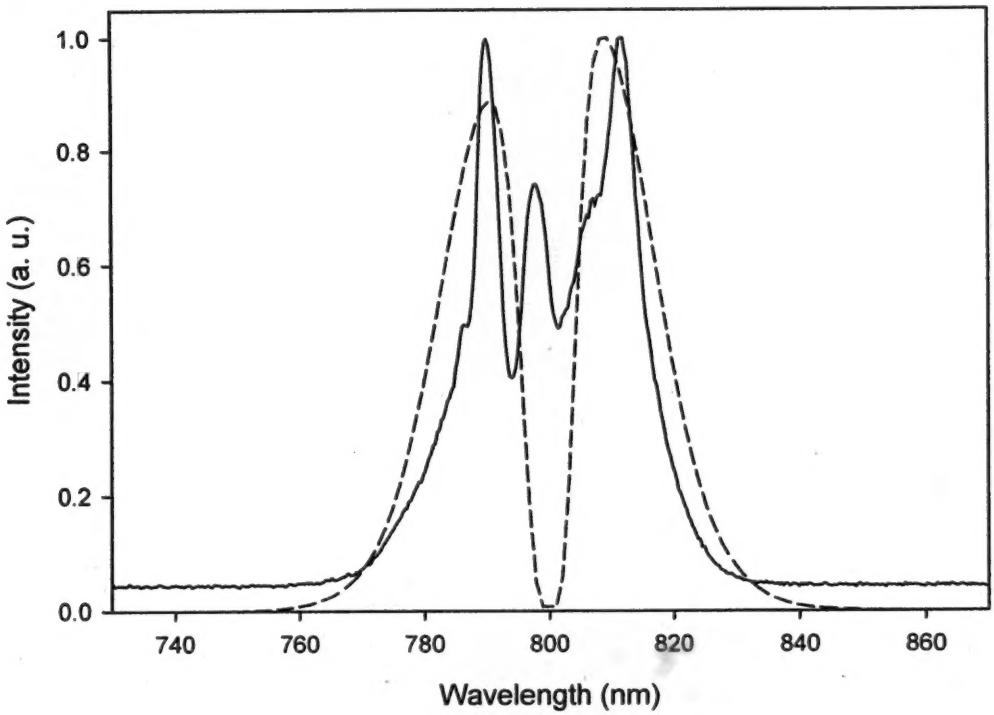

Fig. 5.27 Comparison of output spectrum measured from experiment (solid line) with output spectrum obtained from simulation (dashed line) for the silver coated hollow fiber. The input pulse energy is 250 μJ, the input pulse width is 110 fs, and the argon gas pressure is 1.5 atm.

The pulses exiting the silver coated hollow fiber were collimated and propagated through the fused silica prism pair. The pulses leaving the second prism were reflected back traveling along the same path through the prisms, displaced vertically to separate the beams. The distance between the prisms (apex to apex) was set to 70 cm which was obtained from the simulation. The frequency broadened output pulses of the hollow fiber were compressed to 35 fs. The autocorrelation trace of the compressed pulses is shown in Fig. 5.28. The autocorrelation trace of the calculated compressed pulse, which is shown in Fig. 5.19, has also been plotted for comparison. It can be seen that there is good

agreement between the calculated and experimental results. However, the calculated autocorrelation width is slightly smaller than the measured width, which is due to the larger value of the calculated output spectral width. The autocorrelation of a 35 fs Gaussian pulse is also shown. Using the spectral width of 28 nm and the pulse width of 35 fs, the time bandwidth product is found to be 0.459. Therefore, the compressed pulses are approximately transform limited, assuming a Gaussian pulse shape.

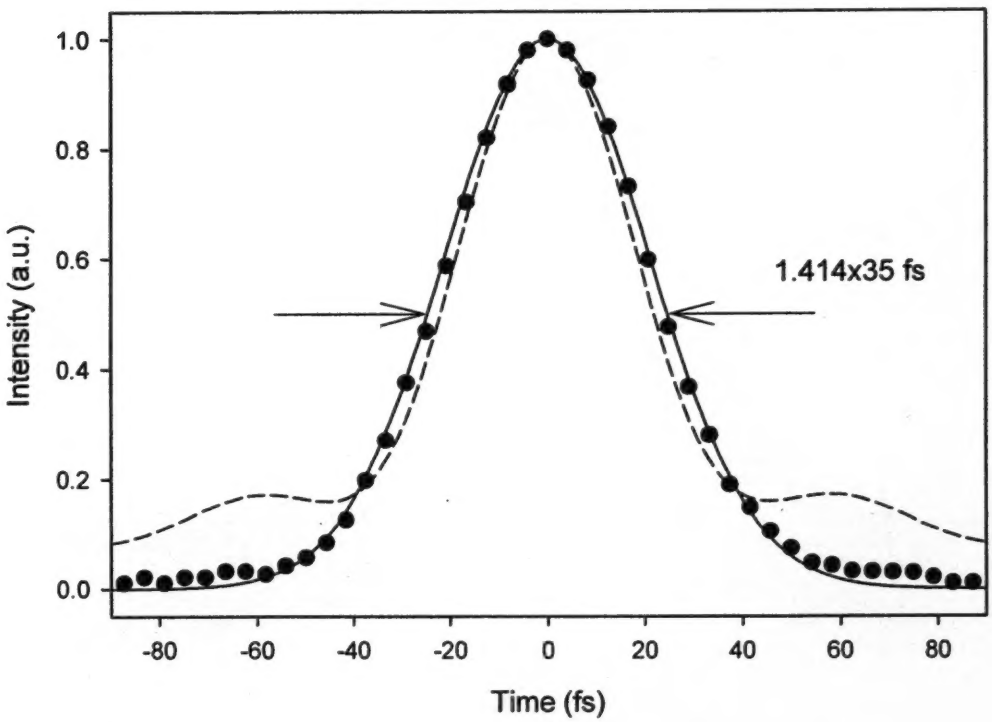

Fig. 5.28 Measured autocorrelation trace (dots) of the compressed pulses and calculated autocorrelation trace (line) assuming a Gaussian pulse shape. The argon pressure is 1.5 atm. The output pulses of the silver coated hollow fiber were compressed using a fused silica prism pair with separation of 70 cm. The autocorrelation of the compressed pulse of Fig. 5.19 is also shown (dashed line).

A 50 cm fused silica hollow fiber with inner diameter of 250 μm was also used for optical pulse compression in order to compare the results with those obtained using the silver coated hollow fiber. Input pulses with energy of 250 μJ and duration of 110 fs were used and the argon gas pressure was set at 2.4 atm. The intensity attenuation constant for the HE_{11} mode propagating in a fused silica hollow waveguide is 0.142 m^{-1}. The dispersion parameters β_2 and β_3 are calculated using the propagation constant for the HE_{11} mode in a fused silica hollow fiber, which were given in the previous section. The values for the dispersion and nonlinear lengths are calculated to be L_D=100 m and L_{NL}=6.3 cm, which are the same as those for the silver coated hollow fiber. The optimum separation between the prisms is also calculated to be 60 cm for the shortest compressed pulse width of 20 fs.

The optical pulse compression was performed using the fused silica hollow fiber. The measured output spectrum is shown in Fig. 5.29 and is compared with the measured output spectrum of the silver coated hollow fiber. As can be seen, the measured output spectrum shows spectral broadening which is very similar to the spectral broadening obtained from the silver coated hollow fiber and with the same spectral width of 55.6 nm. The output pulses exiting the fused silica hollow fiber were compressed using the prism pair. The distance between the prisms, from apex to apex, was set to of 60 cm. A pulse width of 20 fs was measured. The autocorrelation trace of the compressed pulses is shown in Fig. 5.30.

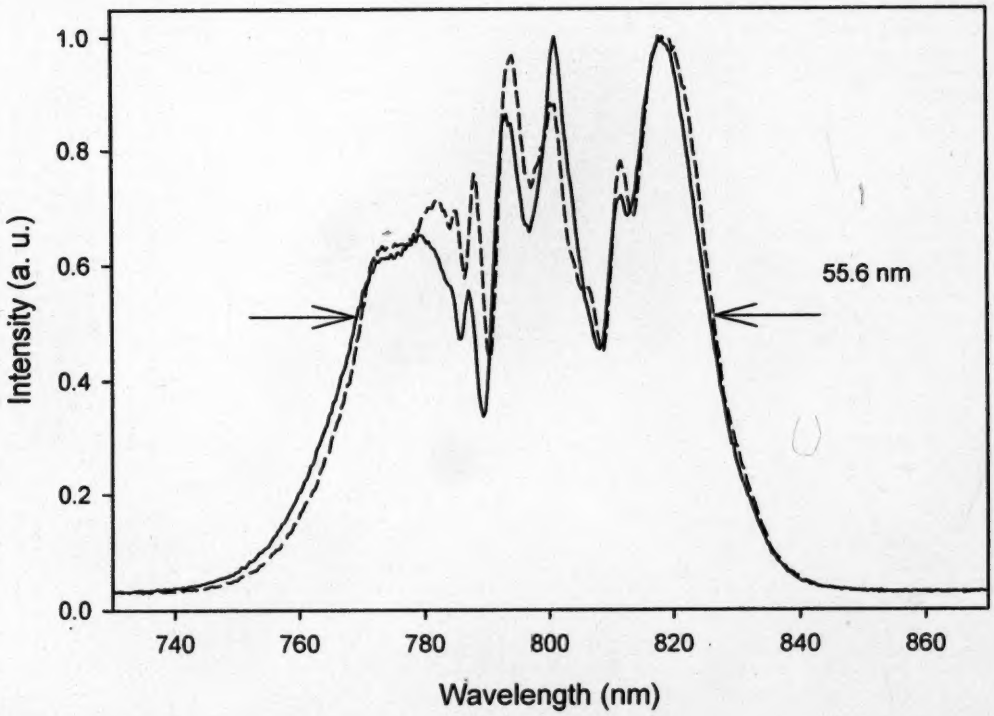

Fig. 5.29 Measured output spectrum (solid line) of the fused silica hollow fiber filled with argon at 2.4 atm. Input pulse energy is 250 μJ and input pulse width is 110 fs. Measured output spectrum of the silver coated hollow fiber (dashed line) is shown for comparison. The spectral width is 55.6 nm.

In a different optical pulse compression experiment using the fused silica hollow fiber, the pulse energy was increased to 300 μJ and the pressure was reduced to 2 atm. These values give the same nonlinear length L_{NL} of 6.3 cm as for pulse energy of 250 μJ and pressure of 2.4 atm. However, the value of the dispersion length L_D changes from 100 m to 126 m. These values of the dispersion length are much greater than the nonlinear length parameter and the length of the hollow fiber. In each case the terms responsible for dispersion in the normalized wave equation (5.3) are not important compared to the nonlinear terms. Therefore, we expect the same amount of spectral

broadening, frequency chirp, and pulse compression in both cases. Simulation of the compressor system with L_D=126 m and L_{NL}=6.3 cm yields a compressed pulse of 20 fs for a prism separation of 60 cm as before. The experiment was performed with pulse energy of 300 μJ and pressure of 2 atm. The prism distance was set to 60 cm as obtained from the simulation and a compressed pulse width of 20 fs was measured.

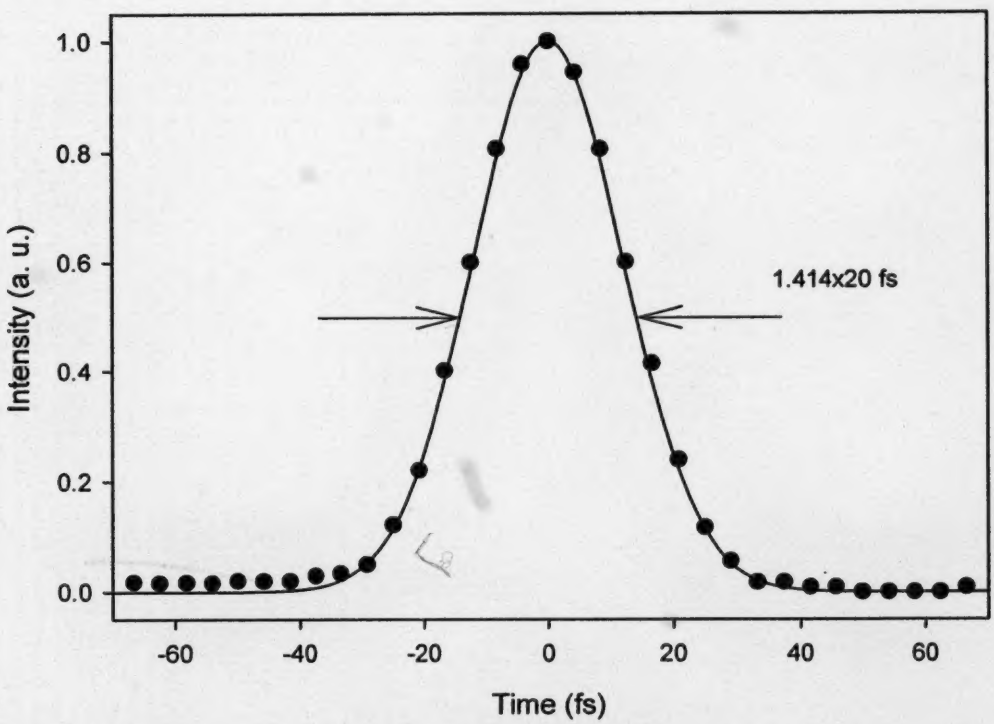

Fig. 5.30 Measured autocorrelation trace (dots) of the compressed pulses and calculated autocorrelation trace (line) assuming a Gaussian pulse shape. The argon pressure is 2.4 atm. The output pulses of the fused silica hollow fiber were compressed using a prism separation of 60 cm.

A transmission of 80% (1.94 dB/m) was measured for the fused silica hollow fiber. For comparison, a typical transmission of 60% for an 85 cm hollow glass fiber (2.61 dB/m) [23], and a transmission of 70% for a 50 cm hollow glass fiber (3.1 dB/m)

[24] have been reported. In Ref. 23 internal diameter of the hollow fiber is 260 μm and the wavelength is 780 nm. In Ref. 24 internal diameter of the hollow fiber is 250 μm and the wavelength is 800 nm. The transmission obtained for the silver coated hollow fiber (0.44 dB/m) is much higher than the above values. The overall transmission of the compressor using the silver coated hollow fiber was 88%. This is significantly higher than the 76% compressor transmission obtained using the fused silica hollow fiber.

5.4 Design considerations for hollow fiber chamber

The silver coated hollow fiber used for optical pulse compression experiment is kept straight in a V groove in an aluminum bar. The aluminum bar is placed in a tube made of plexiglass. Antireflection coated fused silica windows are used in each end of the tube to couple the beam in and out of the hollow fiber. The tube is filled with argon gas and its pressure is kept constant using a pressure gauge. The thickness of the tube must be sufficient to tolerate pressures of a few atmospheres. A wall thickness of 1/4 inch was chosen which according to the manufacturer's specifications has a working pressure of up to 15 atm.

The nonlinear effects in the fused silica windows are very important. It is desired to reduce these effects in order to have a beam with good quality. One nonlinear effect that can be detrimental to the beam quality is the nonlinear phase shift, which is quantified using the *B*-integral given by

$$B = \frac{2\pi}{\lambda}\int_0^L n_2 I(z)dz \qquad (5.12)$$

where λ is the wavelength, n_2 is the nonlinear refractive index of fused silica, and $I(z)$ is the intensity of the beam. We can obtain the maximum value of the B-integral, by using the peak value of the intensity in equation (5.12), yielding

$$B = \frac{2\pi}{\lambda} n_2 IL \tag{5.13}$$

where I is the peak intensity and L is the thickness of the fused silica windows. For good beam quality, it is generally required to keep the value of the B-integral less than one (B<1). Figure 5.31 shows the hollow fiber enclosure with fused silica windows at each end and the coupling lens used to couple the beam into the hollow fiber. In order to calculate the B-integral, we need to know the value of the beam radius at the fused silica window. The beam radius is used to find the intensity. We will choose the beam radius such that the B-integral is less than one.

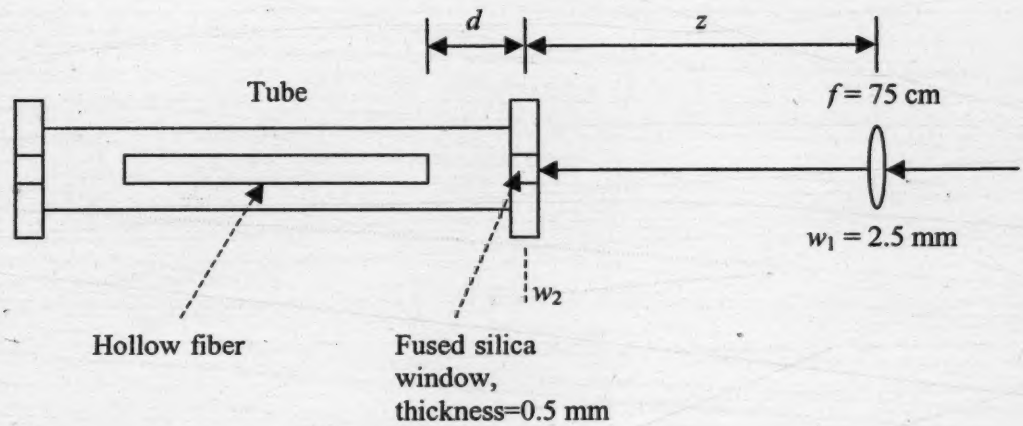

Fig. 5.31 The B-integral of the fused silica window is obtained by finding the beam waist w_2. The maximum distance from the lens with focal length f to the fused silica window is found to be 64.3 cm. Therefore, the distance d between the window and the input end of the fiber must be greater than 10.7 cm. This result was obtained for pulse energy of 400 μJ and pulse width of 110 fs.

A pulse energy of 400 μJ is assumed. The input pulse width is 110 fs. A lens with focal length of 75 cm is used to couple the input beam into the hollow fiber. The measured beam radius at the lens is 2.5 mm. The nonlinear refractive index of fused silica is 3.18×10^{-16} cm^2/W [30]. The thickness of the fused silica window is 0.5 mm. The beam radius at a distance z from the coupling lens is given by

$$w_2 = \left[w_1^2 \left(1 - \frac{z}{f}\right)^2 + \left(\frac{z\lambda}{\pi w_1}\right)^2 \right]^{\frac{1}{2}} \tag{5.14}$$

where w_1 is the beam radius at the lens, w_2 is the beam radius at distance z from the lens, and f is the focal length of the lens. For small values of $(z\lambda/\pi w_1)^2$, equation (5.14) can be approximated by

$$w_2 \cong w_1\left(1 - \frac{z}{f}\right) \tag{5.15}$$

The peak intensity at a distance z from the lens can be calculated by using the peak power and the beam radius w_2, giving

$$I = \frac{\text{Peak power}}{\pi w_2^2} \tag{5.16}$$

where the peak power is 3.2 GW. Using the values for the peak power, wavelength λ, nonlinear refractive index of fused silica n_2, and the window thickness L, in the inequality $B < 1$, we get the requirements

$$I < 8\times10^{11} \text{ W/cm}^2 \tag{5.17}$$

$$w_2 > 0.0357 \text{ cm} \tag{5.18}$$

This result indicates that in order to have $B < 1$, the beam radius at the fused silica window must be greater than 0.0357 cm. By using this value in equation (5.15), we can

find the maximum distance between the lens and the window, or the minimum distance between the window and the entrance of the hollow fiber, which gives

$$z < 64.3\,\text{cm} \tag{5.19}$$

$$d > 10.7\,\text{cm} \tag{5.20}$$

Choosing the distance between the input window and hollow fiber's input end greater than 10.7 cm results in a *B*-integral that is less than one. If we choose the distance d=20 cm, the *B*-integral becomes 0.284.

Similar calculations can be carried out for the output side. It was shown that the mode exiting the hollow fiber is HE_{11}. The beam radius at a distance of 20 cm from the output end of the hollow fiber is calculated to be 0.719 mm. The transmission of the silver coated hollow fiber is 95% as was reported in chapter 3. Therefore, the output pulse has an energy of 380 μJ. Since the output pulse broadens very little, the pulse width is approximately 110 fs. Using these values the output pulse intensity at a distance of 20 cm is calculated to be 1.87×10^{11} W/cm^2, which is less than 8×10^{11} W/cm^2. Therefore, the *B*-integral of the output window is 0.234. In practice, the distance from each hollow fiber end to the fused silica window was chosen to be 20 cm.

5.5 Discussion

Silver coated and fused silica hollow fibers were used to compress 110 fs input pulses from a Ti:sapphire laser to 20 fs. The dispersion parameters for both waveguides were obtained and shown to be almost the same. Therefore, a silver coated hollow fiber can be used in the same manner as a fused silica hollow fiber for optical pulse compression applications. This is also seen by a comparison of the spectral broadening

obtained for both waveguides which were very similar and had the same spectral width. Different experiments were performed for both hollow fibers using different pulse energies and argon gas pressures. In order to examine the scalability with the argon gas pressure, the pulse energy was kept at 250 μJ and the pressure was reduced to 1.5 atm. The pulse duration increased from 20 fs to 35 fs which was expected due to the higher value of the nonlinear length for 1.5 atm resulting in less self phase modulation and spectral broadening. In another experiment the input pulse energy was increased from 250 μJ to 300 μJ and the argon pressure was reduced from 2.4 atm to 2 atm, leaving the nonlinear length unchanged. In both cases the input pulses were compressed to 20 fs.

The above experiments showed that there is good agreement between the simulation and experimental results. By varying the input pulse parameters (pulse energy and pulse width), hollow fiber parameters (length and inner diameter), and the argon gas pressure, the optical compressor system can be simulated and optical compressors with different characteristics can be designed. This has been shown by other reported optical pulse compression experiments using uncoated fused silica hollow fibers [15, 16, 23, 24].

In Ref. 23, an 85 cm long fused silica hollow fiber with core diameter of 260 μm and filled with argon was used to compress 20 fs input pulses with an energy of 1 mJ to 5 fs with an energy of 0.5 mJ. The bore size of their fused silica hollow fiber is similar to the silver coated waveguide used in the present experiments. They reported a typical transmission of 60% (2.61 dB/m) for their fused silica hollow fiber which is much lower than the transmission of the silver coated hollow fiber (0.44 dB/m) examined in this project. Chirped mirrors with high reflectivity were employed for pulse compression in Ref. 23 and the performance of their compressor system was limited by the transmission

of the waveguide. The use of the silver coated hollow fiber in such experiments could improve the efficiency significantly which is important in generation of high energy pulses with femtosecond durations.

In Ref. 24, input pulses with energy of 260 μJ and duration of 120 fs were frequency broadened in a 50 cm hollow glass fiber with inner diameter of 250 μm and filled with argon. The output pulses were subsequently compressed to 28 fs with an energy of 160 μJ using a prism pair compressor. A transmission of 70% for the fused silica hollow fiber was reported in that experiment. They also used the output of their first compressor as input to a second compressor and were able to generate 10 fs pulses with an energy of about 74 μJ. The fused silica hollow fiber in the second compressor had a transmission of 46%. The silver coated hollow fiber, which has the same bore size of 250 μm, has a transmission of 95% and could be used in order to increase the overall performance of such compressor systems.

In other experiments fused silica hollow fibers with various lengths and core diameters have been used to compress input pulses with different pulse energies and durations. In the first optical pulse compression experiment using a hollow core fiber, a 70 cm long hollow glass fiber with inner diameter of 140 μm was used to achieve spectral broadening in krypton [15]. Input pulses with a peak power of 3.5 GW and duration of 140 fs were compressed to 10 fs with an energy of 240 μJ. The transmission of the fused silica waveguide was approximately 50% in that experiment. In another experiment, input pulses with a duration of 20 fs and an energy of 80 μJ were chirped in a krypton filled fused silica hollow fiber with length of 60 cm and internal core diameter of 160 μm [16]. Compressed pulses with duration of 4.5 fs and energy of 40 μJ were

generated by a compressor consisting of a chirped mirror and prisms. The fused silica hollow fibers used in the above mentioned experiments all had much lower transmission than the silver coated hollow fiber examined in this project.

Two additional considerations in designing an optical compressor are self focusing [55] and multiphoton ionization. The self focusing critical power is inversely proportional to the nonlinear refractive index of the noble gas, which is calculated to be 10 GW for argon at 1 atm (4.17 GW at 2.4 atm). Therefore, the type of gas and its pressure should be chosen such that the peak power of the pulse is less than the critical power for self focusing. The peak power used in the experiment was 2 GW. The pulse peak intensity should be smaller than the multiphoton ionization intensity, which is 2×10^{14} W/cm^2 for argon [56, 57]. This problem can be avoided by proper choice of the type of gas and the hollow fiber diameter. In the experiment, the pulse peak intensity at the entrance of the hollow fiber was 9.95×10^{12} W/cm^2.

As discussed in chapter 3, the focal length of the coupling lens and the alignment of the hollow fiber are important in obtaining a good output mode. Accurate measurements of the input beam diameter is needed in order to find the correct focal length for coupling the input beam to the HE_{11} mode of the hollow fiber. The alignment of the input beam into the waveguide is also more difficult when it is placed inside the argon gas tube and requires careful adjustments.

Chapter 6

Nonlinear ellipse rotation in silver coated hollow fiber

6.1 Introduction

In this chapter a preliminary investigation of the propagation of a beam with elliptic polarization through the silver coated hollow glass fiber is presented. The polarization ellipse of such a beam can rotate due to intensity dependence of the nonlinear refractive index of the material filling the hollow core. This effect can be used to increase the pulse contrast of the high intensity part of the pulse with respect to the low intensity pedestals or prepulses. Having clean pulses is essential for developing femtosecond lasers with very high peak powers. For laser matter interactions that require high intensities, it is important that the intensity of the prepulse be many orders of magnitude below the intensity of the main pulse so that no plasma is produced before the high intensity portion of the pulse reaches the target.

A saturable absorber [58, 59] has been considered for use at the preamplifier stage of a laser system in order to eliminate the unwanted components of the pulse. This way the undesired portions of the pulse are not amplified. This scheme requires nonlinear interactions in bulk media and the nonlinear phase shifts accompanying such interactions are of the order of π, thus distorting the spatial beam profile. The peak powers required to achieve this nonlinear saturation are generally more than the critical power for self focusing of the bulk media, which can also distort the spatial profile of the beam. The use of nonlinear ellipse rotation (NER) for achieving pulse contrast for picosecond pulses was previously studied using a CS_2 filled cell [60]. NER has also been investigated in

conventional and birefringent optical fibers [61, 62]. However, an optical fiber is not suitable for high energy pulses because of optical damage to the structure of the fiber. Recently NER in a fused silica hollow fiber filled with xenon gas has been used to improve the pulse contrast of pulses with microjoule energy [17]. In the next section the theory of NER is explained and following that the experimental results of NER using silver coated and uncoated fused silica hollow fibers are presented.

6.2 Theory of NER

The nonlinear polarization that results in the nonlinear refractive index can be written in terms of the third order susceptibility by [63]

$$P_i(\omega) = 3\sum_{jkl} \chi_{ijkl}(-\omega,\omega,\omega,-\omega)E_j(\omega)E_k(\omega)E_l(-\omega) \tag{6.1}$$

The third order nonlinear susceptibility for an isotropic medium has in general three independent elements, where the field frequencies are considered arbitrary. Thus, the nonlinear susceptibility can be written as

$$\chi_{ijkl} = \chi_{1122}\delta_{ij}\delta_{kl} + \chi_{1212}\delta_{ik}\delta_{jl} + \chi_{1221}\delta_{il}\delta_{jk} \tag{6.2}$$

For the case of nonlinear refractive index, the choice of frequencies and the condition of intrinsic permutation symmetry requires that χ_{1122} be equal to χ_{1212}. The nonlinear susceptibility χ_{ijkl} is then represented by

$$\chi_{ijkl}(-\omega,\omega,\omega,-\omega) = \chi_{1122}(-\omega,\omega,\omega,-\omega)\left(\delta_{ij}\delta_{kl} + \delta_{ik}\delta_{jl}\right) + \chi_{1221}(-\omega,\omega,\omega,-\omega)\left(\delta_{il}\delta_{jk}\right) \tag{6.3}$$

Substituting this equation into equation (6.1), the nonlinear polarization can be written in vector form as

$$\vec{P} = 6\chi_{1122}(\vec{E}\cdot\vec{E}^*)\vec{E} + 3\chi_{1221}(\vec{E}\cdot\vec{E})\vec{E}^* \tag{6.4}$$

By introducing the coefficients $A = 6\chi_{1122} = 3\chi_{1122} + 3\chi_{1212}$ and $B = 6\chi_{1221}$, the nonlinear polarization becomes

$$\vec{P} = A(\vec{E}\cdot\vec{E}^*)\vec{E} + \frac{1}{2}B(\vec{E}\cdot\vec{E})\vec{E}^* \tag{6.5}$$

It can be seen that the nonlinear polarization consists of two parts. One has the vector behavior of $\vec{E}$ and the other has the vector behavior of $\vec{E}^*$. Therefore, the nonlinear polarizations produced by each part will be of opposite handedness and their effect on the propagation of a beam of light through a nonlinear optical medium will be different.

Consider a beam of light with arbitrary polarization that is propagating through a nonlinear optical medium in the positive z direction. The electric field of such a beam can be decomposed into a linear combination of left and right hand circularly polarized components given by

$$\vec{E} = E_+\hat{\sigma}_+ + E_-\hat{\sigma}_- \tag{6.6}$$

where the circular polarization unit vectors $\hat{\sigma}_\pm$ are defined by

$$\hat{\sigma}_\pm = \frac{\hat{x} \pm i\hat{y}}{\sqrt{2}} \tag{6.7}$$

Substituting the electric field vector of equation (6.6) into equation (6.5), the nonlinear polarization can be written as

$$\vec{P}_{NL} = A\left(|E_+|^2 + |E_-|^2\right)\vec{E} + B\left(E_+E_-\right)\vec{E}^* \tag{6.8}$$

We can represent the nonlinear polarization in terms of the circular polarization unit vectors, giving

$$\vec{P}_{NL} = P_+\hat{\sigma}_+ + P_-\hat{\sigma}_- \tag{6.9}$$

The coefficients $P_{\pm}$ are the circular components of the nonlinear polarization and can be written in terms of the electric field components $E_{\pm}$ in the form

$$P_{\pm} = \chi_{NL}^{\pm} E_{\pm} \tag{6.10}$$

where $\chi_{NL}^{\pm}$ are the effective nonlinear susceptibilities and are defined by

$$\chi_{NL}^{\pm} = A|E_{\pm}|^2 + (A+B)|E_{\mp}|^2 \tag{6.11}$$

By introducing equations (6.6) and (6.9) for the electric field and nonlinear polarization vectors into the wave equation, we find that each circular component travels with the phase velocity $c/n_{\pm}$, where $n_{\pm}$ is given to the lowest order by

$$n_{\pm} = n_0 + \frac{2\pi}{n_0}\left[A|E_{\pm}|^2 + (A+B)|E_{\mp}|^2\right] \tag{6.12}$$

It can be seen that the right and left circular components of the beam have different refractive indices and propagate with different phase velocities. We can define the difference between the refractive indices by

$$\Delta n = n_+ - n_- = \frac{2\pi B}{n_0}\left(|E_-|^2 - |E_+|^2\right) \tag{6.13}$$

Since the two circular components propagate with different phase velocities, the polarization ellipse of the transmitted wave will rotate with respect to that of the incident wave as the beam propagates through the nonlinear medium. The electric field vector of the traveling wave can be expressed by

$$\vec{E}(z) = A_+ \exp\left(\frac{in_+\omega z}{c}\right)\hat{\sigma}_+ + A_- \exp\left(\frac{in_-\omega z}{c}\right)\hat{\sigma}_- \tag{6.14}$$

By defining the mean propagation constant $k_m = (n_- + \Delta n/2)\omega/c$ and the angle of rotation $\theta = (1/2)\Delta n\omega z/c$, the electric field vector can be written as

$$\vec{E}(z) = [A_+ \exp(i\theta)\hat{\sigma}_+ + A_- \exp(-i\theta)\hat{\sigma}_-]\exp(ik_m z) \qquad (6.15)$$

This equation shows that the polarization ellipse of the transmitted wave is the same as that of the incident wave only rotated by the angle θ. This effect does not occur for the linearly and circularly polarized light. For linearly polarized light the magnitudes of the two circular components of the electric field are equal and the index difference vanishes. For circularly polarized light, we only have one component and the polarization remains circular.

6.3 Experimental results

A fused silica hollow fiber and a silver coated hollow glass fiber filled with argon gas were used to investigate NER and pulse contrast enhancement. The experimental setup is shown in Fig. 6.1. The polarization of the laser output is converted from horizontal to vertical using a half wave plate. A quarter wave plate is used to convert the polarization of the beam to elliptic. The wave plates are made of crystal quartz. The fast axis of the quarter wave plate was set at 10° from the input polarization. Numerical calculations show that by making this angle smaller the transmission of the resultant pulse contrast enhancement system increases, but the intensity required for maximum transmission also becomes higher. The beam is then coupled into the gas filled hollow fiber using a lens with a focal length of 75 cm. The waveguide is in an enclosure pressurized with argon gas. A noble gas is chosen since it has a purely electronic nonlinearity. At the output of the hollow waveguide the beam is recollimated using a lens with a focal length of 40 cm and sent through another quarter wave plate whose fast axis is set at 90° from the fast axis of the first one. If no ellipse rotation occurs, the second

quarter wave plate would undo the retardation imparted by the first one. The ellipse rotation depends on intensity and only that portion of the pulse near the peak undergoes a significant rotation in contrast to the less intense wings before and after the peak. A Glan polarizer made of birefringent calcite is used to separate the horizontal and vertical components of the beam at the output. The components with vertical polarization are rejected and the components with the initial horizontal polarization are passed, which can then be used for experiments or injected into a pulse compressor.

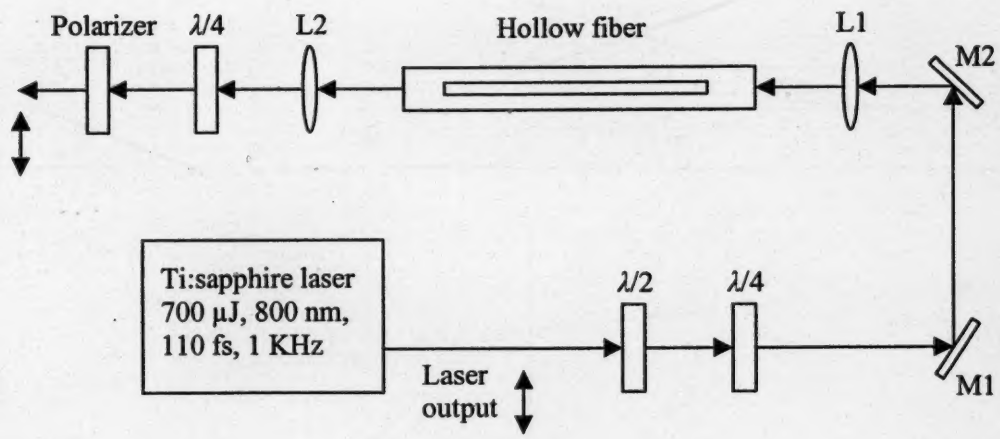

Fig. 6.1 Nonlinear ellipse rotation experimental setup. A half wave plate is used to convert the horizontal input polarization to vertical. The first quarter wave plate changes the polarization of the beam to elliptic. The beam undergoes nonlinear ellipse rotation as it propagates inside the hollow fiber. After passing through the second quarter wave plate, a polarizer rejects the low intensity components of the beam and passes most of the energy near the peak of the pulse with the initial horizontal polarization.

Figure 6.2 shows the fraction of energy in the pulse before and after passing through the second quarter wave plate using the 250 μm diameter and 50 cm long silver coated hollow fiber filled with argon gas at 3 atm. We can clearly see that the NER peaks at a pulse energy of 150 μJ. It is also seen that the transmission decreases for decreasing pulse energy and should reduce to zero as the intensity becomes small for ideal optical components. Figure 6.3 shows the fraction of energy as a function of argon gas pressure for an energy per pulse of 100 μJ at the output of the waveguide. The transmission reduces as pressure is decreased which is expected due to a reduction in the nonlinear effect.

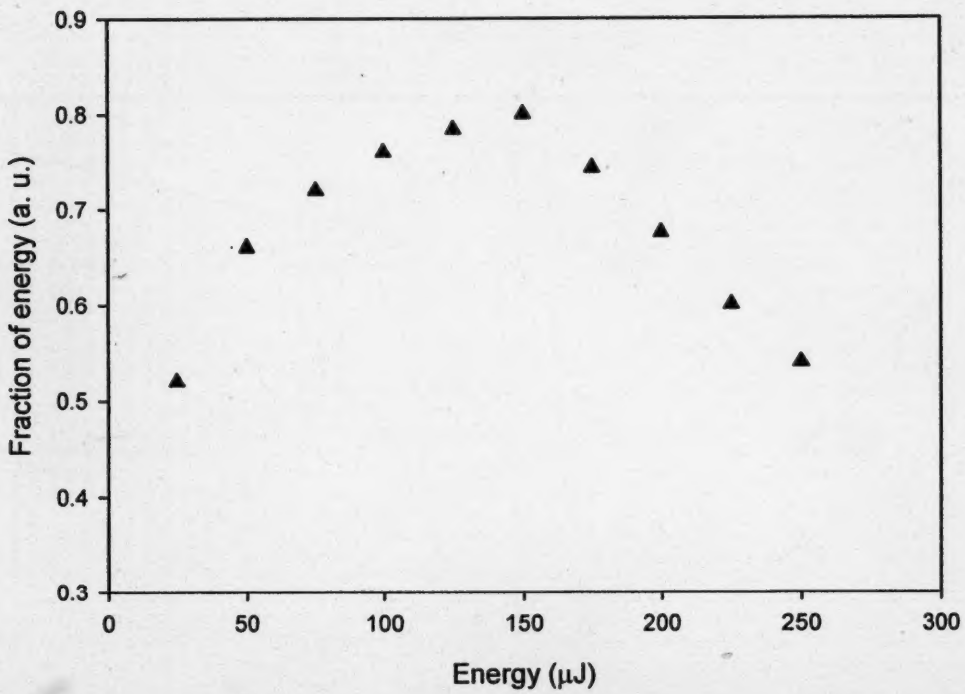

Fig. 6.2 Fraction of energy in the pulse at the output of the polarizer as a function of energy entering the second quarter wave plate for the silver coated hollow fiber filled with argon at 3 atm.

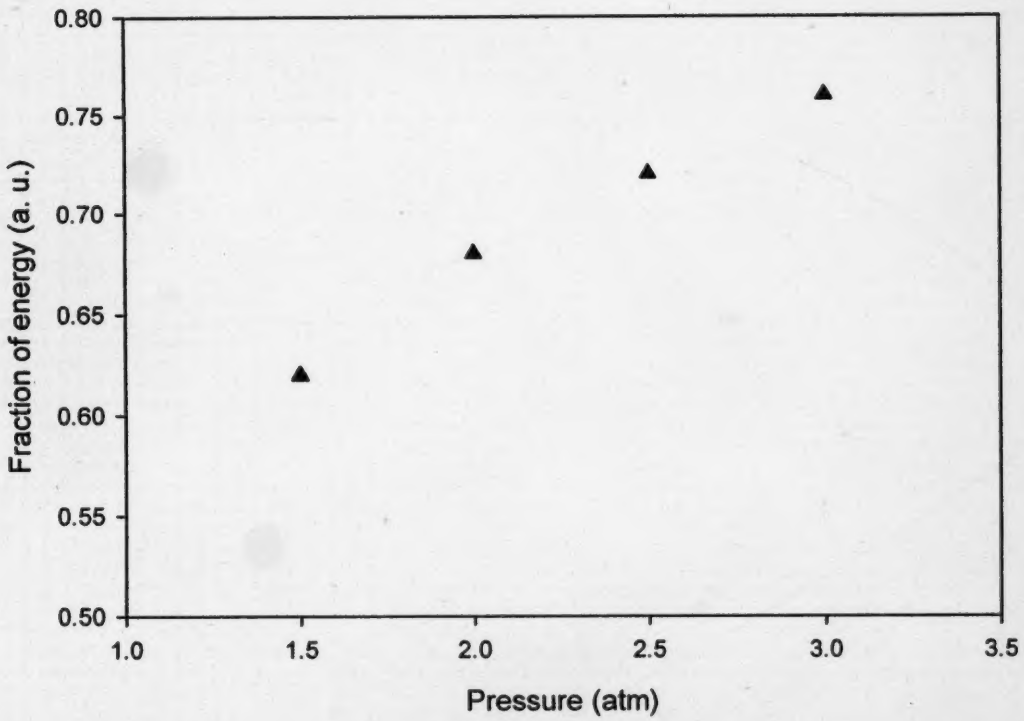

Fig. 6.3 Fraction of energy in the pulse at the output of the polarizer as a function of argon pressure for the silver coated hollow glass fiber. The energy per pulse at the output of the waveguide was set at 100 μJ.

The same experiment was performed using a fused silica hollow fiber. The advantage of the silver coated hollow fiber is that the same amount of NER can be obtained for less input energy and also the overall higher transmission efficiency. It can be seen from Fig. 6.2 that 80% of the energy transmitted by the waveguide is available at the output of the polarizer. Figure 6.4 shows the fraction of energy in the pulse before and after passing through the second quarter wave plate using the 250 μm diameter and 50 cm long fused silica hollow fiber filled with argon gas at 3 atm. The NER peaks at a pulse energy of 150 μJ, but the fraction of energy transmitted is now 73% which is less than

that obtained using the silver coated waveguide. The transmission as a function of argon gas pressure for the fused silica hollow fiber is shown in Fig. 6.5 for an energy per pulse of 100 μJ at the output of the waveguide. The energy at the output of the hollow fiber was kept constant and the argon gas pressure was reduced in steps of 0.5 atm. Similar to Fig. 6.3 for the silver coated waveguide, a reduction in pressure at this energy lowers the amount of rotation as the pulse propagates through the gas filled waveguide. We can see that as the pressure is decreased the fraction of the transmitted energy reduces, but for each value of the pressure the transmission is less than that obtained from the silver coated hollow glass fiber.

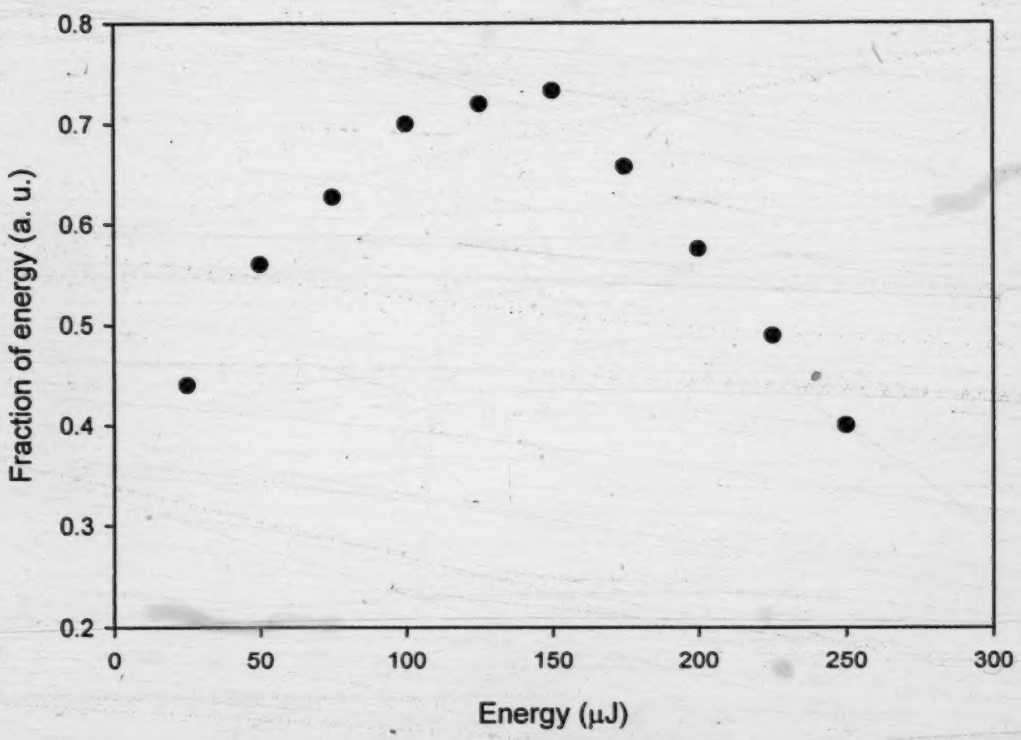

Fig. 6.4 Fraction of energy in the pulse at the output of the polarizer as a function of energy entering the second quarter wave plate for the fused silica hollow fiber at argon pressure of 3 atm.

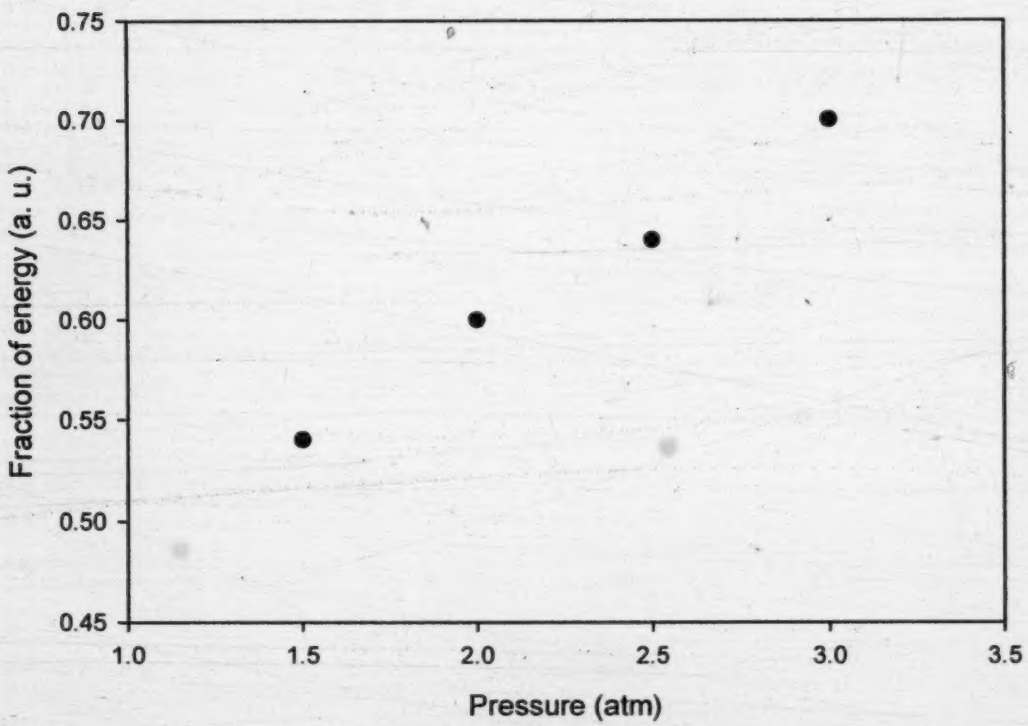

Fig. 6.5 Fraction of energy in the pulse at the output of the polarizer as a function of pressure for the fused silica hollow fiber. The energy at the output of the waveguide was set at 100 μJ.

From the work presented earlier in the thesis it is expected that significant spectral broadening due to self phase modulation would also occur in the waveguide, which can be used to achieve pulse compression. It was shown that the silver coated waveguide can be used to generate compressed pulses with higher transmission. A combination of pulse contrast enhancement and optical pulse compression using the silver coated hollow fiber would result in clean compressed pulses with higher efficiency than using a plain fused silica hollow fiber. Further work will be required to measure the actual prepulse contrast enhancement and pulse compression which can be simultaneously obtained.

6.4 Discussion

In this chapter it was demonstrated that nonlinear ellipse rotation is an effective method for increasing the contrast ratio of femtosecond microjoule pulses. Silver coated and fused silica hollow fibers filled with argon gas were used for the experiments. It was shown that by adjusting the input pulse energy and the gas pressure, the amount of elliptic rotation can be maximized. The fraction of energy transmitted at the polarizer output was higher when the silver coated waveguide was employed. The waveguides had a length of 50 cm and a core diameter of 250 μm. By using different noble gases, gas pressures, core diameters, and waveguide lengths, the rotation and the fraction of the transmitted energy can be optimized for different input pulse energies.

The amount of rotation inside the waveguide and pulse contrast enhancement also depends on the angle between the quarter wave plate fast axis and the input polarization plane. Calculations showed that for a given pulse energy, the smaller values of this angle yield a higher transmission for the output beam. Therefore, it is also possible to tune the nonlinearity by adjusting the orientation of the quarter wave plates. The wave plates and the polarizer used in the experiments had no antireflection coating. Using antireflection coated wave plates and polarizer would increase the transmission of the beam at the polarizer output. The degree of contrast enhancement achievable by this technique is also dependent on the polarization purity that can be maintained by the wave plates. Thus, the ultimate contrast enhancement which can be obtained will depend on the quality of the polarization components employed and residual birefringence in the waveguide cell windows.

Chapter 7

Conclusion

In this thesis a silver coated hollow glass fiber was investigated for beam transport and nonlinear applications at 800 nm. A 50 cm long silver coated hollow glass fiber with inner diameter of 250 μm was used for delivering the laser beam from a Ti:sapphire laser. The measured transmission of this hollow fiber is 95% (0.44 dB/m), which is 15% higher than the transmission of a similar uncoated fused silica hollow fiber measured using the same experimental setup. The measured transmission is still lower than the theoretical value of 99.6% for the silver coated hollow fiber. The increased loss is attributed to the coupling of 2% of the input beam energy to the higher order waveguide modes and the roughness of the silver coating on the inner surface glass. The scattering of light from surface roughness is more important at short wavelengths than the longer infrared wavelengths where hollow waveguides have traditionally been used.

While the TE_{01} mode is the lowest loss mode in the silver coated hollow fiber, an input TEM_{00} free space mode does not couple to the TE_{01} mode. Thus, the lowest order mode excited by a TEM_{00} input laser is the HE_{11} mode. The beam diameters of the output pulse that were obtained experimentally match closely to the values calculated theoretically for the HE_{11} mode confirming such coupling. Single mode propagation of the silver coated hollow fiber is required for most nonlinear applications such as optical pulse compression or Kerr rotation suppression of prepulses.

The measured bending losses of the silver coated hollow fiber were compared with theoretical values based on the solution of Maxwell's equations in the toroidal geometry for bending radii of 30, 50, and 100 cm. The theory of Ref. 5, which uses a

perturbation technique, gave results that were much higher than the measured bending losses and it was concluded that their bending attenuation constants can only be used for very large radii of curvature. The theoretical bending losses calculated for the HE_{11} mode using the attenuation constants given in Ref. 20, which are evaluated numerically, are less than the measured values. The difference is accounted for by increased measured losses due to mode mixing in the bent section and also scattering of light due to the roughness of the silver coating.

This silver coated hollow glass waveguide was also used to compress optical pulses from the Ti:sapphire laser at 800 nm. Input pulses with energy of 250 μJ, duration of 110 fs, and repetition rate of 1 KHz were compressed to 20 fs with energy of 220 μJ at argon pressure of 2.4 atm. The same input pulses were compressed to 35 fs at argon pressure of 1.5 atm. There was good agreement between the numerical modeling and experimental results. It was shown that the group velocity and third order dispersions in the 800 nm region are essentially the same for silver coated and uncoated fused silica hollow fibers filled with argon. A fused silica hollow fiber filled with argon at 2.4 atm was also used for optical pulse compression. The measured output spectrum showed spectral broadening which was very similar to the spectral broadening obtained from the silver coated hollow fiber and with the same spectral width. The output pulses of the fused silica hollow fiber were compressed to 20 fs with energy of 190 μJ. Therefore, the compression of the output pulse from the silver coated hollow fiber leads to results similar to the fused silica hollow fiber but at higher optical efficiency.

Nonlinear ellipse rotation for pulse contrast enhancement was demonstrated using the silver coated waveguide. The effects of pulse energy and gas pressure on the

polarization ellipse of the input beam were investigated. It was shown that the fraction of energy in the output pulse increases for higher input pulse energies. The fraction of energy then peaks at a certain input pulse energy which depends on the gas pressure, the waveguide parameters, and the angle between the fast axis of the quarter wave plate and the input polarization plane. For a pulse energy of 100 μJ at the output of the waveguide, decreasing the argon gas pressure resulted in reduced transmission due to a reduction in the nonlinear effect. The same experiments were performed using a fused silica hollow waveguide which yielded similar results, but with lower transmission.

This technique has a number of advantages including high transmission, good spatial mode quality, and scalability by adjustment of the quarter wave plate angles. Calculations showed that transmission of the output beam increases for smaller angles between the fast axis of the quarter wave plate and the input polarization plane. The significant spectral broadening due to self phase modulation which occurs in the waveguide can be used to achieve pulse compression. Therefore, pulse contrast enhancement and optical pulse compression using the silver coated hollow fiber would result in clean compressed pulses with higher efficiency than using a fused silica hollow fiber.

The performance of the silver coated hollow fiber for beam delivery and nonlinear applications may be improved by depositing a smoother silver film. It may be possible to reduce the roughness of the silver film by changing some of the fabrication parameters such as lowering the temperature of the reacting solutions or reducing the temperature of the silica substrate. It may also be possible to improve the performance of this hollow waveguide further by the application of a suitable dielectric coating to the surface of the

silver layer. A hollow fiber with a different metallic coating such as gold may also be suitable for transmission of femtosecond optical pulses at 800 nm with high efficiency. The refractive index of gold is similar to that of silver and we expect that the dispersion parameters for a gold coated hollow fiber filled with argon would be similar to that of silver. Therefore, a gold coated hollow fiber may also be used for optical pulse compression or other nonlinear applications.

Overall, this thesis has demonstrated that a high quality silver coated hollow fiber can be used to produce single mode 800 nm femtosecond pulses compressed up to six times from the starting pulse width. The optical efficiency is significantly higher than that which can be obtained using uncoated fused silica hollow fibers. The present results should stimulate the application of such metal coated hollow waveguides in femtosecond pulse compressor and enhancement systems.

References

[1] J. A. Harrington, ed., Selected Papers on Infrared Fiber Optics, (SPIE, Bellingham, 1990).

[2] J. A. Harrington, Fiber Integrated Opt. 19, 211 (2000).

[3] T. Hidaka, T. Morikawa, and J. Shimada, J. Appl. Phys. 52, 4467 (1981).

[4] J. A. Harrington and C. C. Gregory, Opt. Lett. 15, 541 (1990).

[5] A. J. Marcatili and R. A. Schmeltzer, Bell Syst. Tech. J. 43, 1783 (1964).

[6] M. Miyagi, A. Hongo, Y. Aizawa, and S. Kawakami, Appl. Phys. Lett. 43, 430 (1983).

[7] Y. Matsuura and J. A. Harrington, Opt. Lett. 20, 2078 (1995).

[8] H. K. Pulker, Thin Films Science and Technology (Elsevier Science, Amsterdam, 1985).

[9] T. Abel, J. Hirsch, and J. A. Harrington, Opt. Lett. 19, 1034 (1994).

[10] C. D. Rabii, D. J. Gibson, and J. A. Harrington, Appl. Opt. 38, 4486 (1999).

[11] C. P. J. Barty, W. White, W. Sibbett, and R. Trebino, eds., Special Issue on Ultrafast Optics, IEEE J. Sel. Topics QE 4, 157 (1998).

[12] L. Xu, C. Spielmann, F. Krausz, and R. Szipöcs, Opt. Lett. 21, 1259 (1996).

[13] A. Baltuska, Z. Wei, M. S. Pshenichnikov, and D. A. Wiersma, Opt. Lett. 22, 102 (1997).

[14] A. Baltuska, Z. Wei, M. S. Pshenichnikov, D. A. Wiersma, and R. Szipöcs, Appl. Phys. B 65, 175 (1997).

[15] M. Nisoli, S. De Silvestri, and O. Svelto, Appl. Phys. Lett. 68, 2793 (1996).

[16] M. Nisoli, S. Stagira, S. De Silvestri, O. Svelto, S. Sartania, Z. Cheng, M. Lenzner, C. Spielmann, and F. Krausz, Appl. Phys. B 65, 189 (1997).

[17] D. Homoelle, A. L. Gaeta, V. Yanovsky, and G. Mourou, Opt. Lett. 27, 1646 (2002).

[18] J. A. Stratton, Electromagnetic Theory (McGraw-Hill, New York, 1941).

[19] M. J. Weber, ed., CRC Handbook of Laser Science and Technology (CRC Press, Boca Raton, 1986).

[20] S. Abe and M. Miyagi, IEEE Trans. Microwave Theory Tech. 39, 230 (1991).

[21] D. N. Nikogosyan, Properties of Optical and Laser Related Materials (Wiley, Chichester, 1997).

[22] R. L. Abrams, IEEE J. QE 8, 838 (1972).

[23] S. Sartania, Z. Cheng, M. Lenzner, G. Tempea, C. Spielmann, F. Krausz, and K. Ferencz, Opt. Lett. 22, 1562 (1997).

[24] J. Thogersen, A. Borowiec, and H. K. Haugen, CLEO Technical Digest, 497 (2000).

[25] K. Matsuura, Y. Matsuura, and J. A. Harrington, Opt. Eng. 35, 3418 (1996).

[26] Y. Matsuura, G. Takada, T. Yamamoto, Y. Shi, and M. Miyagi, Appl. Opt. 41, 442 (2002).

[27] S. J. Wilson, R. M. Jenkins, and R. W. J. Devereux, IEEE J. QE 23, 52 (1987).

[28] Y. Matsuura, T. Abel, and J. A. Harrington, Appl. Opt. 34, 6842 (1995).

[29] Y. Matsuura, M. Miyagi, K. Shihoyama, and M. Kawachi, J. Appl. Phys. 91, 887 (2002).

[30] G. P. Agrawal, Nonlinear Fiber Optics (Academic Press, San Diego, 2001).

[31] K. J. Blow and D. Wood, IEEE J. QE 25, 2665 (1989).

[32] P. V. Mamyshev and S. V. Chernikov, Opt. Lett. 15, 1076 (1990).

[33] G. P. Agrawal, Applications of Nonlinear Fiber Optics (Academic Press, San Diego, 2001).

[34] E. B. Treacy, IEEE J. QE 5, 454 (1969).

[35] R. H. Stolen and C. Lin, Phys. Rev. A 17, 1448 (1978).

[36] M. Nakazawa, T. Nakashima, H. Kubota, and S. Seikai, J. Opt. Soc. Am. B 5, 215 (1988).

[37] R. L. Fork, C. H. Brito Cruz, P. C. Becker, and C. V. Shank, Opt. Lett. 12, 483 (1987).

[38] W. J. Tomlinson, R. H. Stolen, and C. V. Shank, J. Opt. Soc. Am. B 1, 139 (1984).

[39] O. E. Martinez, J. Opt. Soc. Am. B 3, 929 (1986).

[40] R. L. Fork, O. E. Martinez, and J. P. Jordan, Opt. Lett. 9, 150 (1984).

[41] J. P. Gordon and R. L. Fork, Opt. Lett. 9, 153 (1984).

[42] F. J. Duarte and J. A. Piper, Opt. Comm. 43, 303 (1982).

[43] O. E. Martinez, J. P. Gordon, and R. L. Fork, J. Opt. Soc. Am. A 1, 1003 (1984).

[44] J. Diels and W. Rudolph, Ultrashort Laser Pulse Phenomena (Academic Press, San Diego, 1996).

[45] J. D. Kafka and T. Baer, Opt. Lett. 12, 401 (1987).

[46] Zs. Bor and B. Racz, Opt. Comm. 54, 165 (1985).

[47] M. Born and E. Wolf, Principles of Optics, (Pergamon Press, Oxford, 1980).

[48] F. A. Jenkins and H. E. White, Fundamentals of Optics (McGraw-Hill, New York, 1976).

[49] M. Bass, ed., Handbook of Optics (McGraw-Hill, New York, 1995).

[50] O. Duhr, E. T. J. Nibbering, G. Korn, G. Tempea, and F. Krausz, Opt. Lett. 24, 34 (1999).

[51] M. Schnurer, Z. Cheng, S. Sartania, M. Hentschel, G. Tempea, T. Brabec, and F. Krausz, Appl. Phys. B 67, 263 (1998).

[52] S. L. Chin, C. Rolland, P. B. Corkum, and P. Kelly, Phys. Rev. Lett. 61, 153 (1988).

[53] A. Dalgarno and A. E. Kingston, Proc. R. Soc. A 259, 424 (1966).

[54] H. J. Lehmeier, W. Leupacher, and A. Penzkofer, Opt. Comm. 56, 67 (1985).

[55] G. Tempea and T. Brabec, Opt. Lett. 23, 762 (1998).

[56] T. S. Luk, T. Graber, H. Jara, U. Johann, K. Boyer, and C. K. Rhodes, J. Opt. Soc. Am. B 4, 847 (1987).

[57] J. Zhou, J. Peatross, M. M. Murnane, and H. C. Kapteyn, Phys. Rev. Lett. 76, 752 (1996).

[58] M. Nantel, J. Itatani, A. C. Tien, J. Faure, D. Kaplan, M. Bouvier, T. Buma, P. Van Rompay, J. Nees, P. Pronko, D. Umstadter, and G. Mourou, IEEE J. QE 4, 449 (1998).

[59] G. Cheriaux, T. Planchon, F. Auge, G. Mourou, and J. P. Chambaret, in Proceedings of Ultrafast Optics (Springer-Verlag, Heidelberg, 2001).

[60] K. Sala and M. C. Richardson, J. Appl. Phys. 49, 2268 (1978).

[61] G. B. Altshuler, V. B. Karasev, S. A. Kozlov, T. A. Murina, and N. N. Rozanov, Opt. Spectrosk. 61, 359 (1986).

[62] J. Tapie and G. Mourou, Opt. Lett. 17, 136 (1992).

[63] R. W. Boyd, Nonlinear Optics (Academic Press, Boston, 1992).